Forest Ecology and Management 526 (2022) 120573

Contents lists available at ScienceDirect

Forest Ecology and Management

journal homepage: www.elsevier.com/locate/foreco

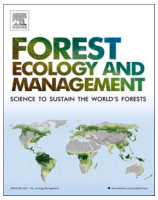

Rangewide climatic sensitivities and non-timber values of tall *Sequoia sempervirens* forests

Stephen C. Sillett [a,*], Marie E. Antoine [a], Allyson L. Carroll [a], Mark E. Graham [a], Alana R.O. Chin [b], Robert Van Pelt [c]

[a] Department of Forestry, Fire, and Rangeland Management, Cal Poly Humboldt, Arcata, CA 95521, USA
[b] Department of Atmospheric and Climate Science, Institute for Integrative Biology, ETH, Zürich, Switzerland
[c] School of Environmental and Forest Science, University of Washington, Seattle, WA 98195, USA

ARTICLE INFO

Keywords:
Redwood
Growth efficiency
Hotter drought
Heartwood
Carbon sequestration
Biodiversity

ABSTRACT

Heavily exploited for its reddish, decay-resistant heartwood, the tallest conifer, *Sequoia sempervirens*, is a major component of coastal forests from extreme southwestern Oregon to California's Santa Lucia Mountains. Primary *Sequoia* forests are now restricted to < 5 % of their former distribution, and mature secondary forests with trees over 60 m tall are even scarcer due to repeated logging. Leveraging allometric equations recently derived from intensive work in both forest types, we climbed, measured, and core-sampled 235 trees in 45 locations distributed across the species range to examine growth trends and understand how tall *Sequoia* are responding to recent environmental changes. Paired samples of sapwood and heartwood collected along the height gradient were used to quantify *Sequoia* investment in decay resistance. During the 20th century, trees in most locations began producing more wood than expected for their size with this growth surge becoming pronounced after 1970 and ending around 2000. Radial increments—ring widths—correlate with climatic variables related to water availability, and these relationships are strengthening as temperatures rise. Sensitivity to drought increased from north to south along a 6° latitudinal gradient of decreasing precipitation and summer fog frequency. *Sequoia* trees north of 40° were least sensitive to drought, producing similar biomass annually during dry and wet years, whereas trees farther south produced less biomass during individual drought years. Hotter 21st century drought barely affected *Sequoia* growth efficiency (biomass increment per unit leaf mass) north of 40° until the fourth consecutive year (2015), when growth efficiency dropped precipitously, recovering within two years. South of 40°, *Sequoia* trees exhibited steadily declining growth efficiency during the multi-year drought followed by recovery, but recovery did not occur south of 37° despite ample precipitation in 2017. *Sequoia* growth efficiency is currently highest in secondary forests north of 40°, where trees produce relatively small amounts of heartwood with the lowest decay resistance (least fungicide) while receiving the most nocturnal summer fog. Increasing sink limitations, whereby rising temperatures, drier air at night, and extreme tree height collectively lower turgor pressure to inhibit cambial activity, may reduce *Sequoia* growth efficiency while contributing to more durable biomass production. Heartwood and fungicide increments are higher in primary than secondary forests across the species range. Crown structural complexity promotes development of vascular epiphytes and arboreal soil habitats in *Sequoia* forests with sufficient moisture availability. These habitats are lacking in secondary forests and rare in primary forests south of 40°. After logging, restoration of tall *Sequoia* forests can be achieved via silviculture that maximizes height increments during early stand development and then retains some dominant trees in perpetuity, allowing them to gain full stature, produce increasingly decay-resistant heartwood, and support significant arboreal biodiversity.

1. Introduction

The species responsible for global maximum forest leaf area and biomass—*Sequoia sempervirens* (hereafter *Sequoia*)—occupies a restricted range along the US Pacific coast (Fig. 1). Combining extreme resistance to fire, fungal decay, and herbivory with shade tolerance and

* Corresponding author.
E-mail address: prof.sillett@gmail.com (S.C. Sillett).

https://doi.org/10.1016/j.foreco.2022.120573
Received 13 August 2022; Received in revised form 28 September 2022; Accepted 30 September 2022
Available online 18 October 2022

clonal reproduction, *Sequoia* trees over 100 m tall, 100 Mg biomass, and 1000 yr old are widely distributed in primary forests (Van Pelt et al. 2016, Sillett et al. 2020). Since 1850, 27 % of these forests were lost to development, 93 % of the remainder were logged, and all but 2 % of the resulting secondary forests were logged again, leaving just 457 km^2 of primary forests and 109 km^2 of mature secondary forests (> 100 yr, trees up 87 m tall, Sillett et al. 2019a) in scattered parks and reserves (Burns et al. 2018). The superlative nature and increasing rarity of tall *Sequoia* forests inspired not only long-term conservation efforts (Engbeck 2018), but also silviculture designed to accelerate tree size development in previously logged forests toward primary (old-growth) reference conditions (Berrill et al. 2013, Dagley et al. 2018, Soland et al. 2021). Substantial climatic, topographic, and edaphic variation across its 740-km-long, relatively narrow, and highly fragmented distribution makes establishing realistic targets for *Sequoia* restoration challenging.

Uncertainty about appropriate reference conditions for *Sequoia* forests is compounded by the global climatic emergency caused by anthropogenic emissions of CO_2 and other greenhouse gases (Ripple

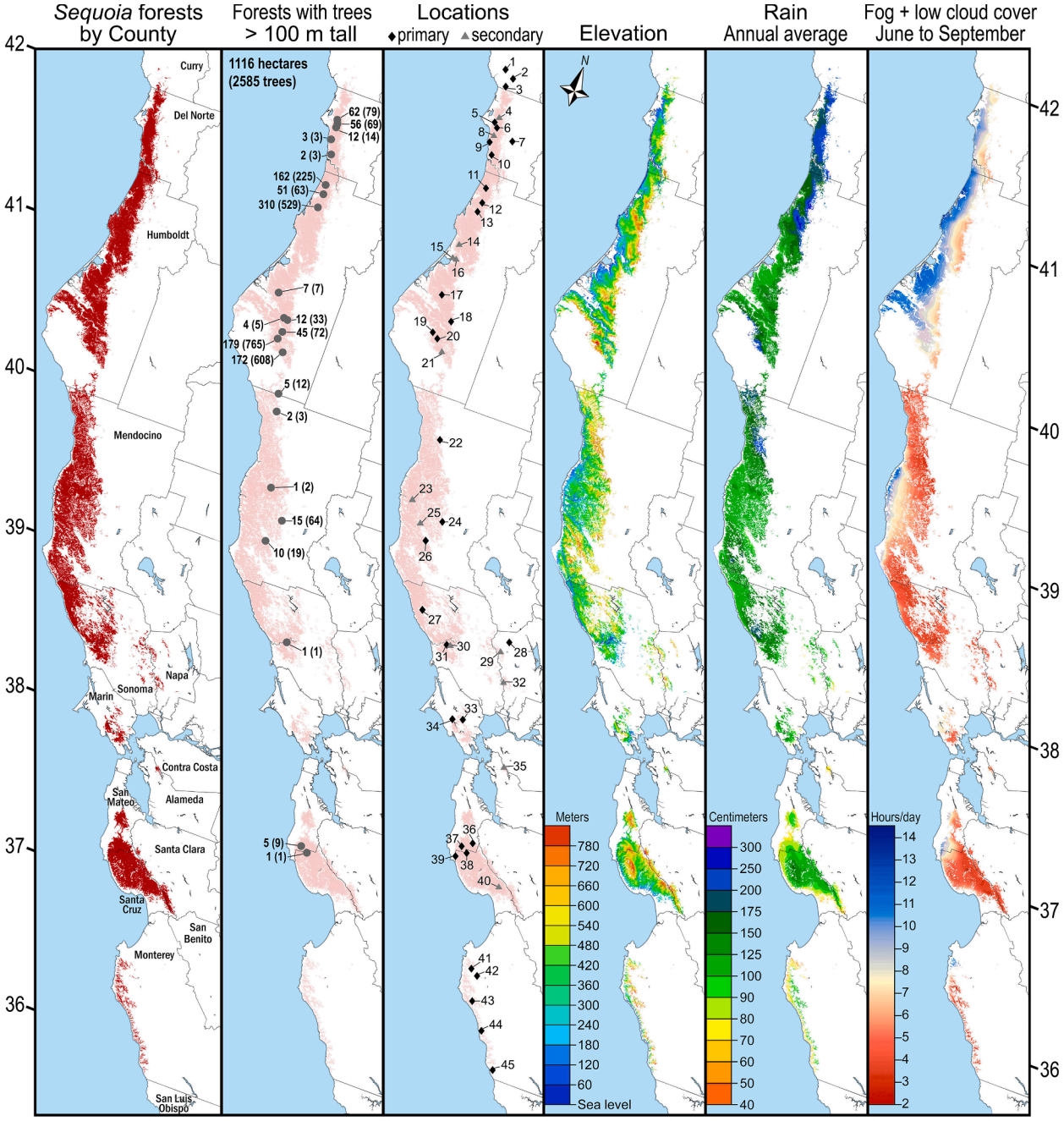

Fig. 1. Natural range of *Sequoia sempervirens*. From left, first panel shows original species distribution in red covering 8900 km^2 (compiled by R. Van Pelt from available sources). Second panel locates all forests with living trees > 100 m tall based on direct measurements and LiDAR canopy height analysis of virtually all suitable habitat (compiled by M. Graham from available sources, **Supplementary Table 1**). Numbers are hectares per reserve (or watershed) containing trees > 100 m tall with number of trees in parentheses. Third panel shows 45 study locations of two forest types (32 primary, 13 secondary). Fourth through sixth panels show elevation (m), rain (cm), and summer fog + low cloud cover (h/d) exclusively for *Sequoia* forests. Elevations are derived from US National Map. Rain is most recent 30-yr annual mean precipitation (PRISM Climate Group 2020). June to September fog and low cloud cover is derived from analysis of Geostationary Operational Environmental Satellite data for period 1999–2009 (Torregrosa et al. 2016). (For interpretation of the references to color in this figure legend, the reader is referred to the web version of this article.)

et al. 2021). Since the start of the 20th century, average air temperatures in California, which holds > 99 % of the *Sequoia* range, have risen nearly 2 °C and are expected to increase at least 1–3 °C more by the end of the 21st century with a much higher frequency of unusually warm nights (Zhao et al. 2020, Frankson et al. 2022). Nocturnal temperature is of critical importance to tree productivity, because cell division and enlargement in the vascular cambium, which controls radial growth, occurs predominantly at night when air temperature and vapor pressure deficit (VPD) are minimal and turgor pressure is maximal (Zweifel et al. 2021). During the day, high VPD, which increases exponentially with temperature, leads to lowered turgor pressure, early stomatal closure, reduced photosynthesis, and diminished growth (Grossiord et al. 2020). Global warming is also associated with increased frequency and severity of extreme climatic events in California, including multi-year hotter droughts and extensive, high-severity fires (Diffenbaugh et al. 2015, Swain et al. 2018, Stephenson et al. 2018, Keeley & Syphard 2021, Shive et al. 2022). The vulnerability of *Sequoia* to such changes is still poorly understood. Models using projected monthly or seasonal climate combined with species occurrence data predict major vulnerability and contraction of suitable habitat in the southern range under projected warming even without substantial changes in annual precipitation (Fernández et al. 2015, Coffield et al. 2021). Habitat suitability for this species is strongly linked to topographic gradients in soil water availability and fog frequency (Francis et al. 2020), though modeling based upon species occurrence does not account for variation in *Sequoia* productivity or its long-term persistence by virtue of great longevity (> 2000 yr) and clonal reproduction via trunk reiteration (i.e., sprouting, O'Hara et al. 2017, Sillett et al. 2020). Were it not for the remarkable ability to sprout after fire, many southern forests may have lost their *Sequoia* component long ago.

Like other trees in temperate forests, *Sequoia* produces wood in annual rings that can be crossdated and used to quantify radial growth trends as they relate to both climatic variation and disturbances (Carroll et al. 2014). Identifying climatic correlates of interannual growth variation is an important first step toward understanding how trees may respond to future conditions, but dendroclimatic relationships may be unstable over time (D'Arrigo et al. 2008, Babst et al. 2019) and inappropriate for predicting tree growth responses to a rapidly changing climate via space-for-time substitutions (Canham et al. 2018, Klesse et al. 2020). Tree-ring indices provide a unitless metric of radial growth, as ring widths are standardized to remove the geometric growth trend—larger rings toward the pith—prior to analysis. Tree-ring sampling usually occurs at breast height (BH), where changes in trunk diameter are used to compute biomass increments as differences in DBH-predicted biomass between time steps (Evans et al. 2022, Piponiot et al. 2022). Comparison of biomass increments predicted by DBH changes and those obtained by repeated diameter measurements at all heights above the ground reveals underestimation of biomass increments in tall trees with the DBH-only method (Sillett et al. 2015a, 2019a,b, 2020). This underestimation is exacerbated in *Sequoia*, because lower trunks of large trees are often highly buttressed with poor circuit uniformity and produce very small (or missing) rings at BH that cannot be crossdated without reference to those produced higher on the trunk (Carroll et al. 2014, Sillett et al. 2019a). Thus, while providing a basis for climatic reconstructions and other practical applications requiring precise dating (Fritts 2012, Cook & Kairiuskstis 2013), ring widths have limited utility for quantifying biomass production or carbon sequestration by tall *Sequoia* unless they are measured at multiple heights above the ground and combined with other measurements.

Intensive study of *Sequoia* in primary forests—trunk diameter measurements from base to top; core-sampling at regular height intervals to quantify bark, cambium, sapwood, heartwood, and annual rings; non-destructive mapping of all appendages; and dissecting subsets of branches into leaf, bark, and wood for predicting these components on all appendages—yielded allometric equations capable of estimating aboveground attributes of any tree regardless of its size or age using ground-based measurements (Sillett et al. 2015b, Van Pelt et al. 2016). Development of these equations—independently evaluated for accuracy by terrestrial laser scanning (Disney et al. 2020)—was a major goal of our previous sampling, which focused on six plots north and five plots south of 40° latitude. Superlative forests, including the tallest, largest, and oldest trees available, were necessary to achieve this goal. A late 20th century growth surge was evident in nine of 11 one-hectare plots (Sillett et al. 2015b), though neither the cause of this surge nor its geographic extent were understood. Focusing on superlative forests, which may be climatically buffered, left potential sources of growth limitation in landscape positions at higher elevations, on steeper terrain, farther from the ocean, and near northern and southern range limits unconsidered.

A multi-year drought (2012–2015) accompanied by unusually warm temperatures occurred during the 5-yr measurement interval of the 11 plots. Unlike extensive areas of Sierra Nevada mixed conifer forests, where this event caused sustained canopy water loss and unprecedented tree mortality (Brodrick & Asner 2017, Fettig et al. 2019), no drought-related tree mortality was evident in any of the *Sequoia* plots (S.C. Sillett and R. Van Pelt, unpublished). In primary and secondary forests, however, *Sequoia* trees produced less biomass than expected for their size by the end of the drought (see Fig. 10 in Sillett et al. 2021), but no attempt was made to quantify the growth response or to determine how its effects varied geographically or by forest type. Continued sampling after the drought resulted in two realizations: (1) key attributes related to crown structure and wood density differ between primary and secondary forests, making allometry of one forest type insufficient for use in the other (Sillett et al. 2019a), and (2) trunk wood densities vary considerably with height such that conversion of volume to biomass using fixed multipliers is inadequate (Sillett et al. 2018a, 2020). Improved allometric equations for *Sequoia*—accounting for height-related variation in wood density and based on intensive re-measurements of trees at 3–8-yr intervals—now permit unbiased estimation of biomass increments as multiples of wood volume increments in both forest types (Sillett et al. 2019a, 2020). Allometry combined with dendrochronology also permits reconstruction of *Sequoia* size and growth increments for developmental analyses, including simulation of aboveground biomass and heartwood production on a per hectare basis (Sillett et al. 2021).

The heartwood component of *Sequoia* is important to quantify separately. This red-colored, polyphenolic-infused material represents a substantially higher proportion of biomass in primary than secondary forests, accumulating at an increasing rate and contributing to declining growth efficiency as trees enlarge with age (Sillett et al. 2019a, 2020). The decay resistance of heartwood may increase during *Sequoia* development with profound implications for management of non-timber values, especially carbon sequestration and conservation of biodiversity. Lower average sapwood and heartwood densities in secondary compared to primary forests (sapwood = 301 vs. 334, heartwood = 316 vs. 376 kg m^{-3} for secondary vs primary forests; data from Sillett et al. 2019a, 2020) indicate that *Sequoia* biomass in secondary forests may be less durable than in primary forests. The density difference between paired heartwood and sapwood samples can be used to estimate the amount of extractives (fungicide) deposited during heartwood formation (Sillett et al. 2021), suggesting that tall *Sequoia* in primary forests invest heartwood with nearly-three times as much fungicide as those in secondary forests (42 vs. 15 kg m^{-3}). The amount of heartwood extractives, which possess both fungicidal and termiticidal properties, correlates with resistance to fungal decay and termites and is highly variable within and between tree species (Clark & Scheffer 1983, Hillis 1987, Taylor et al. 2002, 2006). If not only the amount of heartwood produced annually but also its fungicide content increase during *Sequoia* development, the capacity of regenerating forests to sequester carbon in durable biomass may be substantially overestimated. Moreover, decay resistance should be considered when intentionally damaging relatively young trees in secondary forests to accelerate development of crown

structural complexity (Sillett et al. 2018a). In upper crowns of primary forests, slowly decaying heartwood provides a critical water-holding resource for epiphytic vascular plants and associated arboreal biota (Sillett & Van Pelt 2007, Williams & Sillett 2007). Given high levels of variation observed within trees and between forest types (Luxford & Markwardt 1932), more wood density sampling is necessary to understand *Sequoia* heartwood development and its consequences for both carbon sequestration and conservation of biodiversity.

Our purpose in this rangewide study is to integrate *Sequoia* performance by modeling growth increments as functions of tree attributes, latitude, topography, and climate. Our dendrochronological approach allows individual trees to be examined over many years, back to previous centuries when tall trees in today's primary forests were much shorter and when the largest trees in today's secondary forests were mere saplings. By expanding geographic coverage, increasing replication, improving estimation of heartwood quantities, and extending time series of tree performance further into the 21st century, we hope to answer five main questions: (1) How do long-term growth trends of *Sequoia* trees vary across the species range? (2) What are the climatic drivers of tree-ring width variation, and how stable are these dendroclimatic relationships? (3) How do forest type and latitude influence *Sequoia* growth responses to hotter drought? (4) Which biotic and abiotic factors best explain *Sequoia* growth variation in the 21st century? (5) What are realistic targets for *Sequoia* forest restoration, including tree size, carbon sequestration, and arboreal biodiversity? Organization of this study, which attempts to answer these interrelated questions by quantifying *Sequoia* growth responses at multiple spatial and temporal scales, is summarized in Table 1.

2. Method

2.1. Study locations and tree selection

Primary and secondary forests were selected across the full extent of *Sequoia sempervirens*' natural range if the following criteria were met: some trees exceeded 60 m tall, the forest was protected and available for long-term study, and permission to climb and measure trees was obtained. The 235 trees and 45 locations ultimately selected were distributed among 11 counties, embraced diverse public and private ownerships, and spanned 6° latitude, 56 km distance from the ocean, and 645 m elevation above sea level (Fig. 1, Table 2). These locations included 13 from previous studies—eight primary forests receiving 1-ha plot installations and 5-yr remeasurements (5, 11, 13, 20, 24, 34, 38, 44), one primary forest in Napa County with five trees (28, Carroll et al. 2018b), and four secondary forests in Del Norte and Humboldt Counties with 24 trees measured in an experiment (4, 8, 15, 21, (Sillett et al., 2018a). Since 2017, we added locations in 23 primary forests and nine secondary forests, including 164 new trees—all in dominant or codominant canopy positions. The new trees included a representative set of tall individuals from each location ranging in size from the smallest codominants to the largest dominants. The 71 individuals utilized from previous work were a subset of trees available, including only stand dominants and codominants whose main trunks received a full set of measurements, making their datasets comparable to the new trees (see *2.3. Tree measurements and core sampling*).

Table 1
Organization of article into sections showing locations of figures and tables in Introduction, Methods, and with respect to five main research questions: (1) How do long-term growth trends of *Sequoia* trees vary across the species range? (2) What are the climatic drivers of tree-ring width variation, and how stable are these dendroclimatic relationships? (3) How do forest type and latitude influence *Sequoia* growth responses to hotter drought? (4) Which biotic and abiotic factors best explain *Sequoia* growth variation in the 21st century? (5) What are realistic targets for *Sequoia* forest restoration, including tree size, carbon sequestration, and arboreal biodiversity? Text components are indicated by numbers with decimals indicating subheadings in Results and Discussion.

Section	Figures	Tables	Text
Introduction	1	1	1
Methods	1	2, 3, 4, 5	2
Question 1	1, 2, 3	2, 6	3.1, 3.2, 3.3, 4.1
Question 2	4, 5, 6	7	3.4, 3.5, 4.2
Question 3	7	8	3.6, 4.3
Question 4	8, 9, 10	4, 9	3.7, 3.8, 4.4
Question 5	11, 12, 13, 14	5, 10	3.9, 3.10, 3.11, 4.5, 4.6

2.2. Topographic and canopy height analyses

Terrain and forest canopy surrounding all study trees were examined from a variety of sources, including airborne LiDAR point clouds and USGS topographic maps, with ArcGIS Pro (v2.8.2). Tree positions were determined in the field via GPS unit (Oregon 650 t, Garmin ltd.) and waypoint averaging at the treetop or by inspecting LiDAR-derived Canopy Height Models (CHMs) and locating crowns of known height. Where airborne LiDAR data were available, CHMs were created by subtracting average ground elevation (see below) from maximum first return elevation per m^2. Even for study trees whose locations were determined via treetop GPS, CHMs were used to confirm, and if necessary, adjust actual positions to obtain accurate latitude, longitude, and elevation values per tree. In addition to study trees, special effort was devoted to locating all *Sequoia* > 100 m tall across the species range via airborne LiDAR. The point clouds were initially sized to encompass ~ 1 km^2 per location, but this was increased as necessary to include the nearest streams and potential flow accumulations as well as all primary forests with potentially tall trees. Most point clouds were downloaded from the National Map while others came from private LiDAR sources (**Supplementary Table 1**). For all trees > 100 m tall, UTM coordinates were rounded to the nearest 100 m for easting and northing, so that each tree was assigned to a specific hectare (100 m × 100 m). After tallying trees, numbers of unique hectares per reserve (or watershed) with at least one tree > 100 m tall were counted.

Topographic features relevant to each tree were quantified in a consistent way with missing information (e.g., lack of LiDAR) constraining the number of features evaluated in a few locations. Digital Elevation Models (DEMs) were created from airborne LiDAR point clouds. ArcGIS was used to create DEMs by filtering point clouds to ground points only, calculating average elevation per 1 or 0.5 m^2, and using nearest neighbor for any necessary void fill. Several derivative products were created per DEM using ArcGIS. One-meter contours and grayscale hill shades were used to assess tree and stream positions as well as direction of water flow. Maps showing slope-facing directions were used to classify aspect per tree. Slope-in-degrees maps helped to define ground slope around tree positions. Ground slope was calculated by taking DEM elevations 20 m uphill and downhill per tree, following slope direction, calculating the average gradient over 40 m, and applying the arctangent function to compute slope. For trees standing within 20 m of streams, stream elevation was used as the downhill elevation. Latitude, aspect, and slope were used to compute a heat load index per tree via the statistical package HyperNiche (v2.30, MjM Software Design) following specifications in McCune (2007). Potential sources and directions of surface and subsurface water movement around each tree were evaluated. Flow accumulations were quantified as number of m^2 feeding accumulation points that often create line segments representing seasonal streams, hollows, or gulches. The complete set of topographic information assembled per tree included distance (± 0.1 km) from Pacific Ocean (using Ruler tool in Google Earth Pro, v7.3.3.7786), elevation above sea level (± 1 m), slope (± 1°), aspect (± 22.5°), heat load index, vertical and horizontal distances to nearest stream (± 1 m), vertical and horizontal distances to nearest flow accumulation (± 1 m), and size of nearest flow accumulation (± 1 m^2). If nearest flow accumulation was > 10^4 m^2, it was considered a seasonal stream and used to compute nearest distances to water. For three

Table 2
Summary of 45 study locations by forest type (P = primary, S = secondary), county (all in California except Curry in Oregon), ownership (USFS = US Forest Service, CSP = California State Parks, NPS = National Park Service, P = private, Arcata = City of Arcata, BLM = Bureau of Land Management, LTNC = Land Trust of Napa County, MCP = Marin County Parks, EBRPD = East Bay Regional Park District, UC = University of California), latitude, distance to ocean, elevation above sea level, number of study trees, year(s) sampled, tree attributes (age, height, *f*DBH, biomass, leaves, most recent 5-yr mean biomass increment, and reconstructed growth history), and 21st century climate (2001–2019 means, rain = annual precipitation, JJAS rain = % rain from June to September, temp = minimum and maximum March to October mean temperature, VPD = minimum and maximum March to October mean vapor pressure deficit). Rain, temperature, VPD, and SPEI are derived from 800-m resolution data (LT81 model, PRISM Climate Group 2020). Secondary forests with asterisk (*S) have one veteran tree that survived logging. Primary forests with asterisk (*P) are partially logged with one tree regenerated after logging. Tree attributes are listed as ranges among study trees, and last ring is most recent complete annual ring obtained for most trees per location. Locations are ranked by latitude from north (top) to south (bottom).

Location	Type	County	Ownership	Latitude (°N)	Ocean (km)	Elevation (m)	Trees	Sampled	Age (yr)	Height (m)	*f*DBH (cm)	Biomass (Mg)	Leaves (kg)	Increment (kg yr^{-1})	History (yr)	Rain (cm yr^{-1})	JJAS rain (%)	Temp (°C)	VPD (hPa)
1	P	Curry	USFS	42.12	10.1	134	5	2020	207 – 382	68 – 89	162 – 257	19 – 48	271 – 510	156 – 362	153 – 320	213	7.0	9 – 22	1 – 17
2	P	Curry	USFS	42.08	11.9	439	5	2020	336 – 1078	65 – 77	117 – 310	9 – 67	149 – 436	44 – 152	224 – 945	234	6.5	8 – 22	1 – 17
3	P	Curry	USFS	42.02	5.4	165	5	2019	357 – 871	84 – 93	195 – 588	30 – 142	303 – 862	149 – 345	319 – 488	207	6.6	9 – 19	0 – 11
4	S	Del Norte	CSP	41.82	9.5	36	4	2017	127 – 144	62 – 72	108 – 169	7 – 24	113 – 833	97 – 354	98 – 106	191	5.3	8 – 18	0 – 8
5	P	Del Norte	CSP	41.78	5.7	84	6	2014–18	485 – 1278	87 – 108	352 – 750	58 – 350	559 – 1533	320 – 738	272 – 547	200	5.2	8 – 19	0 – 10
6	P	Del Norte	NPS	41.75	4.2	182	5	2020	367 – 1753	73 – 86	235 – 543	41 – 185	314 – 574	114 – 500	291 – 1032	201	5.2	8 – 20	0 – 11
7	P	Del Norte	USFS	41.71	16.9	181	5	2019	229 – 460	65 – 74	159 – 235	17 – 41	187 – 527	63 – 296	149 – 404	229	5.3	8 – 24	1 – 20
8	S	Del Norte	CSP	41.70	3.2	193	8	2017	96 – 122	58 – 66	96 – 188	6 – 23	71 – 538	86 – 411	62 – 71	211	5.2	8 – 21	0 – 13
9	P	Del Norte	CSP	41.66	0.9	232	6	2019	408 – 1158	82 – 108	199 – 387	25 – 115	301 – 568	208 – 435	308 – 879	209	5.1	8 – 20	0 – 12
10	P	Del Norte	USFS	41.58	2.7	57	5	2018–19	246 – 1449	74 – 98	190 – 690	23 – 254	289 – 1600	237 – 1135	226 – 811	197	5.1	8 – 18	0 – 8
11	P	Humboldt	CSP	41.37	5.1	79	5	2011–16	331 – 1258	80 – 110	248 – 681	43 – 320	386 – 1358	299 – 636	198 – 918	165	5.0	7 – 19	0 – 10
12	P	Humboldt	NPS	41.27	8.0	527	5	2020	405 – 859	69 – 86	198 – 340	27 – 97	251 – 510	99 – 261	368 – 748	229	4.4	10 – 20	3 – 12
13	P	Humboldt	NPS	41.22	7.6	79	8	2012–15	122 – 2342	84 – 116	172 – 632	28 – 240	371 – 1178	154 – 814	85 – 884	156	4.9	8 – 19	0 – 10
14	*S	Humboldt	P	40.96	5.5	106	5	2021	108 – 278	56 – 70	130 – 227	8 – 42	132 – 453	149 – 685	73 – 212	125	5.5	8 – 17	0 – 7
15	S	Humboldt	Arcata	40.87	7.5	117	8	2017	138 – 156	61 – 70	122 – 184	10 – 19	130 – 330	135 – 317	100 – 118	118	4.9	8 – 18	0 – 9
16	S	Humboldt	Arcata	40.87	9.1	296	5	2020	120 – 139	62 – 65	145 – 250	12 – 24	210 – 379	223 – 398	95 – 104	125	4.9	8 – 20	0 – 12
17	P	Humboldt	BLM	40.62	20.2	426	5	2020	532 – 1232	83 – 101	214 – 405	33 – 126	437 – 751	226 – 643	288 – 713	148	4.5	9 – 21	2 – 14
18	P	Humboldt	CSP	40.48	39.0	171	5	2019	601 – 1552	81 – 85	200 – 366	31 – 109	379 – 550	164 – 366	469 – 1287	127	3.9	8 – 19	1 – 11
19	P	Humboldt	CSP	40.38	29.0	654	5	2018	227 – 1094	69 – 90	213 – 504	28 – 127	374 – 759	347 – 524	181 – 647	192	3.3	8 – 22	2 – 16
20	P	Humboldt	CSP	40.33	29.5	59	7	2006–18	634 – 1261	93 – 113	266 – 598	60 – 250	463 – 1039	225 – 646	146 – 732	139	3.5	8 – 23	1 – 18
21	S	Humboldt	CSP	40.27	26.8	56	4	2017	101 – 169	65 – 76	128 – 182	11 – 20	162 – 268	224 – 436	67 – 126	133	3.3	8 – 23	0 – 17
22	P	Mendocino	UC	39.73	13.3	439	5	2019	442 – 689	74 – 88	218 – 272	30 – 64	336 – 603	101 – 215	346 – 570	192	2.8	7 – 22	1 – 17
23	*S	Mendocino	CSP	39.29	8.8	9	5	2017		78 – 82		17 – 30		221 – 277		109	2.9	8 – 21	0 – 11

(*continued on next page*)

Table 2 (*continued*)

Location	Type	County	Ownership	Latitude (°N)	Ocean (km)	Elevation (m)	Trees	Sampled	Age (yr)	Height (m)	*f*DBH (cm)	Biomass (Mg)	Leaves (kg)	Increment (kg yr^{-1})	History (yr)	Rain (cm yr^{-1})	JJAS rain (%)	Temp (°C)	VPD (hPa)
									152 – 302		155 – 261		215 – 437		132 – 234				
24	P	Mendocino	CSP	39.23	30.4	279	4	2015	506 – 1558	91 – 112	181 – 481	21 – 160	191 – 709	140 – 372	70 – 616	117	2.3	7 – 24	1 – 20
25	*S	Mendocino	CSP	39.16	12.8	29	5	2021	159 – 252	75 – 81	132 – 205	18 – 36	362 – 511	140 – 496	120 – 151	100	2.5	8 – 22	0 – 15
26	P	Mendocino	CSP	39.07	19.7	50	5	2020	421 – 921	88 – 106	225 – 293	31 – 78	339 – 495	287 – 453	284 – 619	92	2.2	9 – 26	1 – 24
27	P	Sonoma	P	38.63	6.1	223	5	2018	543 – 1643	73 – 98	212 – 672	38 – 163	347 – 517	228 – 337	158 – 603	134	2.1	9 – 22	1 – 15
28	P	Napa	LTNC	38.62	57.1	481	5	2016–20	241 – 783	46 – 62	115 – 220	9 – 33	167 – 268	50 – 156	190 – 542	103	2.2	10 – 25	4 – 24
29	S	Napa	CSP	38.54	48.6	280	5	2020	151 – 169	62 – 72	108 – 143	8 – 16	193 – 355	77 – 188	102 – 147	100	2.4	10 – 27	3 – 27
30	S	Sonoma	P	38.47	13.2	151	5	2019	121 – 127	67 – 71	110 – 129	7 – 9	168 – 295	100 – 163	104 – 111	130	2.1	9 – 24	1 – 19
31	P	Sonoma	P	38.46	12.2	141	6	2013–19	367 – 782	64 – 94	205 – 329	25 – 80	265 – 601	144 – 457	330 – 712	131	2.1	9 – 24	1 – 19
32	*S	Napa	LTNC	38.36	48.9	390	5	2018	145 – 238	67 – 70	130 – 184	10 – 19	250 – 381	71 – 180	112 – 149	106	2.2	10 – 24	3 – 22
33	P	Marin	MCP	38.02	12.6	134	5	2021	175 – 340	72 – 84	123 – 244	13 – 48	245 – 556	261 – 522	127 – 272	108	2.4	10 – 24	2 – 20
34	P	Marin	CSP	38.01	28.2	68	4	2014–16	371 – 755	72 – 91	152 – 381	11 – 58	146 – 411	105 – 424	233 – 548	104	2.9	9 – 24	1 – 18
35	S	Contra Costa	EBRPD	37.82	26.9	305	5	2018	147 – 153	63 – 65	129 – 197	10 – 19	162 – 300	125 – 180	108 – 134	71	3.0	10 – 21	2 – 15
36	*P	San Mateo	P	37.27	18.1	199	5	2020	130 – 608	63 – 85	120 – 223	8 – 39	164 – 403	82 – 291	110 – 507	83	2.4	9 – 26	1 – 23
37	P	San Mateo	CSP	37.23	9.6	359	5	2018	599 – 1388	102 – 108	322 – 487	76 – 135	407 – 669	164 – 509	401 – 1103	87	3.1	11 – 23	3 – 18
38	P	Santa Cruz	CSP	37.19	11.4	349	5	2012–14	457 – 843	75 – 100	248 – 342	38 – 71	324 – 584	170 – 340	99 – 341	100	2.7	11 – 24	3 – 20
39	*P	Santa Cruz	P	37.15	3.3	141	5	2019	100 – 528	62 – 72	136 – 242	9 – 32	133 – 499	53 – 178	88 – 414	83	3.2	9 – 21	1 – 13
40	S	Santa Cruz	CSP	37.05	9.6	284	5	2018	132 – 144	83 – 87	144 – 193	15 – 27	378 – 695	121 – 270	114 – 118	110	1.4	10 – 24	3 – 20
41	P	Monterey	P	36.46	7.3	466	6	2018–20	177 – 1286	68 – 93	153 – 474	17 – 149	157 – 815	73 – 274	148 – 822	77	1.1	9 – 23	3 – 19
42	P	Monterey	P	36.43	11.4	461	5	2019	153 – 740	65 – 74	110 – 454	7 – 83	103 – 470	26 – 188	124 – 432	79	1.0	9 – 24	3 – 21
43	P	Monterey	USFS	36.24	4.1	431	5	2021	220 – 830	65 – 77	139 – 213	15 – 43	164 – 445	30 – 98	137 – 709	114	1.0	9 – 24	3 – 22
44	P	Monterey	UC	36.09	2.0	148	4	2011–16	317 – 324	70 – 80	182 – 334	21 – 44	200 – 312	109 – 286	248 – 311	83	1.0	10 – 22	2 – 16
45	P	Monterey	USFS	35.86	2.4	346	5	2020	242 – 563	64 – 75	165 – 270	18 – 40	158 – 341	56 – 139	193 – 501	101	0.9	12 – 22	5 – 18

locations (2, 7, 36) lacking airborne LiDAR, no information on flow accumulations was obtained. One other topographically influenced variable pertaining to climate was computed: summer fog and low cloud cover (FLCC) indices were derived for study trees from analysis of Geostationary Operational Environmental Satellite data June-September 1999–2009 (Torregrosa et al. 2016). Raster layers were downloaded from the online data source (http://climate.calcommons.org/), loaded in QGIS (v 3.22.1), and reviewed to isolate values for individual trees. We used the diurnal, nocturnal, and total daily FLCC (h/d) for modeling. Note that these were 11-yr mean values per tree and not time series.

2.3. Tree measurements and core sampling

Trees were climbed using standard low-impact methods—no spikes—as in our previous studies. Main trunks were tape-measured for diameter at breast height (1.37 m), top of buttress (TB), and 5-m intervals into the crown, where measurement intervals decreased to < 2 m toward the treetop for accuracy. All heights were referenced to average ground level determined as the mean of highest and lowest points around the trunk perimeter where it entered the soil. Trunk bases received footprint analysis involving scaled photogrammetry or iPhone LiDAR (Tatsumi et al. 2022) to account for asymmetries such as buttressing, burls, and fire caves. All diameters from TB to ground level were converted to *functional* diameters (*f*D) based on cross-sectional analysis of 3D footprint models as previously described (Kramer et al. 2018, Sillett et al. 2019b). Reiterated trunks and limbs (if any) were measured for base and top heights, diameters, distances, and azimuths from reference trunk, and percent dead to construct 3D crown models for error-checking and to compute appendage volumes and areas as previously described (Sillett et al. 2015b, Kramer et al. 2018). Crowns were measured for depth (vertical distance from highest leaf to crown base) and radius (mean of 4–8 horizontal distances from crown edge to trunk center) to compute ellipsoid volume ($4/3 \times \pi \times \text{depth}/2 \times \text{radius}^2$).

Trunks were sampled with increment borers up to 99 cm long to obtain 5-mm-diameter core samples (series) for dendrochronology and to measure bark, sapwood, and heartwood radii. Pairs of cores were collected from trunks unless they exceeded 2 m or 3 m diameter in which case three or four samples were obtained, respectively. Samples were collected at BH, TB, and 10-m intervals from base to near treetop, where measurement intervals decreased as necessary to account for trunk reiteration and to permit dendrochronological reconstruction of top heights (see *2.5. Tree size and growth increments*). Samples were spaced around trunk circumference to avoid branch collars, burls, and other irregularities. No cores were collected from trunks ≤ 10 cm diameter, only shallow cores (< 25 cm) were collected at BH and TB to avoid seepage, and holes were plugged with bark after extraction. Additional pairs of short cores (~ 15 cm) were collected at three or more 10-m height intervals on most trees to quantify sapwood and heartwood densities. Excluding the sapwood-heartwood transition zone by ~ 1 cm on each side, paired samples separated most of the recent sapwood from 5 to 10 cm of heartwood per core. Sealed in airtight tubes immediately after extraction, samples were individually measured for fresh volume (via Archimedes method) and dry mass (101 °C for 48 h) to obtain dry-mass-to-fresh-volume ratios. The resulting values were used to model sapwood and heartwood densities (kg m^{-3}) as quadratic functions of height for conversion of trunk wood volumes to biomass (see *2.6. Tree size and growth increments*). The heartwood – sapwood density difference of paired samples was also used to estimate the amount of heartwood extractives (fungicide) deposited during conversion of sapwood to heartwood (see *2.7. Heartwood characteristics*).

2.4. Crossdating and ring indices

Assignment of calendar years to annual rings (crossdating) was accomplished by a combination of listing visual marker years and patterns (Yamaguchi 1991) and staggered correlation analysis on overlapping segments using COFECHA (Holmes 1983). Core samples were air-dried, glued to wooden mounts, sanded with progressively finer grit paper (>600), and digitally scanned at 1200 dpi. While viewing cores under a microscope to verify ring boundaries, rings were measured to 0.001 mm using WinDendro (v.2009b). Cores from each tree were crossdated first and then compared to other trees per location. Each ring was categorized based on crossdating confidence (Carroll et al. 2014). High confidence equated to absolute dating, while moderate confidence occurred when missing rings were placed in the most likely position, but a feasible alternative existed, or when multiple missing rings were placed in a region of very narrow rings. Undated rings were either 1) bound by dated rings so that radial growth over that interval was known or 2) unbound such that crossdating stopped before the innermost ring was dated. In the latter case, wood radius was measured farther toward the pith (trunk center) than crossdating extended, and ring count of the undated section was added to the number of crossdated and predicted rings to compute trunk age (see *2.5. Estimating tree age*).

Standardized ring-width chronologies (ring indices) were created for each location to facilitate estimation of tree ages and growth increments and to characterize inter-annual variation as a basis for dendroclimatic analyses (Table 3). For each tree, ring-width series ≥ 30 years with high crossdating confidence were detrended with a 32-year spline to remove low-frequency variation—including any geometric growth trends—and standardized around a dimensionless index of 1.0 via ARSTAN (Cook 1985, Grissino-Mayer 2001, Carroll et al. 2014). In addition to these standardized chronologies, we removed 1st order autocorrelation and generated residual chronologies per tree for comparison. Individual tree chronologies were then combined to generate standardized and residual ring indices for 45 locations with no further detrending applied in ARSTAN. We used the dplR package in R (Bunn 2008, R Core Team 2021) to report rbar and EPS statistics per ring index since 1901. Whereas rbar was the mean Pearson correlation (*r*) among series, EPS measured signal strength per chronology and depended on rbar and sample depth (Wigley et al. 1984, Briffa 1995). While some location chronologies exceeded 1000 yr, only ring indices since 1901 were utilized for dendroclimatic analyses, because reliable climate data were unavailable prior to the 20th century.

2.5. Estimating tree age

Because study trees were not core-sampled to pith at ground level—and even if they could be, many had hollow or decayed centers incapable of yielding annual rings—we estimated tree age by combining dendrochronology and measurements of wood radii at 10-m height intervals. This method was founded on the observation that *Sequoia* gains height at approximately linear rates when young, until gravitational constraints curtail treetop shoot elongation above ~60 m tall (Koch et al. 2004; Ishii et al. 2008; Ishii et al., 2014; Sillett et al. 2010, 2021). Thus, by knowing trunk age at 10-m height intervals, we predicted tree age—trunk age at ground level (0 m)—as the *y*-intercept of a linear relationship between height (*x*) and trunk age (*y*). This was easy when pith was reached at all heights because trunk ages were known. When pith was not reached at a given height on the trunk, ring widths to pith were estimated as power functions of wood radius using location-specific equations derived from crossdated portions of wood radii at that height (**Supplementary Table 2**). Predicted ring widths were subtracted from the remaining wood radius, and the total number of predicted rings required to reach the pith was added to the number of crossdated and undated rings to compute trunk age at that height. Prediction errors in tree age estimates were reported as one standard error of the *y*-intercept derived from linear regression of height (*x*) against trunk age (*y*). To be conservative, trunk age estimates at 50 or 60 m were excluded from regressions if curvilinearity was apparent, which was frequent in primary forests with maximum tree heights under 90 m.

Table 3
Summary of core sampling and tree-ring analysis in 45 study locations separated into primary (P) and secondary (S) forest types. Sampling 235 trees yields 5427 core series containing 1.186 million annual rings (radial increments) extending from year 328 to 2020, including 36.7 thousand missing rings. Annual rings are classified by crossdating confidence into high, moderate, undated, and unusable percentages. Undated rings are not crossdated, and unusable rings are lost or too decayed to measure. Standardized (STD) and residual (RES) ring indices, which utilize only annual rings since 1901 with high crossdating confidence and 4445 series containing at least 30 radial increments, are described by two statistics—rbar (mean Pearson correlation coefficient [*r*] among series) and EPS (expressed population signal). Locations are ranked by latitude from north (top) to south (bottom) within forest type.

	All rings sampled					Crossdating (% rings)				Ring index statistics (1901–2020)			
Location	Series	Rings	First	Last	Missing	High	Moderate	Undated	Unusable	STD rbar	RES rbar	STD EPS	RES EPS
Primary forests													
1	117	14,372	1699	2019	11	99.8	0.2	0.0	0.0	0.85	0.86	0.97	0.97
2	122	41,294	1057	2019	2058	71.8	8.0	20.0	0.1	0.71	0.71	0.93	0.93
3	152	37,132	1501	2018	1222	94.0	1.9	3.9	0.1	0.79	0.76	0.95	0.94
5	169	54,398	1109	2017	3433	67.0	4.0	29.0	0.0	0.60	0.59	0.90	0.89
6	130	64,055	988	2019	4253	77.4	5.9	16.6	0.1	0.55	0.50	0.85	0.82
7	108	18,213	1602	2018	6	99.7	0.0	0.0	0.3	0.53	0.56	0.85	0.86
9	202	57,832	1091	2018	2250	87.5	4.5	8.0	0.1	0.69	0.68	0.93	0.93
10	154	52,788	1018	2018	2591	83.5	3.7	12.7	0.1	0.56	0.54	0.86	0.86
11	136	48,923	1049	2015	3192	65.5	7.4	26.7	0.4	0.58	0.53	0.87	0.85
12	128	37,433	1240	2019	517	92.7	2.0	5.0	0.3	0.71	0.74	0.93	0.94
13	165	65,156	328	2014	4201	72.9	6.6	20.3	0.1	0.42	0.36	0.85	0.81
17	144	47,262	1226	2019	1133	92.5	1.1	6.4	0.1	0.55	0.57	0.86	0.87
18	131	51,910	668	2018	2740	64.6	2.3	33.0	0.1	0.57	0.55	0.87	0.86
19	131	35,805	1333	2017	190	98.8	0.4	0.1	0.7	0.65	0.64	0.90	0.90
20	165	35,387	1266	2017	1377	77.3	2.9	18.7	1.1	0.44	0.46	0.83	0.85
22	123	33,808	1406	2018	258	98.3	0.9	0.5	0.2	0.74	0.72	0.94	0.93
24	97	27,012	822	2014	649	79.9	4.3	12.9	2.8	0.53	0.53	0.82	0.82
26	146	35,579	1402	2019	271	93.5	1.4	4.9	0.1	0.73	0.70	0.93	0.92
27	123	32,062	1206	2017	237	85.6	1.0	13.2	0.2	0.55	0.61	0.86	0.89
28	72	17,673	1507	2019	99	87.3	5.5	6.8	0.4	0.59	0.55	0.88	0.86
31	143	38,307	1289	2018	405	93.5	2.0	3.8	0.7	0.57	0.58	0.89	0.89
33	121	11,473	1740	2020	58	95.6	0.8	3.7	0.0	0.65	0.64	0.90	0.90
34	102	17,809	1422	2015	185	93.6	1.9	4.5	0.0	0.52	0.55	0.81	0.83
36	117	18,368	1495	2019	88	97.9	0.2	1.8	0.2	0.54	0.52	0.85	0.84
37	155	64,381	705	2017	3300	65.9	5.6	27.9	0.6	0.55	0.51	0.86	0.84
38	95	16,922	1415	2014	191	91.0	2.7	6.3	0.0	0.48	0.46	0.82	0.81
39	102	17,060	1596	2018	255	88.7	3.2	7.6	0.6	0.48	0.53	0.81	0.84
41	143	34,202	1156	2019	240	96.6	1.1	1.3	1.0	0.53	0.59	0.87	0.90
42	102	20,430	1418	2018	416	83.6	4.0	12.5	0.0	0.61	0.60	0.89	0.88
43	107	25,536	1297	2020	200	95.8	0.9	2.3	1.0	0.58	0.55	0.88	0.86
44	87	11,161	1706	2015	121	97.6	0.8	1.5	0.0	0.72	0.69	0.91	0.90
45	106	21,730	1508	2019	456	89.0	2.6	8.3	0.0	0.59	0.60	0.88	0.88
Secondary forests													
4	78	4231	1899	2016	0	99.6	0.0	0.0	0.4	0.58	0.57	0.84	0.83
8	140	5495	1931	2016	1	98.3	0.0	1.6	0.1	0.58	0.60	0.91	0.91
14	106	6137	1795	2020	46	99.2	0.8	0.0	0.0	0.35	0.40	0.70	0.74
15	144	8945	1887	2016	18	98.4	0.3	0.7	0.5	0.45	0.49	0.87	0.88
16	93	4871	1906	2019	3	99.8	0.2	0.0	0.0	0.53	0.53	0.84	0.84
21	74	3503	1879	2016	0	97.1	2.9	0.0	0.0	0.39	0.41	0.67	0.69
23	107	8286	1743	2016	4	99.3	0.7	0.0	0.0	0.57	0.51	0.87	0.81
25	125	8566	1883	2020	4	95.5	2.5	1.7	0.3	0.43	0.45	0.79	0.81
29	104	6874	1867	2019	1	99.9	0.0	0.0	0.1	0.49	0.51	0.83	0.84
30	91	5278	1906	2018	2	99.6	0.3	0.0	0.0	0.48	0.47	0.82	0.81
32	87	6697	1808	2017	1	99.3	0.1	0.0	0.6	0.44	0.42	0.80	0.78
35	83	5718	1884	2017	0	99.8	0.0	0.0	0.2	0.66	0.62	0.91	0.89
40	100	6669	1888	2017	0	100.0	0.0	0.0	0.0	0.63	0.62	0.89	0.89

Confirmed tree age was computed as the number of crossdated (plus undated) years accessed by core sampling divided by estimated tree age.

2.6. Tree size and growth increments

Measurements obtained from the ground and by virtue of climbing and core-sampling yielded key size predictors for 235 trees, allowing accurate estimation of total aboveground volume and biomass (separately for bark, sapwood, heartwood) as well as leaf quantities (mass, projected area, number). In primary forests, these metrics included main trunk masses and volumes (total, bark, sapwood, heartwood), main trunk areas (bark, cambium, heartwood deposition), reiterated trunk and limb volume and area, crown volume, and sapwood cross sectional area at top of buttress (SA_{TB}, Sillett et al. 2020). In secondary forests, these metrics included crown volume as well as main trunk total mass, wood mass, total volume, bark volume, sapwood volume, heartwood volume, cambium area, and heartwood deposition area (Sillett et al. 2019a, 2021). Sapwood and heartwood densities per tree were predicted as quadratic functions of height above ground using separate equations for primary and secondary forests. In trees also sampled for wood density, prediction of trunk masses was adjusted via scaling relationships between observed and height-predicted wood densities, improving allometric estimates for trees with unusually low- or high-density wood.

Time series of tree size were reconstructed from current measurements via dendrochronology using only rings with high or moderate crossdating confidence. At each measurement height, annual rings of replicate samples were averaged and extended as far back in time as possible using local relationships between multi-core averages when only single cores remained. Wood radius at measurement height was computed by subtracting adjusted bark radius from total radius, where bark radius was first predicted from diameter and height using separate equations for primary and secondary forests (Sillett et al., 2015, 2019a)

and then adjusted by scaling relationships between observed and predicted radii. A similar procedure was applied to sapwood and heartwood radii to accommodate tree-to-tree variability—some trees had unusually thin or thick bark or sapwood. Measured rings were scaled to fresh widths using the ratio of freshly extracted and mounted core lengths (± 1 mm) per location. The sum of measured ring widths from cambium to pith (if reached) was forced to equal wood radius. Wood radii were decremented by annual rings across the trunk height gradient with rings at intervening heights of measurement (no crossdated core samples) computed by interpolation. Above the highest core samples per tree, rings were assumed equivalent, and live top heights were decremented in proportion to ring width, allowing top heights to be reconstructed back through time by pith position (e.g., if core reaches pith at 60 m, tree exceeded 60 m tall that year). Below the lowest core samples per tree, ring widths at measurement heights to ground level were computed as averages of two quantities: 1) ring width of the lowest samples and 2) the ring-width-to-wood-radius ratio of the lowest samples multiplied by wood radius at measurement height. This accounted for buttress formation in the lower trunk, maintaining a consistent rate of taper change and allowing buttressing to diminish gradually. By sequentially subtracting ring widths from all wood radii, we used conic equations to compute main trunk wood volume and cambium area at annual increments as far back as crossdating allowed and terminating when no samples remained at 10 m. The resulting time series of trunk wood volume increment (WVI, $m^3\ yr^{-1}$) were used to predict biomass increments (kg yr^{-1}) via separate multipliers for trees in primary (WVI × 538, Sillett et al. 2020) and secondary (WVI × 431, Sillett et al. 2018a) forests. Ultimately, we reconstructed 77.7 thousand years of sizes (height, wood volume, cambium, biomass) to quantify growth histories of 235 trees (Table 2). These time series were cross-referenced to identify calendar years when trees first reached 60 m tall for recording age, biomass, biomass increment (centered 5-yr mean), and height increment (centered 5-yr mean). Excluding trees < 60 m tall, with trunks too small to core at 60 m, or with long-dead and broken tops, we quantified 60-m-height thresholds for 169 trees in primary (108) and secondary (61) forests.

In addition to reconstructing tree size, we generated times series of several growth increments for modeling. Specific volume increment (SVI) was the trunk-averaged radial increment (mm yr^{-1}) calculated as WVI divided by the average of current and previous year cambium area. Residual wood volume increment (RWVI) was the amount of wood produced relative to a null hypothesis of uniform growing conditions over a fixed interval. As described in previous studies (Sillett et al., 2015b, 2018b, 2019b, 2020), RWVI was computed as observed minus expected WVI, where cambium expanded at the mean annual rate, and expected WVI was proportional to trunk size (cambium area). Since RWVI and WVI had identical units ($m^3\ yr^{-1}$) and were derived from a common source, RWVI was converted to residual biomass increment (kg yr^{-1}, hereafter residual increment) via the same multipliers used to convert WVI to biomass increment in primary (538) and secondary (431) forests. We generated residual increment time series for one fixed interval per tree—all complete years since 1901. Growth efficiency (kg $kg^{-1}\ yr^{-1}$) was computed as biomass increment divided by leaf mass. Each tree's current leaf mass was predicted allometrically using separate equations for primary and secondary forests (Sillett et al. 2019a, 2020). Time series of leaf mass needed for computation of growth efficiency were obtained by a 3-step algorithm utilizing the linear relationship between leaf quantities and trunk sapwood cross-sectional area. First, each tree's measured trunk heartwood radii (base to top) were regressed against corresponding wood radii, and the best linear or quadratic equation ($R^2 \geq 0.99$) was used to predict heartwood radii from measured wood radii at all heights back to 1998. Second, SA_{TB} (cm^2) was computed in annual increments back to 1998, and a correction factor was computed per year as the ratio of current SA_{TB} divided by each year's allometrically predicted SA_{TB} such that correction factor for current year = 1. Third, leaf mass back to 1998 was computed as current leaf mass multiplied by the correction factor. We computed growth efficiency (GE) back to 1999 as the ratio of each year's biomass increment (BI) to the average of current and previous year predicted leaf mass (e.g., 1999 GE = 1999 BI ÷ 1998–1999 average leaf mass).

2.7. Heartwood characteristics

Each tree's current trunk heartwood volume was computed from measured and predicted heartwood radii at ≤ 5 m height intervals from ground level to treetop via the conic equation. Heartwood volume per trunk frustum was converted to mass using the height-predicted density as previously described. We used time series of tree age and trunk wood volume to predict the heartwood proportion of aboveground biomass back to 1900 (Table 4). Preliminary time series of heartwood mass were computed as the product of biomass and the predicted heartwood proportion of biomass, and we used each tree's current measured-to-predicted-heartwood-mass ratio as a scalar to adjust time series such that current measured and predicted heartwood mass were equivalent. We quantified heartwood investment as trees enlarged with age by expressing the resulting heartwood mass increments (to 1901) as proportions of biomass increments for 120 trees in three age classes (120–180 yr in secondary forests, 480–750 yr and 750–2100 yr in primary forests) such that each age class had constant sample size ($N = 40$ trees, 1918–2016 for secondary forests, 1901–2006 for primary forests).

The fungicide content of *Sequoia* trunks was quantified via a 4-step algorithm involving separate equations for primary and secondary forests in regions defined by latitude (> 40°, 37-40°, < 37°). First, volume of each trunk heartwood frustum (to 1998) was converted to mass using the appropriate height-predicted heartwood density (Table 4). Second, heartwood mass per frustum was converted to fungicide mass using the appropriate height-predicted fungicide proportion (Table 4). The latter equations were based on density differences between 727 pairs of heartwood and sapwood samples collected at 10-m height intervals from 121 trees in primary forests and 51 trees in secondary forests. Third, summing all trunk heartwood frusta measured per tree yielded time series of trunk heartwood mass (to 1998) and trunk heartwood mass increment (to 1999). Finally, heartwood deposition area per frustum was used to compute the weighted-average fungicide proportion of heartwood mass per trunk, and fungicide increment (to 1999) was computed as the product of heartwood mass increment and the weighted-average fungicide proportion per trunk for 235 trees.

2.8. Analysis of tree growth trends

We used a moving-window correlation analysis to examine temporal trends in radial and wood volume increments—SVI and WVI. Pearson correlations (r) between growth increments and year were evaluated using 21-yr moving windows (1-yr offset) centered on year of measurement, truncated to 11-yr at beginning (first year + following decade) and end (last year + preceding decade) per series. We considered positive (increasing) and negative (decreasing) growth trends statistically significant at $P < 0.01$. Time series stopped when number of trees dropped below three per location.

2.9. Dendroclimatic analyses

Our source of climatic information was 800-m resolution monthly data on precipitation (rain), minimum temperature (T_{min}), maximum temperature (T_{max}), minimum vapor pressure deficit (V_{min}), and maximum vapor pressure deficit (V_{max}) available for 235 individual tree locations from 1900 to 2020 (LT81 model, PRISM Climate Group 2020). Climatic variables were summarized for 45 locations by averaging tree-level values (Table 2). We combined monthly rain, T_{min}, and T_{max} to compute the standardized precipitation evapotranspiration index (hereafter SPEI) via the spei package in R (R Core Team 2021). SPEI calculations employed the Hargreaves equation to model

Table 4
Summary of equations for estimating *Sequoia* heartwood characteristics in primary and secondary forests at different latitudes. Dependent variables are heartwood proportion of aboveground biomass, sapwood (SW) density, heartwood (HW) density, and fungicide percent of heartwood mass (see Fig. 9**a**). Predictors (V1, V2) are listed from left to right in descending order of importance (trunk wood volume, tree age, height above ground level) followed by regression coefficients (*a*-*e*), sample size (*N*), goodness of fit (R^2), root mean square error (RMSE), average of dependent variable (mean), coefficient of variation (CV) computed as RMSE ÷ mean, and form of equation. Samples are trees ($N = 235$) or 10-m height interval averages ($N = 6$–10) based on paired samples from primary forests north of 40° (70 trees, 255 pairs), primary forests between 37 and 40° (28 trees, 136 pairs), primary forests south of 37° (23 trees, 109 pairs), secondary forests north of 40° (26 trees, 98 pairs), and secondary forests between 37 and 40° (25 trees, 129 pairs).

Forest type	Latitude	Dependent variable	V1	V2	*a*	*b*	*c*	*d*	*e*	*N*	R^2	RMSE	Mean	CV	Form
Both	All	Heartwood (% biomass)	Wood volume (m^3)	Age (yr)	2.78E + 01	1.26E-01	8.42E + 00	1.47E-01	−4.75E + 00	235	0.796	4.18E + 00	6.39E + 01	7 %	$aV1^b + cV2^d + e$
Primary	> 40°	SW density (kg m^{-3})	Height (m)	—	3.17E-02	−2.66E + 00	3.47E + 02	—	—	10	0.941	9.30E + 00	3.23E + 02	3 %	$aV1^2 + bV1 + c$
Primary	> 40°	HW density (kg m^{-3})	Height (m)	—	4.45E-02	−3.00E + 00	3.76E + 02	—	—	10	0.958	1.48E + 01	3.82E + 02	4 %	$aV1^2 + bV1 + c$
Primary	> 40°	Fungicide (% heartwood mass)	Height (m)	—	5.09E-02	1.27E + 00	5.82E + 00	—	—	10	0.949	1.42E + 00	1.46E + 01	10 %	$aV1^b + c$
Primary	37 to 40°	SW density (kg m^{-3})	Height (m)	—	1.73E-02	−1.89E + 00	3.70E + 02	—	—	9	0.737	7.41E + 00	3.31E + 02	2 %	$aV1^2 + bV1 + c$
Primary	37 to 40°	HW density (kg m^{-3})	Height (m)	—	1.86E-02	−1.26E + 00	3.77E + 02	—	—	9	0.750	1.23E + 01	3.73E + 02	3 %	$aV1^2 + bV1 + c$
Primary	37 to 40°	Fungicide (% heartwood mass)	Height (m)	—	3.58E-01	8.58E-01	9.43E-01	—	—	9	0.944	1.28E + 00	1.10E + 01	12 %	$aV1^b + c$
Primary	< 37°	SW density (kg m^{-3})	Height (m)	—	2.49E-02	−2.48E + 00	4.19E + 02	—	—	7	0.775	8.35E + 00	3.69E + 02	2 %	$aV1^2 + bV1 + c$
Primary	< 37°	HW density (kg m^{-3})	Height (m)	—	6.11E-02	−3.82E + 00	4.54E + 02	—	—	7	0.919	1.06E + 01	4.23E + 02	2 %	$aV1^2 + bV1 + c$
Primary	< 37°	Fungicide (% heartwood mass)	Height (m)	—	2.89E-02	1.19E + 00	—	—	—	7	0.942	1.96E + 00	1.24E + 01	16 %	$\exp(aV1 + b)$
Secondary	> 40°	SW density (kg m^{-3})	Height (m)	—	4.12E-02	−2.63E + 00	3.29E + 02	—	—	6	0.886	4.92E + 00	3.00E + 02	2 %	$aV1^2 + bV1 + c$
Secondary	> 40°	HW density (kg m^{-3})	Height (m)	—	7.98E-02	−4.08E + 00	3.45E + 02	—	—	6	0.985	4.90E + 00	3.23E + 02	2 %	$aV1^2 + bV1 + c$
Secondary	> 40°	Fungicide (% heartwood mass)	Height (m)	—	5.60E-02	−4.77E-01	—	—	—	6	0.970	1.29E + 00	6.57E + 00	20 %	$\exp(aV1 + b)$
Secondary	37 to 40°	SW density (kg m^{-3})	Height (m)	—	2.55E-02	−2.85E + 00	3.97E + 02	—	—	7	0.948	5.12E + 00	3.33E + 02	2 %	$aV1^2 + bV1 + c$
Secondary	37 to 40°	HW density (kg m^{-3})	Height (m)	—	5.25E-02	−3.90E + 00	4.18E + 02	—	—	7	0.988	2.45E + 00	3.67E + 02	1 %	$aV1^2 + bV1 + c$
Secondary	37 to 40°	Fungicide (% heartwood mass)	Height (m)	—	3.72E-02	4.19E-01	—	—	—	7	0.984	9.06E-01	8.85E + 00	10 %	$\exp(aV1 + b)$

evapotranspiration as a function of T_{min}, T_{max}, and latitude (Beguería et al. 2014), considered monthly water balance over a 12-month window (1 + preceding 11), and were standardized with respect to a 20th century reference period (1901–2000). Unlike rain and SPEI, temperature and vapor pressure deficit time series were strongly trended, so these variables were detrended using a 32-yr spline prior to dendroclimatic analysis.

We identified climatic predictors of interannual growth variation by applying bootstrapped Pearson's correlation and response function analysis (RFA) to ring indices and monthly climatic variables via the treeclim package in R (Zang & Biondi 2015, R Core Team 2021). Prior to assessing dendroclimatic relationships, RFA removed multicollinearity (if any) between months. Preliminary analyses investigated a full array of input variables to verify consistency of relationships. Standardized and residual chronologies were run with six sets of monthly climate variables (rain, SPEI, T_{min}, T_{max}, V_{min}, V_{max}) using both standard and stationary bootstrapping. These analyses considered each year's previous and current growing seasons across a 20-month window—previous March to current October. Final selection of analyses and input variables eliminated redundancy and focused on the strongest signals. Ultimately, standardized ring indices were used with stationary bootstrapping (1000 iterations) to account for temporal autocorrelation (Zang & Biondi 2015) and to identify key climatic predictors. We also used the treeclim package in R to assess the temporal stability of dendroclimatic relationships across 45 locations by examining Pearson's correlations (r) on 30-year moving windows (1-yr offset) starting in 1901 using standard bootstrapping due to window length.

For quantifying growth responses to tree-level, topographic, and

climatic predictors, we preferred nonparametric multiplicative regression (NPMR) via the statistical package HyperNiche (v2.30, MjM Software Design), because this method considers any response shape while automatically and parsimoniously modeling complex interactions among predictors (McCune 2011). Response variables included two growth metrics (biomass increment, growth efficiency) as well as trends (τ) between climatic variables and two growth metrics (ring index, biomass increment). Here we preferred Kendall's rank coefficient (τ)—generated with the Real Statistics Resource Pack (real-statistics.com) for Excel (v16.56, Microsoft Inc.)—to examine trends, because it does not assume linearity and is less susceptible to outliers than Pearson *r* coefficient. Predictors included tree attributes (leaf mass, age, heartwood proportion of biomass increment, fungicide proportion of heartwood increment), topographic variables (latitude, elevation, distance to ocean, vertical and horizontal distances to streams, slope steepness, heat load index, FLCC), and monthly climatic variables. NPMR models used a local multiplicative kernel smoothing function and leave-one-out cross validation to estimate response variables. Local linear quantitative model form was deployed in forward stepwise regressions of individual responses against all sets of predictors. Minimum data-to-predictor ratio was set to 40. Minimum average neighborhood size was set to 20 % of sample size ($N = 45$ locations or 235 trees) for multi-decadal models (1901–1960, 1961–2020) and 10 % of sample size ($N = 235$ trees) for annual models (1999–2020). Model fit was expressed as a cross-validated correlation—xR^2—differing from traditional R^2 in that each datum was excluded from the basis for estimating the response at that point (McCune & Mefford 2009). Predictors of growth responses were ignored unless they contributed at least 5 % of model xR^2.

We isolated effects of extreme drought by ranking individual years according to SPEI (March to October mean). After splitting 1901–2020 time series into two 60-yr series, the three highest and three lowest annual values per tree were used to compute 3-yr average maximum and minimum biomass increments, respectively. Each tree's maximum and minimum biomass increments were then divided by its 1901–1960 or 1961–2020 mean biomass increment to compute its wettest and driest relative increments, which were modeled as functions of latitude using NPMR.

2.10. Effects of hotter drought

We assessed the relationship between *Sequoia* growth efficiency and 21st century drought with mixed-effects analysis of covariance (ANCOVA). Tree data were split into groups on the basis of forest type (1° = primary, 2° = secondary) and latitude (N = northern > 40°, C = central 37-40°, S = southern < 37°). No study locations in secondary forests occurred south of 37°, so comparisons between forest types were only made across northern and central latitudes. Both locations and trees within locations were included as random effects on model intercepts to account for repeated measurements over the course of our reference period and use of 4–8 trees per location. Focusing on the hotter drought event of 2012–2015, we coded these years consecutively as 1–4 and bounding non-drought years 2011, 2016, and 2017 as 0. The years 2011, 2016, and 2017 were coded as non-drought because March to October mean SPEI averaged 0.8, 0.4, and 1.7 (range 0.4 to 1.4, −0.3 to 0.8, 1.4 to 2.2), whereas 2012 to 2015 were coded as drought because March to October mean SPEI averaged −0.3, −0.6, −1.6, and −0.8 (range −0.9 to 0.3, −1.3 to −0.3, −2.1 to −1.3, −1.3 to −0.5), respectively. This sequential 0–4 representation of the non-drought, drought, and non-drought sequence was included in all models as the continuous fixed effect *consecutive drought years*. Models included categorical variables for forest type (1° / 2°) or latitude (N / C or N / C / S) as fixed effects and assessed the interaction of these variables with consecutive drought years to determine their influence on the growth efficiency response to drought.

We complemented analyses of consecutive drought years with an assessment of growth efficiency recovery from drought. Here we coded recovery as 0–2 with drought year 2015 = 0 and post-drought years 2016 = 1 and 2017 = 2. The mixed-effects ANCOVA models described above were repeated with *post-drought recovery* used as the continuous fixed effect. All models were fit with restricted maximum likelihood (REML) estimators and used the Satterthwaite approximation to estimate degrees of freedom and *P*-values. Models were implemented using the packages lme4 and LmerTest in R 4.1.1 (R Core Team 2021). Because ANCOVA degrees of freedom and *P*-values were approximated, we only considered *F* tests to be significant at the $\alpha = 0.01$ level, relying on size of the *F* statistic to interpret model quality as well as strength of observed effects and avoiding use of the term "significant" when reporting results (Bates et al. 2015, 2018). We evaluated impacts of fixed effects on slopes of GE responses to both consecutive drought years and post-drought recovery by comparing interaction trends with the lstrends() function in the R package emmeans.

2.11. Plot measurements and time series

In addition to climbing and measuring study trees in 45 locations, we quantified dominant and codominant neighboring trees plus other vegetation in fixed-area plots at 41 locations (Table 5). No plots were established in four secondary forest locations (4, 8, 15, 21) that were part of an experiment (Sillett et al. 2018a). Plots at eight locations (5, 11, 13, 20, 24, 34, 38, 44) included complete vegetation inventories made at 5-yr intervals (Sillett et al. 2020) with pairs of 1-ha plots combined at three locations (5, 11, 13). Plots at 33 locations were aggregations of 20-m-radius circular plots centered on each study tree with plot size accounting for overlapping areas where study trees stood < 20 m apart. From atop each study tree, all visible treetops within 20 m horizontal distance were identified by species and measured for azimuth and height above ground using compass and laser rangefinder. Trees were located on the ground and measured for trunk diameter and crown volume to estimate aboveground biomass and leaf mass via published allometric equations per species (Van Pelt et al. 2016; Kramer et al. 2018; Sillett et al. 2018b, 2019a, 2020, 2021). Average ground level at the base of each neighboring tree was compared to that of its focal tree to adjust height (and computed crown volume) accordingly. All species of vascular plants occurring per plot were recorded to quantify species richness, and special effort was made to identify all vascular plants occurring as epiphytes in the crowns of study trees.

We generated time series of per-hectare quantities of leaves, heartwood, fungicide, and other biomass (to 1998) as well as growth increments (to 1999) for all dominant and codominant *Sequoia* trees per plot. Heartwood mass of a neighboring tree was predicted using separate allometric equations for primary and secondary forests (Sillett et al. 2019a, 2020). Fungicide mass of a neighboring tree was estimated by multiplying its predicted heartwood mass by the average fungicide proportion of heartwood mass among study trees per location. Biomass increment and heartwood increment of a neighboring tree—measured only for trunk diameter and crown volume—were estimated by multiplying its allometrically predicted leaf mass (kg) by growth efficiency (kg kg^{-1} yr^{-1}) and the heartwood-increment-to-leaf-mass ratio (kg kg^{-1} yr^{-1}) of combined study trees per location, respectively. Prior to computing growth efficiencies per location, leaf masses of neighboring trees were adjusted by average correction factors derived from allometrically predicted changes in SA_{TB} of study trees (see *2.6. Tree size and growth increments*). Fungicide increment of a neighboring tree was estimated by multiplying its heartwood increment by the average fungicide proportion of heartwood mass increment among study trees per location. Biomass increments and residual increments of 4–8 study trees per location were calculated as multiples of main trunk wood volume increment (WVI) and residual wood volume increment (RWVI), respectively. Subtracting biomass and residual increments yielded expected biomass increment per study tree under a null hypothesis of uniform growing conditions since 1901 (see *2.6. Tree size and growth increments*). Expected biomass increment of a neighboring tree was

Table 5
Summary of fixed-area plots used to measure study trees, codominant neighboring trees, and other vegetation in 41 locations separated into primary (P) and secondary (S) forest types. For dominant and codominant *Sequoia*, stand density (trees ha^{-1}), aboveground biomass (Mg ha^{-1}), leaves (Mg ha^{-1}), and biomass increment (Mg ha^{-1} yr^{-1}) are listed. Biomass and leaf mass are best estimates at most recent measurement. Biomass increment is 21st century mean. For eight locations with complete vegetation inventories and 5-yr remeasurements, percentages are proportions of total plot quantities attributable to dominant and codominant *Sequoia*. For codominant neighboring trees of other species (PSME = *Pseudotsuga menziesii*, CHLA = *Chamaecyparis lawsoniana*, PISI = *Picea sitchensis*, TSHE = *Tsuga heterophylla*, NODE = *Notholithocarpus densiflorus*), if any, stand density and aboveground biomass are given on right. Locations are ranked by latitude from north (top) to south (bottom) within forest type.

				Dominant and codominant *Sequoia*						Neighbors (non-*Sequoia*)			
Location	Type	Latitude	Plot size (ha)	Trees ha^{-1}	Biomass (Mg ha^{-1})		Leaves (Mg ha^{-1})		Increment (Mg ha^{-1} yr^{-1})	Species	Trees ha^{-1}	Biomass (Mg ha^{-1})	Leaves (Mg ha^{-1})
Primary forests													
1	P	42.12	0.52	29	655	—	8.3	—	5.3	—	PM	6	87	0.7
2	P	42.08	0.53	32	843	—	7.4	—	2.6	—	PM	19	210	2.8
3	P	42.02	0.55	24	1345	—	10.8	—	5.4	—	PM	2	43	0.3
5	P	41.78	2.00	29	3195	86 %	15.9	60 %	8.2	70 %	—	—	—	—
6	P	41.75	0.50	30	1578	—	10.0	—	7.1	—	—	—	—	—
7	P	41.71	0.59	10	238	—	3.0	—	1.5	—	PM	22	260	3.0
9	P	41.66	0.70	33	2230	—	15.1	—	13.3	—	—	—	—	—
10	P	41.58	0.63	24	1839	—	11.3	—	6.7	—	PS, PM, TH	6	90	1.8
11	P	41.37	2.00	31	2611	79 %	15.2	58 %	7.3	64 %	PM	2	43	0.3
12	P	41.27	0.57	32	1170	—	9.5	—	4.6	—	PM	7	143	1.5
13	P	41.22	2.00	27	2014	62 %	12.8	44 %	9.4	49 %	PM	2	44	0.5
17	P	40.62	0.58	26	1103	—	8.7	—	6.8	—	PM	7	123	1.0
18	P	40.48	0.43	28	1024	—	9.5	—	5.1	—	—	—	—	—
19	P	40.38	0.58	26	1334	—	11.7	—	7.6	—	ND, PM	9	228	1.7
20	P	40.33	1.00	43	3240	83 %	21.5	71 %	17.1	71 %	—	—	—	—
22	P	39.73	0.63	11	472	—	4.8	—	1.9	—	—	—	—	—
24	P	39.23	1.00	43	2838	83 %	18.7	66 %	9.0	69 %	—	—	—	—
26	P	39.07	0.51	29	1569	—	11.9	—	10.1	—	—	—	—	—
27	P	38.63	0.63	27	989	—	8.4	—	5.7	—	PM	10	161	1.9
28	P	38.62	0.58	21	345	—	4.1	—	1.9	—	PM	2	33	0.4
31	P	38.46	0.58	19	635	—	6.1	—	4.1	—	PM	9	132	1.9
33	P	38.02	0.46	30	838	—	9.4	—	8.4	—	—	—	—	—
34	P	38.01	1.00	46	1202	83 %	11.5	65 %	10.3	79 %	PM	4	58	0.5
36	P	37.27	0.63	45	847	—	9.5	—	6.5	—	PM	2	16	0.2
37	P	37.23	0.56	27	2047	—	15.3	—	10.0	—	—	—	—	—
38	P	37.19	1.00	30	1318	63 %	9.4	45 %	5.9	41 %	PM	10	243	2.2
39	P	37.15	0.52	36	450	—	7.0	—	4.0	—	PM	8	71	1.6
41	P	36.46	0.55	40	1336	—	10.9	—	6.8	—	—	—	—	—
42	P	36.43	0.43	63	1225	—	11.7	—	5.1	—	—	—	—	—
43	P	36.24	0.45	45	759	—	9.5	—	3.1	—	—	—	—	—
44	P	36.09	1.00	37	787	49 %	7.1	38 %	4.3	28 %	—	—	—	—
45	P	35.86	0.48	36	632	—	6.4	—	2.9	—	—	—	—	—
Secondary forests													
14	S	40.96	0.50	36	314	—	5.9	—	6.7	—	PS, PM	14	91	2.5
16	S	40.87	0.60	57	565	—	11.4	—	12.4	—	PS, PM	3	14	2.5
23	S	39.29	0.57	58	818	—	15.9	—	10.3	—	—	—	—	—
25	S	39.16	0.48	70	872	—	17.8	—	9.5	—	PM	2	32	0.4
29	S	38.54	0.50	57	499	—	10.1	—	4.6	—	PM	2	24	2.1
30	S	38.47	0.54	59	369	—	7.3	—	3.9	—	PM	6	65	2.2
32	S	38.36	0.63	32	302	—	6.6	—	2.9	—	PM	19	212	3.4
35	S	37.82	0.63	72	452	—	9.2	—	5.6	—	—	—	—	—
40	S	37.05	0.50	75	901	—	21.7	—	8.4	—	—	—	—	—

computed by multiplying its estimated leaf mass by the average expected-biomass-increment-to-leaf-mass ratio among study trees per location. Finally, plot residual increments were computed as the difference between observed and expected biomass increments (Mg ha^{-1} yr^{-1}).

3. Results

3.1. Crossdating

Among 235 study trees in 45 locations, we sampled 1.187 million annual rings, including 37 thousand with undetectable widths (missing rings), and were able to crossdate 1.003 million (84 %) with high confidence and 38 thousand (3 %) with moderate confidence (Table 3). Crossdating was generally less successful in primary forests (89.6 ± 1.7

% rings) than secondary forests (99.5 ± 0.2 % rings, mean ± 1 S_E) with six primary forests having < 80 % of rings crossdated. Of the 146 thousand remaining rings, 97 % were usable for scaling radial growth via interpolation from nearby crossdated rings or computing tree age even though they were undated. On average, standardized and residual ring indices exhibited identical correlations among series (rbar 0.57 ± 0.02) and signal strength (EPS 0.86 ± 0.01, mean ± 1 S_E). For standardized ring indices, rbar and EPS were generally higher in primary than secondary forests (rbar 0.60 ± 0.02 vs. 0.50 ± 0.03, EPS 0.88 ± 0.01 vs. 0.82 ± 0.02).

Crossdating yielded sufficient rings for accurately estimating tree ages and reconstructing growth histories. Among 164 new trees measured since 2017, the confirmed portion of tree age averaged 84 %, and 59.1 thousand years of growth history were reconstructed (primary forests = 451 ± 27 yr tree^{-1}, secondary forests = 121 ± 4 yr tree^{-1}, mean ± 1 S_E). Among 71 trees measured previously, the confirmed portion of tree age averaged 73 %, and 18.5 thousand years of growth history were reconstructed (primary forests = 347 ± 26 yr tree^{-1}, secondary forests = 92 ± 1 yr tree^{-1}, mean ± 1 S_E). Smaller time series from previous work were attributable to shallower cores and less intensive sampling along the height gradient than in this study. Overall, one standard error (S_E) of tree age estimates averaged 3 % of the estimate, ranging from 0 to 16 % with the greatest uncertainty occurring in a 1643 ± 269-yr-old tree (location 27) possessing a massive fire cave and extensive heartwood decay extending to a height of 59 m. Tree ages were 100–2342 yr in primary forests (mean 671 yr) and 96–181 yr (mean 139 yr) in secondary forests with growth histories up to 1287 yr in primary forests and up to 147 yr in secondary forests, excluding five obvious veterans (122–302 yr) that survived logging of neighbors in the late 19th or early 20th century (Table 2).

3.2. Climatic and topographic gradients

Since 2001, climatic variation among locations was pronounced in primary and secondary forests (**Supplementary Fig. 1**). The amount of annual precipitation (rain) increased strongly with latitude and exhibited high interannual variability with summer precipitation representing a small proportion of the annual total across the *Sequoia* range (Table 2). Growing season (March to October mean) T_{min} had a strong temporal trend, frequently averaging 1–4 standard deviations above the 20th century mean during the 21st century. According to the standardized precipitation evapotranspiration index (SPEI), 2014 was the driest growing season. Across locations, the 2013–2015 growing seasons were unusually dry, while the 2006, 2011, and 2017 growing seasons were unusually wet.

Topographic and 21st century climatic variables exhibited many statistically significant ($P < 0.001$) pairwise trends (τ) among the 45 locations (Table 6). Whereas rain, the proportion of summer rain, and summer fog and low cloud cover (FLCC) were higher in the north, T_{min}, T_{max}, and vapor pressure deficit (VPD) were higher in the south (Fig. 1, Table 2). Temperature and VPD were positively trended, which was not surprising since the former were used to compute the latter (PRISM Climate Group 2020). In contrast, rain and FLCC were negatively trended with temperature and VPD, as these variables co-varied with latitude. Regardless of latitude, minimum VPD (V_{min}, March to October mean) increased with elevation, and T_{max} (March to October mean) increased with distance to ocean. Preliminary analyses revealed unexplainable step changes in VPD time series, so given the strong trends between temperature and VPD, we excluded VPD time series from further analyses.

3.3. Tree growth trends

Both radial and volume increments exhibited correlations (r) with year at various intervals during tree growth histories (Fig. 2). Among 32 primary forests, statistically significant positive and negative correlations (hereafter increasing and decreasing trends, respectively) occurred with similar frequency (8 %) in radial increment, whereas increasing trends occurred with higher frequency than decreasing trends in volume increment (13 vs. 5 %). In contrast, among 13 secondary forests, decreasing trends were more frequent than increasing trends in radial increment (27 vs. 5 %), and increasing trends were far more frequent than decreasing trends in volume increment (46 vs. 2 %). Decades where most trees exhibited decreasing trends were sporadically distributed in primary forests since 1700 with two notable exceptions. First, decreasing trends were prevalent in 13 locations between 1940 and 1960. Second, decreasing trends were prevalent in four locations (7, 22, 42, 45) during the 21st century. Decades where most trees had increasing trends were sporadic until the 20th century, and then all but four locations (10, 13, 33, 44) exhibited increasing trends from 1920 to 1940 and most locations exhibited multiple consecutive decades with increasing trends from 1960 to 2000. In primary forests, durations of these 20th century growth surges were the longest since at least 1700. In secondary forests, decreasing radial increments were prevalent until ~1960, whereas increasing volume increments predominated until the 21st century. Decreasing radial increments occurred in all but one secondary forest (29) from 1940 to 1960, and three of these locations (4, 15, 16) also exhibited decreasing volume increments during this interval. Only the southernmost secondary forest (40) exhibited decreasing volume increments during the 21st century.

Time series of biomass increments revealed long-term trends (τ) with substantial interannual and tree-to-tree variability (**Supplementary Fig. 2**). Among 32 primary forests (166 trees), biomass increments were positively trended ($P < 0.001$) in 139 trees (84 %), negatively trended ($P < 0.001$) in 13 trees (8 %), and not trended in 14 trees (8 %). Only primary forests north of 40° (3, 5, 6, 10, 11, 13, 17, 20) had trees

Table 6
Pairwise trends among landscape and 21st century climatic variables for 45 study locations. Values are Kendall rank coefficients (τ) highlighted **bold** if statistically significant ($P < 0.001$). Landscape variables are latitude (°N), elevation above sea level (m), distance to ocean (km), slope steepness (%), vertical distance to water (VDW, m), and June to September fog + low cloud cover (FLCC, h d^{-1}). Climatic variables—derived from 800-m resolution data (LT81 model, PRISM Climate Group 2020)—are averaged for 2001–2019 (rain = annual precipitation, JJAS% = percent annual precipitation occurring June to September, T_{min} and T_{max} = minimum and maximum March to October mean temperature, V_{min} and V_{max} = minimum and maximum March to October mean vapor pressure deficit, Table 2).

	Latitude	Elevation	Ocean	Slope	VDW	FLCC	JJAS%	Rain	T_{min}	T_{max}	V_{min}
Elevation	−0.19										
Ocean	−0.05	0.12									
Slope	−0.10	0.19	−0.18								
VDW	0.24	0.06	−0.09	0.16							
FLCC	**0.39**	−0.12	−0.26	−0.16	0.14						
JJAS%	**0.76**	−0.19	−0.14	−0.05	0.26	**0.51**					
Rain	**0.66**	−0.05	−0.13	0.03	0.31	0.27	**0.51**				
T_{min}	**−0.44**	0.18	0.12	0.22	−0.26	**−0.34**	**−0.35**	**−0.36**			
T_{max}	**−0.42**	0.18	**0.35**	0.01	−0.22	**−0.51**	**−0.49**	−0.32	0.34		
V_{min}	**−0.51**	**0.46**	0.21	0.21	−0.15	**−0.38**	**−0.46**	−0.31	**0.62**	**0.42**	
V_{max}	**−0.43**	0.25	0.34	0.00	−0.17	**−0.47**	**−0.50**	−0.32	**0.34**	**0.82**	**0.49**

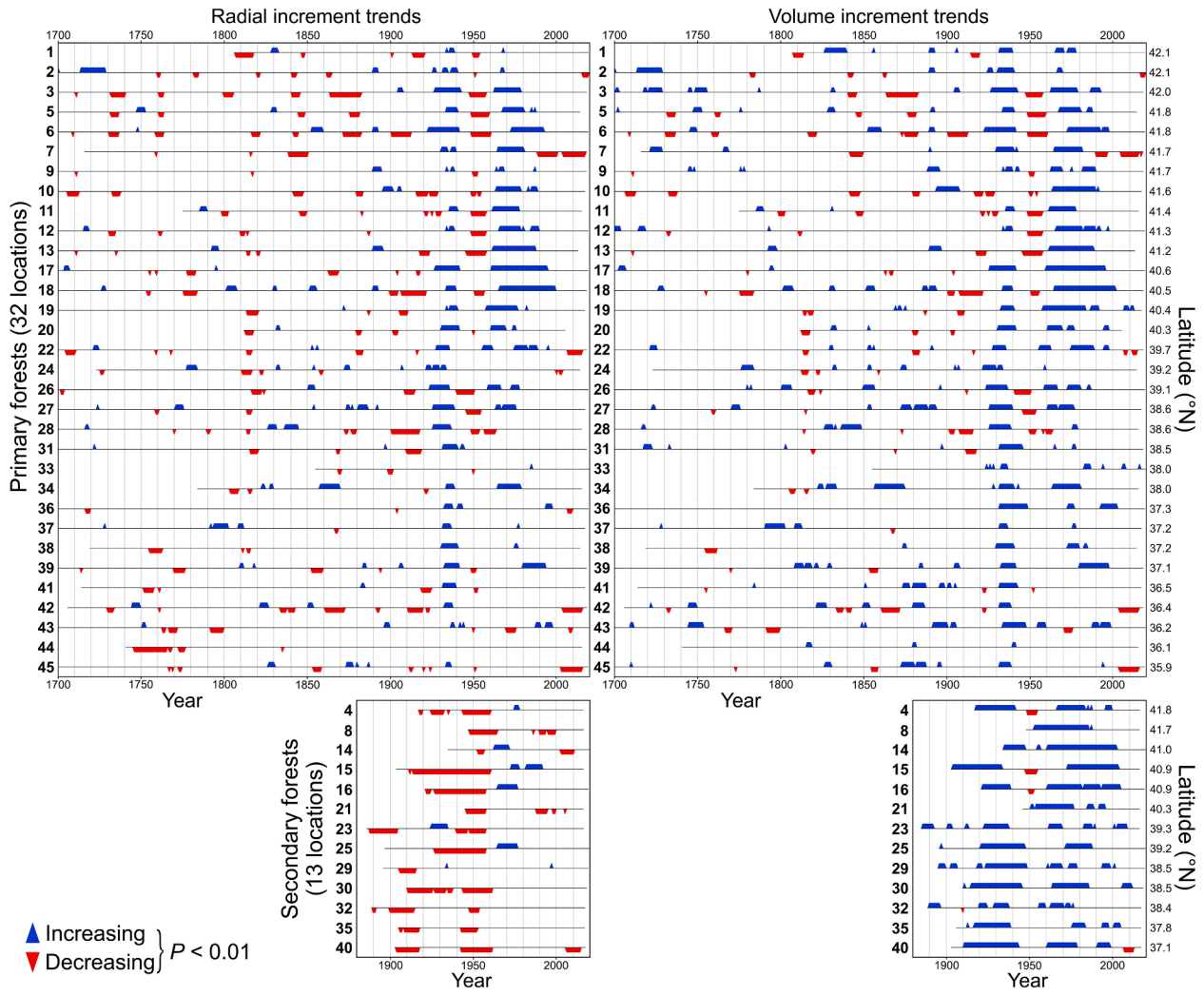

Fig. 2. Incremental growth trends in 32 primary forests since 1700 and in 13 secondary forests since 1880 (4–8 trees per location). Radial increment is specific volume increment computed as trunk wood volume increment (WVI) divided by trunk cambium area. Volume increment is WVI. Only years with statistically significant Pearson correlations (r, $P < 0.01$) occurring in majority of trees per location are highlighted as increasing (blue) or decreasing (red). Correlations are evaluated using 21-yr moving windows centered on year of measurement, truncated to 11-yr at beginning (first year + following decade) and end (last year + preceding decade) per series (horizontal lines). Locations are ranked by latitude from north (top) to south (bottom) per forest type. Vertical lines indicate decades. (For interpretation of the references to color in this figure legend, the reader is referred to the web version of this article.)

producing > 700 kg yr^{-1} with three of these (5, 10, 11) having trees occasionally producing > 1000 kg yr^{-1}. In seven primary forests (2, 12, 28, 39, 42, 43, 45), trees never produced > 400 kg yr^{-1}. Among 13 secondary forests (69 trees), biomass increments were positively trended ($P < 0.001$) without exception. The most productive tree in any secondary forest (14) was a 278-yr-old veteran that produced ~ 700 kg yr^{-1} during the most recent decade. Only one secondary forest (25) had a non-veteran tree producing > 500 kg yr^{-1}. Trees producing > 400 kg yr^{-1} were rare in secondary forests, including seven other individuals in five locations (4, 8, 15, 16, 40). The least productive secondary forest (30) had no trees producing > 100 kg yr^{-1} until late in the 20th century.

Time series of residual increments emphasized variation in tree productivity since 1901 (Fig. 3). Among primary forests, a substantial increase (> 100 kg yr^{-1}) in residual increment occurred during the late 20th century in most locations north of 37°. Short-term disruption of these growth surges occurred in several locations during 21st century drought, but overall trees in these forests produced more biomass than expected for their size since ~ 1970. Another, shorter duration surge occurred during the 1940 s in several locations. Primary forests at northern (> 42°), eastern (locations 7, 22, 24), and southern (< 37°) range margins exhibited sharply or gradually declining residual increments such that trees produced less biomass than expected for their size during the 21st century. Protracted growth suppressions, where trees produced > 100 kg yr^{-1} less than expected for their size over an extended period, were also apparent in several primary forests north of 39° prior to 1940 and from ~ 1950–1970. Among secondary forests, most trees exhibited declining residual increments with faster-than-expected growth occurring when they were < 100 yr old. During the 21st century, a substantial decrease (> 50 kg yr^{-1}) in residual increment occurred in most locations associated with 21st century drought. A sharp decline followed by quick recovery of residual increment was also associated with the 1977 drought at four locations (21, 25, 35, 40).

3.4. Identifying key dendroclimatic relationships

Prior to initial analyses, we detrended climatic variables, if necessary, by the same method (32-yr spline) used to detrend standardized ring indices across 45 locations. Correlation and response function analyses revealed which monthly climatic predictors explained significant variation in each location's ring index (Fig. 4). Among the four sets of monthly predictors—SPEI, rain, T_{min}, T_{max}—SPEI was by far the most influential, accounting for 64 % of statistically significant ($P < 0.001$)

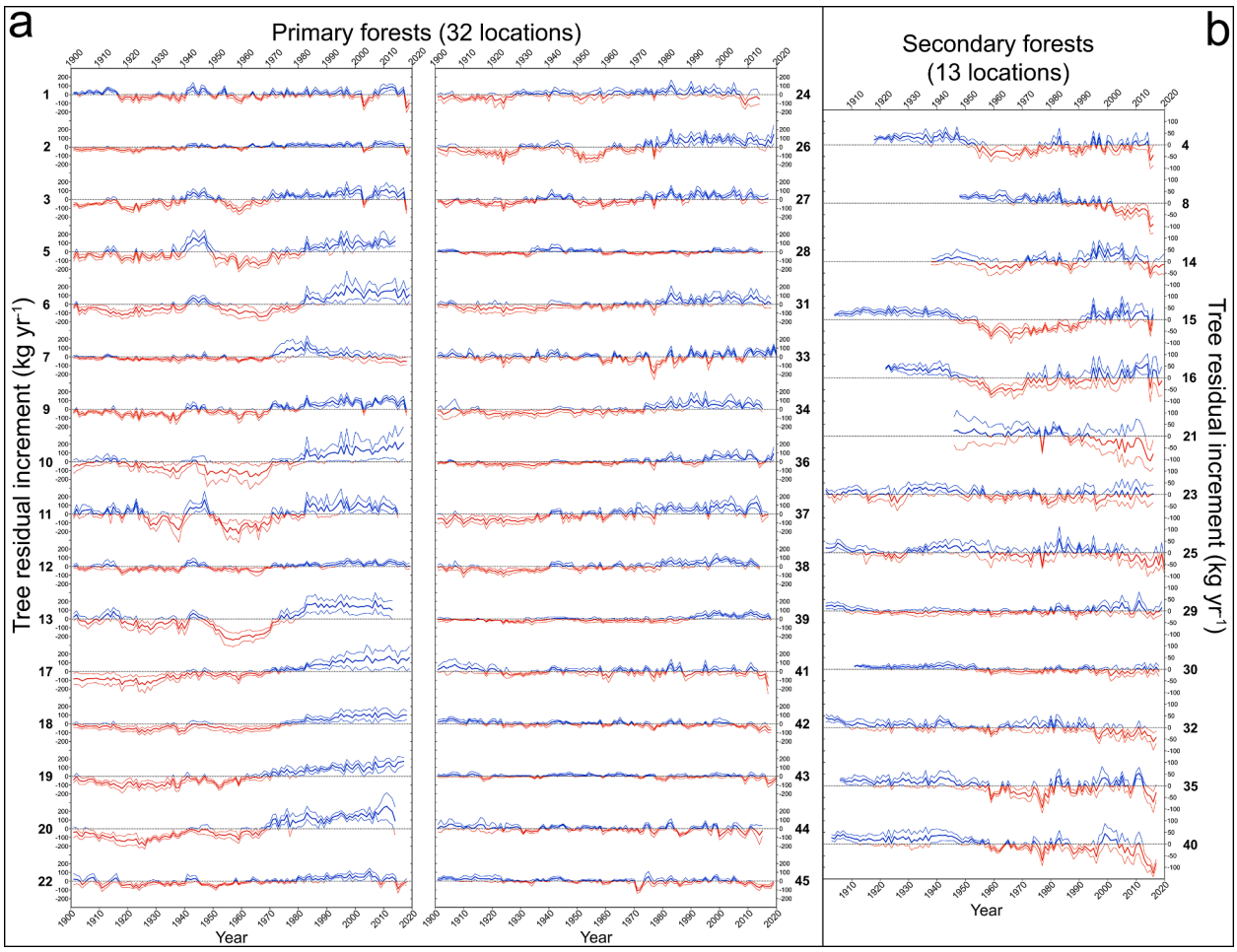

Fig. 3. Tree residual increments since 1901 in 32 primary (**a**) and 13 secondary (**b**) forests (4–8 trees per location). Residual increment (kg yr^{-1}) expresses annual biomass production relative to null hypothesis of uniform growing conditions since 1901, where trunk cambium expands at mean annual rate and growth is proportional to size (trunk cambium area). Values are mean (thick line) and 95 % confidence intervals (thin lines). Faster-than-expected growth is highlighted blue, and slower-than-expected growth is highlighted red. Locations are ranked by latitude from north (top left) to south (bottom right). Note that *y*-axis scales differ between primary and secondary forests with ticks at 100 and 50 kg yr^{-1} intervals, respectively. (For interpretation of the references to color in this figure legend, the reader is referred to the web version of this article.)

correlations and 77 % of statistically significant ($P < 0.01$) response functions. During nearly every month of the current growing season, SPEI correlated positively—more growth during wet years, less during dry years—and significantly with ring indices south of 39°, except in four locations (34, 37, 38, 43). Thirteen locations (6 primary, 7 secondary) exhibited significant SPEI response functions during several months per current growing season, including one location north of 40° (15). The southernmost secondary forest (40) had significant SPEI correlations for all 20 months considered. Correlations between ring indices and monthly rain were significant in three main bands—previous October to November (6 locations), current March to April (11 locations), and current June to July (11 locations). All significant response functions for rain occurred during current June to July (7 locations), except for previous March in one location (25). Correlations between ring indices and monthly T_{min} were significant during current July and August in six locations with most other locations showing positive T_{min} correlations (but $P > 0.001$) during these months. A secondary forest in Napa County (32) exhibited the only significant response function to T_{min} observed—radial increment was less in years with high current June T_{min}. Significant monthly T_{max} correlations occurred in two main bands—previous October to November (11 locations) and current April to June (25 locations). Response functions for the former were significant in three primary forests (9, 11, 38), whereas response functions for the latter were significant in one secondary forest (29) and five primary forests (1, 3, 6, 7, 27). The seven key climatic variables identified by initial dendroclimatic analysis—gs SPEI (current March to October mean), pON rain (previous October to November mean), MA rain (current March to April mean), JJ rain (current June to July mean), JA T_{min} (current July to August mean), pON T_{max} (prior October to November mean), and AMJ T_{max} (current April to June mean)—were confirmed by independent analyses using residual instead of standardized ring indices (results not shown).

3.5. Temporal stability of dendroclimatic relationships

Moving-window correlation (r) analysis revealed how key dendroclimatic relationships changed since 1901 (Fig. 5). The heatmap indicated general stability in the direction of correlations. Whereas all significant SPEI, rain, and T_{min} correlations were positive (more growth during wet years and at high T_{min}), all significant T_{max} correlations were negative (less growth at high T_{max}). Trend (τ) analysis of moving-window correlations highlighted which dendroclimatic relationships were strengthening, stable, or weakening (Fig. 5). Strengthening positive correlations with gs SPEI, pON rain, and MA rain occurred in 18 locations south of 40° but only one location (21) north of 40°. Strengthening positive correlations also occurred in 10 locations for JJ rain and one location (14) for JA T_{min}. Stable positive correlations with gs SPEI, pON rain, and MA rain occurred in seven locations south of 39°

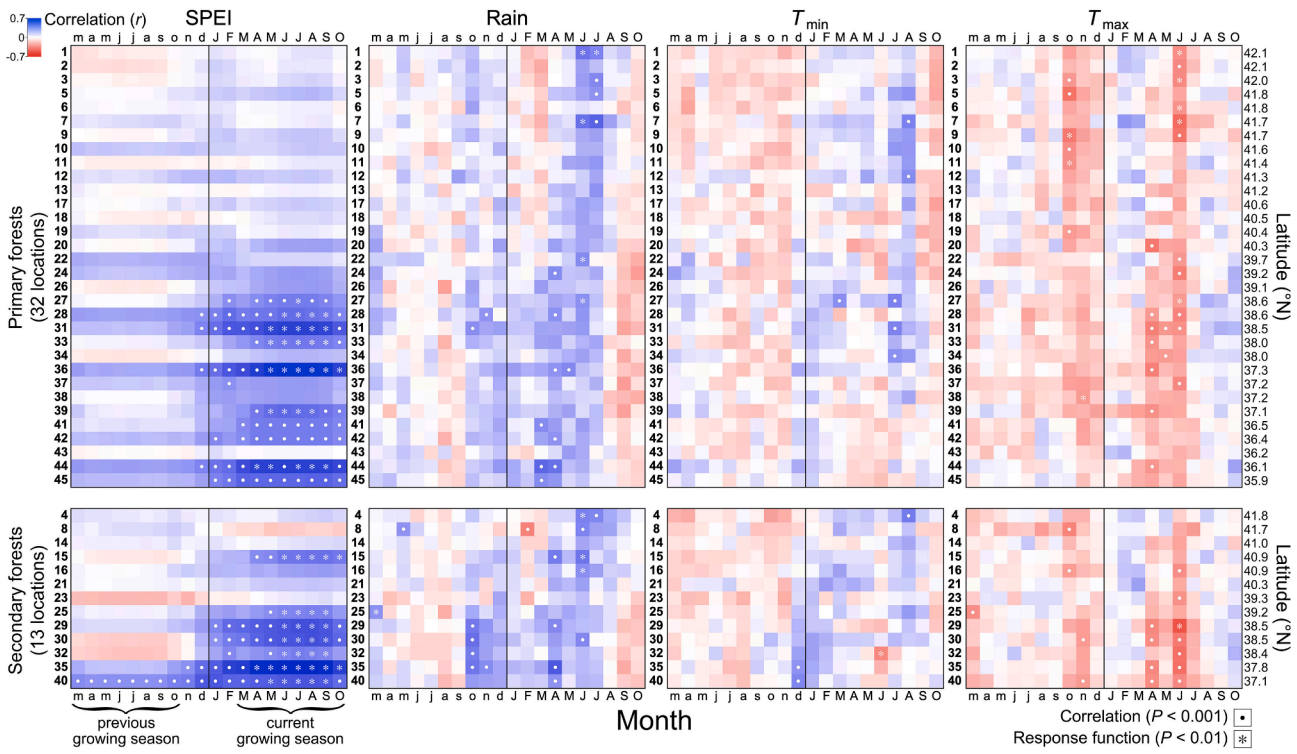

Fig. 4. Relationships between tree-ring indices and monthly climatic variables in 32 primary and 13 secondary forest locations since 1901, extending from beginning of previous growing season (March) to end of current growing season (October). Values per cell are color-coded (blue = positive, red = negative) by Pearson correlations (*r*). Statistically signification correlations ($P < 0.001$) and response functions ($P < 0.01$) are indicated by white dots and asterisks, respectively. All months with significant response functions also have significant correlations. Note that tree-ring indices and trended climatic variables (T_{min}, T_{max}) were detrended by 32-yr spline functions prior to correlation and response function analyses. Monthly SPEI, rain, T_{min}, and T_{max} are derived from 800-m resolution data (LT81 model, PRISM Climate Group 2020). Locations are ranked by latitude from north (top) to south (bottom) per forest type. (For interpretation of the references to color in this figure legend, the reader is referred to the web version of this article.)

and one location (15) north of 40°. Stable positive correlations with JJ rain occurred in 12 locations north of 38°. Dendroclimatic correlations became increasingly positive in many locations with variables related to water availability but in relatively few locations with variables related to temperature. Weakening positive correlations were uncommon with gs SPEI, pON rain, MA rain, and JJ rain but widespread with JA T_{min}. For pON T_{max} and AMJ T_{max}, strengthening negative correlations occurred in six and seven locations, stable negative correlations occurred in three and 10 locations, and weakening negative correlations occurred in nine and 11 locations, respectively. Dendroclimatic correlations became increasingly negative only with temperature variables. Overall, the majority (62 %) of dendroclimatic relationship were unstable over time and exhibited statistically significant ($P < 0.001$) trends since 1901.

We visualized the latitudinal basis of temporal inconsistency in the most influential dendroclimatic variable—March to October mean SPEI—by modeling growth metrics in two 60-yr series (1901–1960, 1961–2020) as functions of latitude using NPMR (Table 7). Trends in both metrics decreased with latitude (highest < 39°), and response curves indicated that ring index was more responsive to SPEI than biomass increment, becoming considerably stronger during the later period at most latitudes (Fig. 6**a**, upper panel). Comparing latitudinal gradients of relative increments between time periods also revealed shifts in tree performance (Fig. 6**a**, lower panel). Dependent variables in these models were computed as 3-yr average biomass increment during the wettest (highest SPEI) and driest (lowest SPEI) years per tree divided by its 1901–1960 or 1961–2020 mean biomass increment. During the wettest years of the earlier period north of 40°, trees produced 10–20 % less biomass than the 1901–1960 mean, yet during the wettest years of the later period, these trees produced up to 15 % more biomass than the 1961–2020 mean. During the driest years of the earlier period, trees produced 10–25 % less biomass than the 1901–1960 mean across the latitudinal gradient, but a dramatic shift occurred during the later period, when trees north of 40° produced up to 10 % more biomass during the driest years compared to the 1961–2020 mean. South of 38°, trees exhibited a consistent dendroclimatic response—relative increments were 30–50 % higher during the wettest than the driest years. Trees generally produced more biomass during the later period with those north of 40° outproducing those south of 40° except during the 1950 s and 1960 s (Fig. 6**b** upper panel). Climatic differences between time periods included higher and more rapidly rising temperatures south of 40° (T_{min} + 1.5°, T_{max} + 0.3 °C per century) than north of 40° (T_{min} + 0.9°, T_{max} + 0.1 °C per century) as well as substantially higher and more rapidly rising atmospheric CO_2 concentrations during the later period (Fig. 6**b** lower panel).

3.6. Growth efficiency and hotter drought

Mixed-effects ANCOVA revealed consistently strong negative effects of four consecutive drought years (2012–15) on *Sequoia* productivity across forest types and latitudes (Table 8). The dependent variable in these models was growth efficiency (GE, biomass increment ÷ leaf mass). In all models, consecutive drought years had a substantial impact where GE progressively decreased as the drought intensified and temperatures increased (Fig. 7). Among primary forests (models A, E), neither latitude nor its interaction with consecutive drought years had additional effects on GE. Among secondary forests (model B), GE was substantially higher in locations north of 40°, where trees were 2.6X more strongly impacted by the multi-year drought than in locations south of 40°, and GE decreased by an additional 0.026 ± 0.008 kg kg^{-1} yr^{-1} with most of this occurring in 2015. Among northern locations

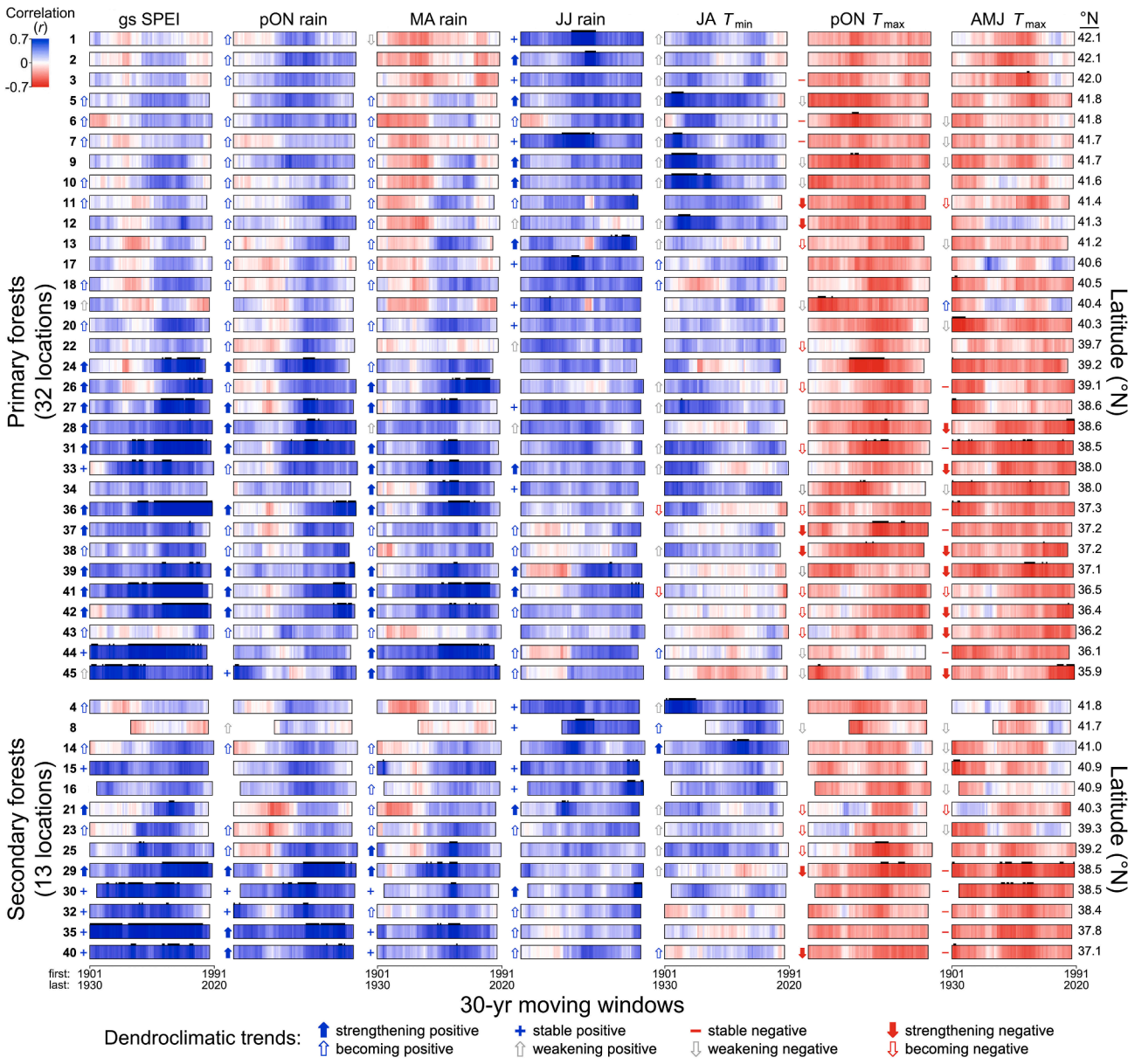

Fig. 5. Changing relationships between tree-ring indices and seven key climatic variables in 32 primary and 13 secondary forest locations. Values are color-coded (blue = positive, red = negative) by Pearson correlations (r) using 30-yr moving windows from 1901 to 2020 at 1-yr intervals. Statistically significant individual correlations ($P < 0.001$) are highlighted by black bars atop each location's heat map. SPEI, rain, T_{min}, and T_{max} are derived from 800-m resolution data (LT81 model, PRISM Climate Group 2020) averaged over months indicated (gs = current March to October, pON = previous October to November, MA = current March to April, JJ = current June to July, AMJ = current April to June). Locations are ranked from north (top) to south (bottom) within forest type. Symbols to left indicate statistically significant ($P < 0.001$) trends (τ) between year and 30-yr moving window correlations (r). Solid arrows indicate locations with strengthening positive (blue) or negative (red) correlations that are statistically significant overall. Unfilled arrows indicate locations with significant correlations that are weakening (gray) as well as locations with insignificant correlations that are approaching statistical significance or changing direction (red, blue). Plus (+) and minus (−) symbols indicate stable (not trended) positive and negative correlations that are statistically significant overall ($P < 0.001$). (For interpretation of the references to color in this figure legend, the reader is referred to the web version of this article.)

(model C), GE was substantially higher in secondary forests, where trees were 2.5X more strongly impacted by the multi-year drought than in primary forests, and GE decreased by an additional 0.025 ± 0.006 kg kg^{-1} yr^{-1}. This was not the case in central locations (model D), where neither forest type nor its interaction with consecutive drought years had additional effects on the GE response.

Mixed-effects ANCOVA also revealed recovery of GE in the two years (2016–17) following the fourth consecutive year of drought (2015) with degree of recovery varying by forest type and latitude (Table 8, Fig. 7). Among northern and central primary forests (model F), GE increased by 0.050 ± 0.008 kg kg^{-1} yr^{-1} after 2015, and neither latitude nor its interaction with post-drought recovery had additional effects on GE. Among northern, central, and southern primary forests (model J), however, the interaction between latitude and post-drought recovery had a major impact on GE. South of 37°, GE failed to recover and decreased by 0.045 ± 0.014 kg kg^{-1} yr^{-1} after 2015. Among secondary forests (model G), post-drought recovery was 5.6X faster in northern than central locations, where GE increased by an additional 0.107 ± 0.017 kg kg^{-1} yr^{-1} after 2015. Among northern locations (model H), GE recovered 2.6X faster in secondary than primary forests with GE increasing by an additional 0.080 ± 0.014 kg kg^{-1} yr^{-1} after 2015, but GE in both forest types recovered to pre-drought (2011) levels by 2017.

Table 7
Summary of nonparametric regression models associated with response curves illustrated in Fig. 6**a**. Predictor in all models is latitude. Dependent variables are ring index vs SPEI trends, biomass increment vs SPEI trends, and two relative increments computed separately for two 60-yr time series (1901–1960 vs 1961–2020). Relative increments are average biomass increments during each tree's three wettest (highest SPEI) and three driest (lowest SPEI) years divided by its mean biomass increment. SPEI (March to October mean standardized precipitation evapotranspiration index) is derived from 800-m resolution monthly rain, T_{min}, and T_{max} data (LT81 model, PRISM Climate Group 2020). Sample size is 45 locations or 235 trees. Average neighborhood size (N^*) is amount of data bearing on response estimate per point. Sensitivity is mean absolute difference resulting from nudging predictor (delta = 0.05) expressed as proportion of dependent variable's range. Cross-validated correlation (xR^2) is computed as 1 – (residual sum of squares / total sum of squares) and based on leave-one-out cross validation.

Dependent variable	Sample size	N^*	60-yr period	Sensitivity	xR^2
Ring index vs SPEI (τ)	45	39	1901–1960	0.60	0.33
			1961–2020	0.50	0.44
Biomass increment vs SPEI (τ)	235	52	1901–1960	0.22	0.13
			1961–2020	0.33	0.53
Wettest relative increment	235	52	1901–1960	0.36	0.38
			1961–2020	0.37	0.29
Driest relative increment	235	52	1901–1960	0.35	0.09
			1961–2020	0.43	0.54

This was not the case in central locations (model I), where neither forest type nor its interaction with post-drought recovery had additional effects on the GE response.

3.7. . Heartwood development

Because increasing investment in defense against wood decay fungi may reduce *Sequoia* growth efficiency as trees enlarge with age (Sillett et al. 2020), we considered tree age and heartwood characteristics as additional predictors of growth responses since 1901. As a proportion of tree biomass, heartwood mass increased nonlinearly with both trunk wood volume and tree age (Fig. 8**a**), allowing a tree's heartwood content to be estimated at annual resolution (Table 4). Heartwood increments were substantially lower in secondary than primary forests. Whereas heartwood increments increased from 52 to 63 % of increments in secondary forests (trees 120–180 yr in 2016), heartwood increments of middle-aged (480–750 yr in 2006) and older (750–2100 yr in 2006) trees in primary forests increased from 72 to 75 % and 80–82 % of biomass increments, respectively, during a century of development (Fig. 8**b**).

Heartwood characteristics varied along height and age gradients in forests at different latitudes. Across the range, *Sequoia* wood densities exhibited quadratic relationships to height such that the least dense wood occurred at intermediate heights. We used the difference between heartwood and sapwood density to estimate the amount of heartwood extractives (fungicide) deposited in sapwood during its conversion to heartwood. Expressed as a proportion of heartwood mass, the amount of fungicide in heartwood increased nonlinearly with height on trunk (Fig. 9**a**). Heartwood density of lower trunks (up to 20 m) exceeded sapwood density by 3–4 kg m^{-3} in northern secondary forests, 9–14 kg m^{-3} in central secondary forests, 12–21 kg m^{-3} in central primary forests, 17–34 kg m^{-3} in southern primary forests, and 20–28 kg m^{-3} in northern primary forests, which represented lower-trunk fungicide contents averaging of 1.3, 3.1, 4.6, 6.1, and 7.1 % of heartwood mass, respectively. In all forests, heartwood density increased more rapidly with height above mid-trunk than sapwood density such that fungicide content approached or exceeded 20 % of heartwood mass in uppermost trunks. The accumulation of heartwood as trees enlarged with age combined with increasing fungicide deposition along the height gradient translated into generally higher fungicide contents of heartwood increments in primary vs. secondary forests, though there was considerable tree-to-tree variation (Fig. 9**b**). Among northern primary forests, the highest estimated whole-trunk fungicide investment (12.5 % of heartwood increment) occurred in a 113-m-tall, 1260-yr-old tree (location 20), and the lowest investment (6.6 %) occurred in an 84-m-tall, 120-yr-old tree (location 13) growing on an alluvial terrace exposed by creek avulsion in the late 19th century. Among central primary forests, the highest fungicide investment (9.3 % of heartwood increment) occurred in a 112-m-tall, 1130-yr-old tree (location 24), and the lowest investment (4.5 %) occurred in a 46-m-tall, 780-yr-old tree (location 28), the shortest in the study. Among southern primary forests, the highest fungicide investment (11.6 % of heartwood increment) occurred in a 93-m-tall, 650-yr-old tree (location 41), and the lowest investment (6.7 %) occurred in a 64-m-tall, 410-yr-old tree (location 42). The oldest trees per region, which were 96, 73, and 68 m tall, had relatively low fungicide investments, because their upper trunks were either mostly dead or replaced by much smaller reiterated trunks. Overall, as a percentage of heartwood mass increment, northern secondary forests invested the least in fungicide (3.1 ± 0.1, $N = 34$ trees) followed by central secondary forests (4.7 ± 0.2, $N = 37$ trees), central primary forests (7.2 ± 0.3, $N = 57$ trees), and southern primary forests (7.9 ± 0.5, $N = 25$ trees), whereas northern primary forests (10.3 ± 0.2, $N = 84$ trees) invested the most (means ± 95 % confidence intervals).

3.8. Biotic and abiotic predictors of growth

We modeled annual productivity of *Sequoia* trees from 2001 to 2019 as well as tree- and plot-level averages for an 11-yr period (1999–2009) to take advantage of a coincident summer fog and low cloud cover index (FLCC) derived from Geostationary Operational Environmental Satellite (GOES) data for this period (Torregrosa et al. 2016). Since FLCC values were 11-yr averages, this index was less of a climatic and more of a topographic predictor (i.e., distinguishing foggy and non-foggy landscape positions) for individual years. Leaf mass was the strongest single predictor of biomass increment for trees and plots, explaining 18–59 % of variation during individual years as well as 57–64 % of variation for the 1999–2009 average (Table 9). Biomass increment increased nearly linearly with leaf mass in trees and plots (Fig. 10**a**). Compared to leaf-only models, models with more than one predictor had considerably lower, but still respectable (minimum = 28), average neighborhood sizes (N^*) and explained up to 64 % of variation (Table 9). Night FLCC explained 5–11 % of variation during 10 of 19 (53 %) of years. Latitude explained 6–10 % of variation during 6 of 19 (32 %) years. Other important predictors of biomass increment during individual years were JJ rain (2009), day FLCC (2014), and pON rain (2018), which explained 5–35 % of variation. Model sensitivity to leaf mass was higher than all predictors every year except 2018, when sensitivity to pON rain was higher.

The fungicide proportion of heartwood increment (hereafter fungicide increment) and night FLCC were the two strongest predictors of growth efficiency for trees and plots. Whereas fungicide increment explained 17–29 % of variation during 15 of 19 (79 %) of years as well as 24–25 % of variation for the 1999–2009 average, night FLCC explained 10–27 % of variation during 18 of 19 (95 %) of years as well as 15–21 % of variation for the 1999–2009 average (Table 9). Growth efficiency was highest in northern secondary forests (8, 14–16, 21) with the lowest fungicide increments and some of the highest values of night FLCC (Fig. 10**b**). Other important predictors of growth efficiency during individual years were tree age (2010–12, 2015), elevation (2003, 2013, 2014), JJ rain (2003, 2004), pON rain (2015, 2018), pON T_{max} (2017), distance to ocean (2017), and latitude (2019), which explained 5–38 % of variation. Model sensitivity to fungicide increment was highest during 11 of 19 (58 %) of years as well as the 1999–2009 average (235-tree model). Model sensitivity to night FLCC was highest during 2016 as well as the 1999–2009 average (45-location model). Model sensitivities to other important predictors (tree age, latitude, pON rain, pON T_{max}) were

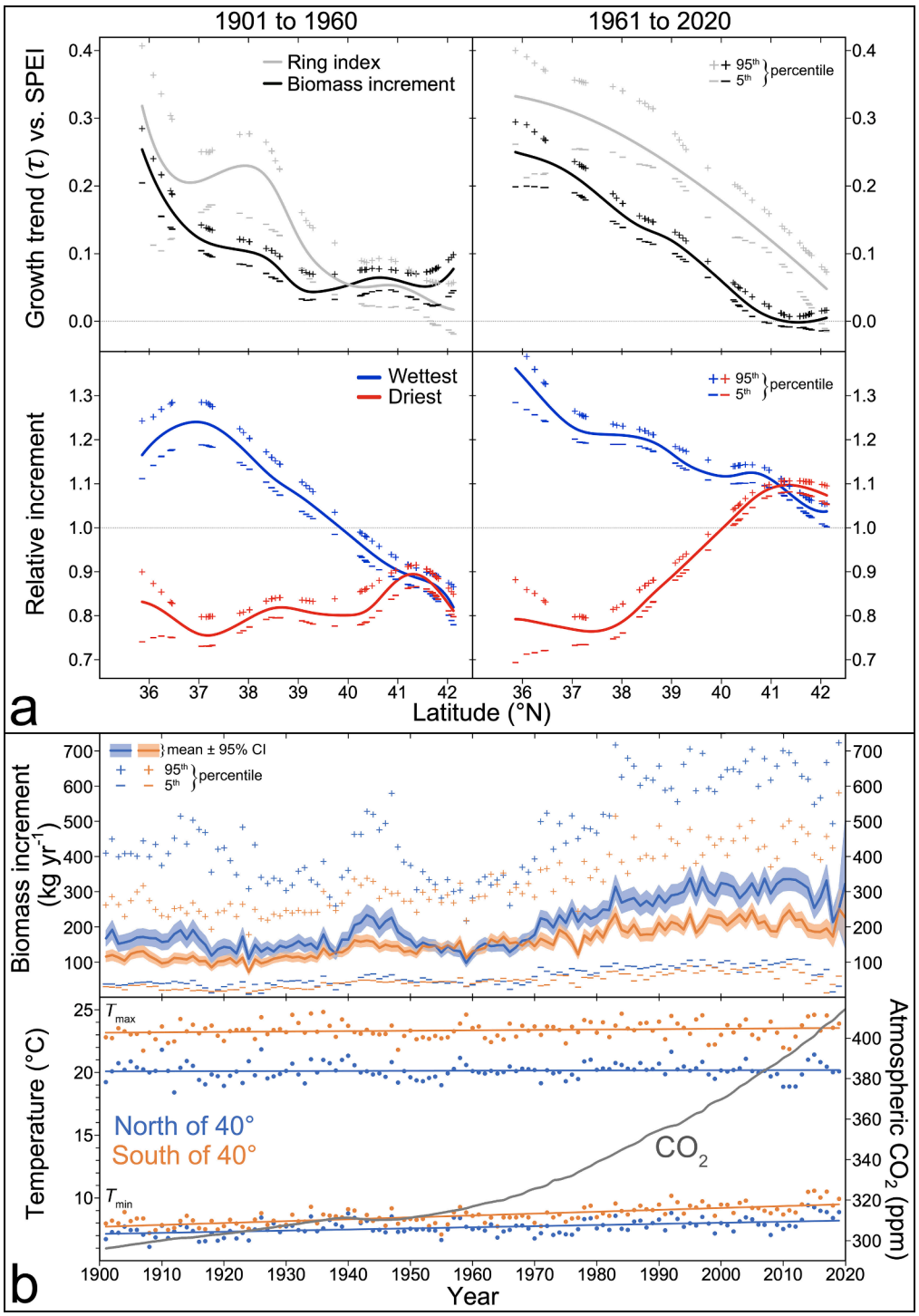

Fig. 6. Shifting *Sequoia* growth responses and climatic context since 1901. (**a**) Latitudinal response curves for *Sequoia* growth trends vs standardized precipitation evapotranspiration index (SPEI, March to October mean) from 1901 to 1960 and 1961 to 2020. In upper panels, Kendall coefficients (τ) between SPEI and two growth metrics—standardized ring index (N = 45 locations) and biomass increment (N = 235 trees)—are modeled as functions of latitude. In lower panels, relative increments (N = 235 trees) during climatic extremes are modeled as functions of latitude. For each 60-yr series, biomass increments of 3 wettest and 3 driest years (ranked by SPEI) are separately averaged per tree and divided by mean biomass increment to compute maximum (wettest) and minimum (driest) relative increments. For each response curve, 95th (+) and 5th (-) percentiles of individual location (ring index) or tree (biomass increment, relative increment) estimates are shown. See Table 7 for details of models. (**b**) Biomass production and climatic context since 1901. Time series of biomass increments (mean ± 95 % confidence interval, N = 116 trees north of 40°, 119 trees south of 40° latitude) as well as 95th (+) and 5th (-) percentiles for individual years are shown in upper panel. Air temperatures and CO_2 concentrations since 1901 are shown in lower panel. Annual temperature data are March to October mean T_{max} (upper) and T_{min} (lower) averaged separately for 21 locations north (blue) and 24 locations south (orange) of 40° latitude with trendlines (R^2 = 0.003, 0.027, 0.260, 0.526 for T_{max} north, T_{max} south, T_{min} north, and T_{min} south, respectively). SPEI and temperature are derived from 800-m resolution data (LT81 model, PRISM Climate Group 2020). Annual CO_2 data are from Mauna Loa observatory (1959–2020, https://gml.noaa.gov/ccgg/trends/data.html) and ice cores (1901–1958, http://data.giss.nasa.gov/modelforce/ghgases/Fig1A.ext.txt). (For interpretation of the references to color in this figure legend, the reader is referred to the web version of this article.)

Table 8
Summary of mixed-effects ANCOVA used to assess *Sequoia* growth responses to 21st century drought. Dependent variable is aboveground growth efficiency (kg kg^{-1} yr^{-1}) in 10 models involving trees in primary (1°) and secondary (2°) forests at northern (N, > 40°), central (C, 37-40°), and southern (S, < 37°) latitudes (Fig. 7). Models A to E examine *consecutive drought years* as continuous fixed effect with drought years 2012–2015 coded 1–4 and bounding non-drought years (2011, 2016, 2017) coded 0. Models H to J examine *post-drought recovery* as continuous fixed effect with last year of drought (2015) coded 0 and non-drought years 2016–2017 coded 1–2. Only models E and J include trees south of 37°, all from primary forests. Each model has one categorical fixed effect (N / C, 1° / 2°, N / C / S), one interaction between continuous and categorical fixed effects, and two random effects on the intercept (locations, trees within locations). Number of locations and trees varies due to 14-yr sampling period (5 trees sampled prior to 2011, 33 trees sampled prior to 2015). Parameter estimate and standard error (S_E) are listed along with sum of squares (sum sq), mean square (mean sq), numerator degrees of freedom (num df), denominator degrees of freedom (den df), *F* statistic, and *P* value. Significant *F* statistics ($P < 0.01$) are highlighted in **bold**.

Model	Locations	Trees	Fixed effects	Sum sq	Mean sq	Num df	Den df	*F*	*P*
A, primary (1°)	27	135	Consecutive drought years (CDY)	0.6139	0.6139	1	704	**69.2**	< 0.0001
			N / C	0.0000	0.0000	1	26	0.0	0.9578
			CDY × N / C	0.0095	0.0095	1	704	1.1	0.3013
B, secondary (2°)	15	71	Consecutive drought years (CDY)	0.8741	0.8741	1	400	**51.2**	< 0.0001
			N / C	0.4416	0.4416	1	12	**25.9**	0.0003
			CDY × N / C	0.1708	0.1708	1	400	**10.0**	0.0017
C, northern (>40°, N)	21	112	Consecutive drought years (CDY)	1.1072	1.1072	1	591	**90.8**	< 0.0001
			1° / 2°	0.3677	0.3677	1	18	**30.1**	< 0.0001
			CDY × 1° / 2°	0.2084	0.2084	1	591	**17.1**	< 0.0001
D, central (37-40°, C)	19	94	Consecutive drought years (CDY)	0.4529	0.4529	1	512	**39.6**	< 0.0001
			1° / 2°	0.0004	0.0004	1	30	0.0	0.8470
			CDY × 1° / 2°	0.0083	0.0083	1	512	0.7	0.3936
E, primary (36-42°, all)	32	160	Consecutive drought years (CDY)	0.8406	0.8406	1	833	**82.8**	< 0.0001
			N / C / S	0.0363	0.0182	2	30	1.8	0.1846
			CDY × N / C / S	0.0396	0.0198	2	833	1.9	0.1431
F, primary (1°)	26	116	Post-drought recovery (PDR)	0.4570	0.4570	1	197	**101.2**	< 0.0001
			N / C	0.0000	0.0000	1	25	0.0	0.9752
			PDR × N / C	0.0000	0.0000	1	197	0.0	0.9938
G, secondary (2°)	15	71	Post-drought recovery (PDR)	0.5271	0.5271	1	116	**84.4**	< 0.0001
			N / C	0.0493	0.0493	1	13	7.9	0.0152
			PDR × N / C	0.2556	0.2556	1	116	**40.9**	< 0.0001
H, northern (>40°, N)	21	101	Post-drought recovery (PDR)	0.8146	0.8146	1	163	**167.3**	< 0.0001
			1° / 2°	0.0499	0.0499	1	18	**10.3**	0.0049
			PDR × 1° / 2°	0.1634	0.1634	1	163	**33.6**	< 0.0001
I, central (37-40°, C)	18	86	Post-drought recovery (PDR)	0.1992	0.1992	1	149	**36.3**	< 0.0001
			1° / 2°	0.0008	0.0008	1	33	0.2	0.6966
			PDR × 1° / 2°	0.0258	0.0258	1	149	4.7	0.0316
J, primary (36-42°, all)	31	140	Post-drought recovery (PDR)	0.0499	0.0499	1	230	**9.6**	0.0022
			N / C / S	0.0057	0.0029	2	29	0.6	0.5824
			PDR × N / C / S	0.2145	0.1073	2	230	**20.7**	< 0.0001

highest during six individual years (2010–12, 2015, 2017, 2018, 2019).

3.9. Per hectare quantities during 21st century

Installation of fixed-area plots that included measurements of all dominant and codominant trees in 41 locations allowed us to estimate per hectare aboveground quantities and annual rates of biomass production during the 21st century (Table 5). Considering only dominant and codominant *Sequoia* trees, primary forests carried 3–21 Mg ha^{-1} of leaves and 238–3240 Mg ha^{-1} of biomass containing 147–2394 Mg ha^{-1} of heartwood (62–75 % of biomass) and 10–247 Mg ha^{-1} of fungicide (5–10 % of heartwood mass), whereas secondary forests carried 6–18 Mg ha^{-1} of leaves and 302–901 Mg ha^{-1} of biomass containing 173–514 Mg ha^{-1} of heartwood (54–59 % of biomass) and 4–21 Mg ha^{-1} of fungicide (2–4 % of heartwood mass, Fig. 11**ab**). Among primary forests, the plot (20) with the most leaves and biomass had 43 trees ha^{-1} averaging 98 m tall that accumulated 17.1 Mg ha^{-1} yr^{-1}, more than any other, and the plot (7) with the least leaves and biomass had 10 trees ha^{-1} averaging 65 m tall that accumulated 1.5 Mg ha^{-1} yr^{-1}, less than any other (Fig. 11**c**). Two other very low-productivity plots (22, 28) in primary forests, which had 4–5 Mg ha^{-1} of leaves and 11–21 trees ha^{-1} averaging 52–79 m tall, also occurred near the eastern range margin. Except for these unusually high- and low-productivity examples, plots in secondary forests had similar biomass increments to those in primary forests—2.9–12.4 (mean 7.2) vs. 2.6–13.3 (mean 6.6) Mg ha^{-1} yr^{-1}—as well as similar leaf masses (Fig. 10**a, 11a**). As a percentage of biomass increments, heartwood increments of secondary forests were significantly lower than those in primary forests—64 ± 3 vs. 73 ± 2 (means ± 95 % confidence intervals, $t = 4.6$, $P < 0.0001$). As a percentage of heartwood increments, fungicide increments of secondary forests were also significantly lower than those in primary forests—4.1 ± 0.7 vs. 8.6 ± 0.6 (means ± 95 % confidence intervals, $t = 7.4$, $P < 0.0001$).

Plot growth efficiencies during the 21st century were comparable between primary and secondary forests (Fig. 11**d**), but only secondary forests in Humboldt County had an average growth efficiency > 1, including two plots (14, 16) and two locations that were part of an experiment (15, 21, Fig. 10**b**). Among remaining locations, unusually high average plot growth efficiencies (> 0.8) occurred in two primary forests of Marin County (33, 34), a primary forest in Del Norte County < 1 km from the ocean (9), and three low-elevation alluvial forests of Humboldt and Mendocino Counties (20, 23, 26). Unusually low average plot growth efficiencies (< 0.5) were prevalent among locations near northern (2), eastern (22, 24, 28, 29, 32), and southern (42, 43, 45) range margins. There was considerable year-to-year variation in plot growth efficiencies during the 21st century with some of the lowest annual values observed during post-fire years in three primary forests (2, 41, 43). Another wildfire barely affected growth efficiency of a primary forest that is a swamp (24), and yet another wildfire occurred during the calendar year preceding our measurements of a secondary forest (32), but this occurred before any post-fire ring had started to form.

Plot residual increments during the 21st century exhibited pronounced latitudinal variation (Fig. 11**e**). Based on measured tree performance since 1901, all primary forests south of 37° produced less biomass than expected or had residual increments indistinguishable from zero, and primary forests north of 37° produced more biomass than expected except those near the eastern range margin in Del Norte (7),

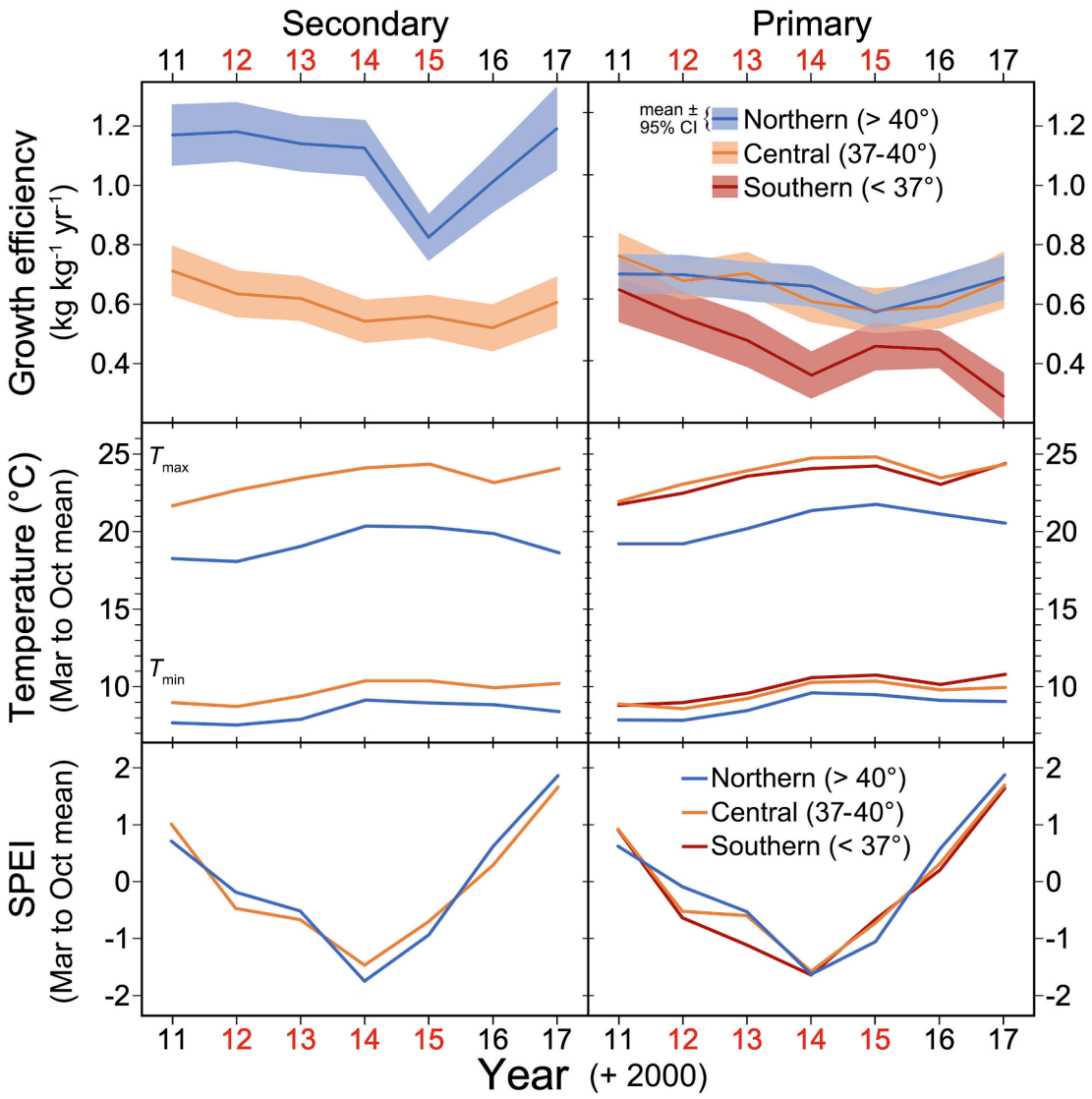

Fig. 7. *Sequoia* growth efficiency and climatic variation before (2011), during (2012–15), and after (2016–17) hotter drought differ by forest type and latitude. Consecutive drought years are highlighted in red. Upper panel shows means and 95 % confidence intervals of growth efficiency (biomass increment per unit leaf mass) in secondary forests (left, 33 trees > 40°, 37 trees 37-40°) and primary forests (right, 67 trees > 40°, 53 trees 37-40°, 24 trees < 37°). Middle panel shows average maximum (T_{max}) and minimum (T_{min}) temperatures in secondary forests (left, 5 locations > 40°, 6 locations 37-40°) and primary forests (right, 15 locations > 40°, 12 locations 37-40°, 5 locations < 37°). Lower panel shows average SPEI per year for corresponding forests. Annual SPEI and temperature values are March to October means derived from 800-m resolution data (LT81 model, PRISM Climate Group 2020). (For interpretation of the references to color in this figure legend, the reader is referred to the web version of this article.)

Mendocino (22, 24), and Napa (28) Counties as well as the two northernmost plots in Curry County, Oregon (1, 2). Among secondary forests, three plots (25, 32, 40) produced less biomass than expected, four plots (16, 23, 30, 35) had residual increments indistinguishable from zero, and only one plot (14) produced more biomass than expected since 2001.

3.10. Long-term tree development

Reconstruction of tree size and growth histories revealed long-term rates of development. Plotting height and aboveground biomass of individual trees against tree age illustrated how quickly dominant and codominant *Sequoia* grew across the species range (Fig. 12). In secondary forests, trees gained height and biomass most rapidly in two locations (23, 40) of Mendocino and Santa Cruz Counties (39.3°, 37.1°) and considerably less rapidly in two locations (29, 32) near the eastern range margin in Napa and Contra Costa Counties (38.5°, 38.4°). The fastest-growing tree in a primary forest (13) of Humboldt County (41.2°) gained height and biomass more rapidly than any trees measured in secondary forests (see arrows in Fig. 12). With few exceptions, however, trees gained height and biomass far more slowly in primary than secondary forests, and many trees acquired dead and broken tops during development in primary forests, greatly slowing their upward height trajectories. Wide variation in developmental rate was apparent in both forest types with some trees greatly outpacing others at similar latitudes. In primary forests, trees accumulated biomass at steady rates for centuries and millennia, especially in Humboldt and Del Norte Counties (40-42°), which contained the only trees > 200 Mg we measured.

By the time our study trees reached 60 m tall, there was great variation in age, biomass, and growth increments across the latitudinal gradient (Fig. 13). Among secondary forests, study trees (excluding veterans) reached 60 m tall in 77–162 yr, whereas primary forest trees required up to 672 yr (276 ± 12 yr, mean ± 1 *SE*). Trees requiring > 500 yr to reach this height were widely distributed, including

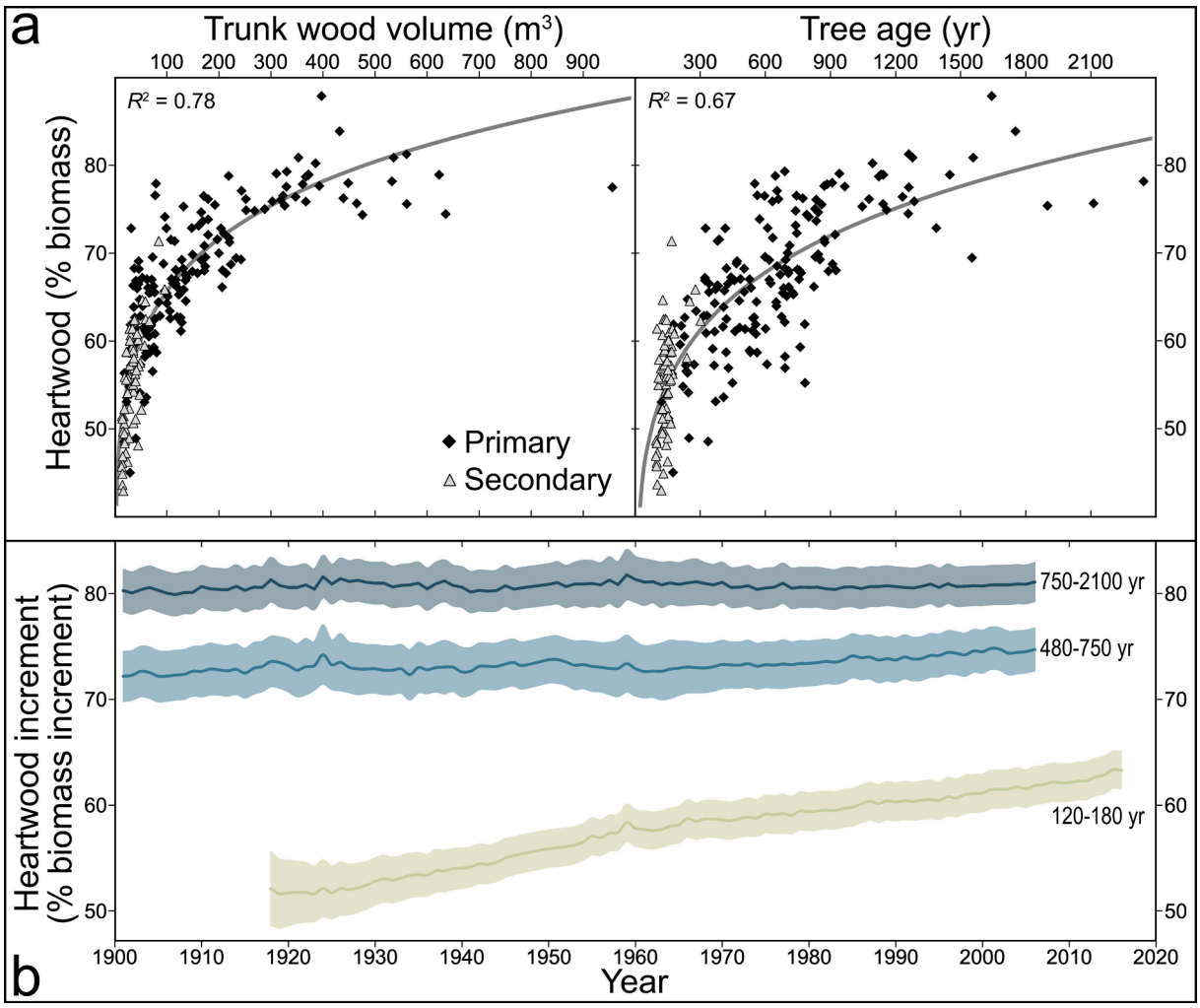

Fig. 8. Allometric estimation of *Sequoia* heartwood increments in primary and secondary forests. (**a**) Heartwood proportions of aboveground biomass are fitted as power functions of trunk wood volume (left) and age (right) for 235 trees (see Table 4). (**b**) Time series of trunk wood volume and tree age are used to predict heartwood proportions of aboveground biomass and generate time series of heartwood biomass for 120 trees. Resulting heartwood increments are expressed as proportions of biomass increments in separate time series for one tree age class in secondary forests (1918–2016) and two tree age classes in primary forests (1901–2006). Tree age ranges per class (in 2006 or 2016) are shown to right. Values are means ± 95 % confidence intervals with constant sample size ($N = 40$ trees per series).

individuals in six locations spanning the latitudinal gradient. At 60 m tall, the only trees producing > 300 kg yr^{-1} were in primary and secondary forests of Humboldt and Del Norte Counties (40-42°). In primary forests, the slowest-growing trees, which produced < 100 kg yr^{-1}, were among the oldest at 60 m tall. Height increments at 60-m tall declined in curvilinear fashion with increasing tree age such that all trees with height increments > 60 cm yr^{-1} were ≤ 110 yr old, and all trees > 400 yr old had height increments < 30 cm yr^{-1}.

3.11. Arboreal biodiversity

Arboreal biodiversity was closely associated with structural complexity in the form of reiterated trunks and limbs, dead spire tops, and hollow trunks (Table 10). Trees in secondary forests (excluding veterans) had no limbs and few (if any) reiterated trunks, all of which were relatively small, averaging < 15 cm diameter with maximum diameters < 25 cm. Whereas in secondary forests only 17 % of trees had any reiterated trunks, in primary forests half the trees had such appendages as well as limbs. The largest and most structurally complex trees in primary forests required hundreds of appendage diameter measurements with average diameters up to 61 cm and maximum diameters up to 197 cm. Trees with high structural complexity and enormous appendages were widely distributed but concentrated in primary forests of Humboldt and Del Norte Counties (40-42°). Vascular plants occurred as epiphytes in the crowns of 34 trees from 15 of 32 primary forests and in none of the trees from secondary forests (**Supplementary Fig. 3**). The evergreen fern *Polypodium scouleri* and the ericaceous shrub (hereafter ericad) *Vaccinium ovatum* were the most frequently encountered species with some trees in Humboldt and Del Norte Counties supporting hundreds of kilograms of these plants plus associated arboreal soil (Sillett & Van Pelt 2007). Two other ferns (*Dryopteris*, *P. glycyrrhiza*) and four other ericads (*Arbutus*, *Gaultheria*, *Rhododendron*, *V. parvifolium*) occurred as epiphytes along with seven angiosperms (*Castanopsis*, *Frangula*, *Gallium*, *Notholithocarpus*, *Ribes*, *Rubus*, *Stachys*, *Umbellularia*) and four conifers (*Picea*, *Pseudotsuga*, *Sequoia, Tsuga*). Only three exceptional trees south of 40° supported any vascular epiphytes, including a 1558-yr-old tree in Mendocino County (24) with a single small *Arbutus*, a 1643-yr-old tree in Sonoma County (27) with several small *Pseudotsuga* and four angiosperms (*Gallium*, *Notholithocarpus*, *Rubus*, *Stachys*), and a 1286-yr-old tree in Monterey County (41) with one tiny *Gallium*. Unlike epiphytes, terrestrial vascular plants were prevalent across the latitudinal gradient, and secondary forests harbored comparable species richness to primary forests (**Supplementary Fig. 3**). In total, we encountered 185 species of vascular

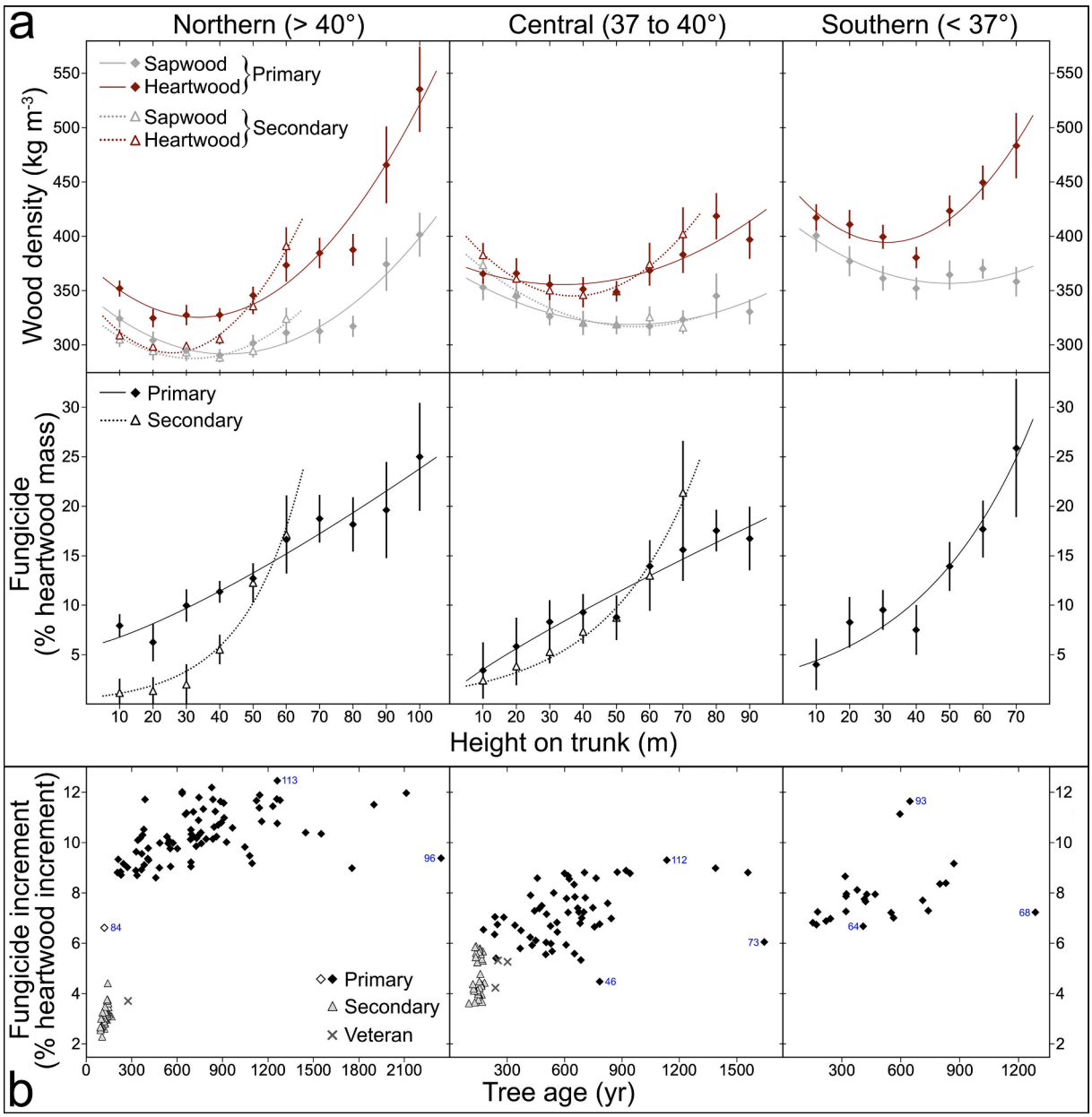

Fig. 9. Variation in *Sequoia* heartwood characteristics by latitude and forest type. (**a**) Paired samples of heartwood and sapwood are used to estimate fungicide deposition during heartwood formation as density differences at 10-m height intervals. In upper panel, heartwood and sapwood densities are fitted as quadratic functions of height. In lower panel, density differences between paired samples are expressed as proportions of heartwood mass and fitted as power functions of height. Values are means ± 1 S_E. See Table 4 for equations. (**b**) Fungicide proportions of whole-trunk heartwood increments are estimated by applying corresponding equations (**a**, lower panel) to midpoints of trunk frusta (sections between measurements) and summing from base to top for 235 trees. Veteran trees (survivors of logging) are distinguished from those in primary and secondary forests. Blue numbers indicate tree height (m) for nine individuals mentioned in text. Note that youngest tree (122 ± 1 yr) in primary forest—tallest (84 m) on alluvial terrace exposed by creek avulsion in late 19th century—has secondary forest heartwood characteristics. (For interpretation of the references to color in this figure legend, the reader is referred to the web version of this article.)

plants among the 41 plots (**Supplementary Fig. 4**).

4. Discussion

Superlative *Sequoia* forests now represent a tiny portion of the species' original distribution. The 2585 known *Sequoia* > 100 m tall occupy only 1135 ha in 22 locations with > 95 % of these trees occurring in relatively large forest reserves of Humboldt and Del Norte Counties (Fig. 1). Globally, only one standing non-*Sequoia* tree > 100 m tall is known, a 100.2-m-tall *Picea sitchensis* in Humboldt County, though a few standing individuals ≥ 99 m tall of three other species—*Pseudotsuga menziesii*, *Eucalyptus regnans*, *Shorea faguetiana*—have been reliably measured (Sillett et al. 2015a, Shenkin et al. 2019, M.W. Taylor & S.C. Sillett unpublished). In an attempt to be comprehensive, we sampled *Sequoia* in 13 locations with trees > 100 m tall as well as 19 primary forests with maximum tree heights < 100 m (62–98 m) and nearly every secondary forest we could find with trees > 60 m tall. Our *Sequoia* dataset includes measurements of 30 trees > 100 m tall, 37 trees > 100 Mg biomass, and 23 trees > 1000 yr old as well as a variety of landscape positions spanning the latitudinal gradient (Fig. 1, Table 2). Compared to many dendrochronology studies, the number of trees sampled (235) is relatively small, but each tree was measured intensively from base to top and core-sampled at multiple heights, averaging 23 core series per tree (Table 3). We use these measurements not only to quantify

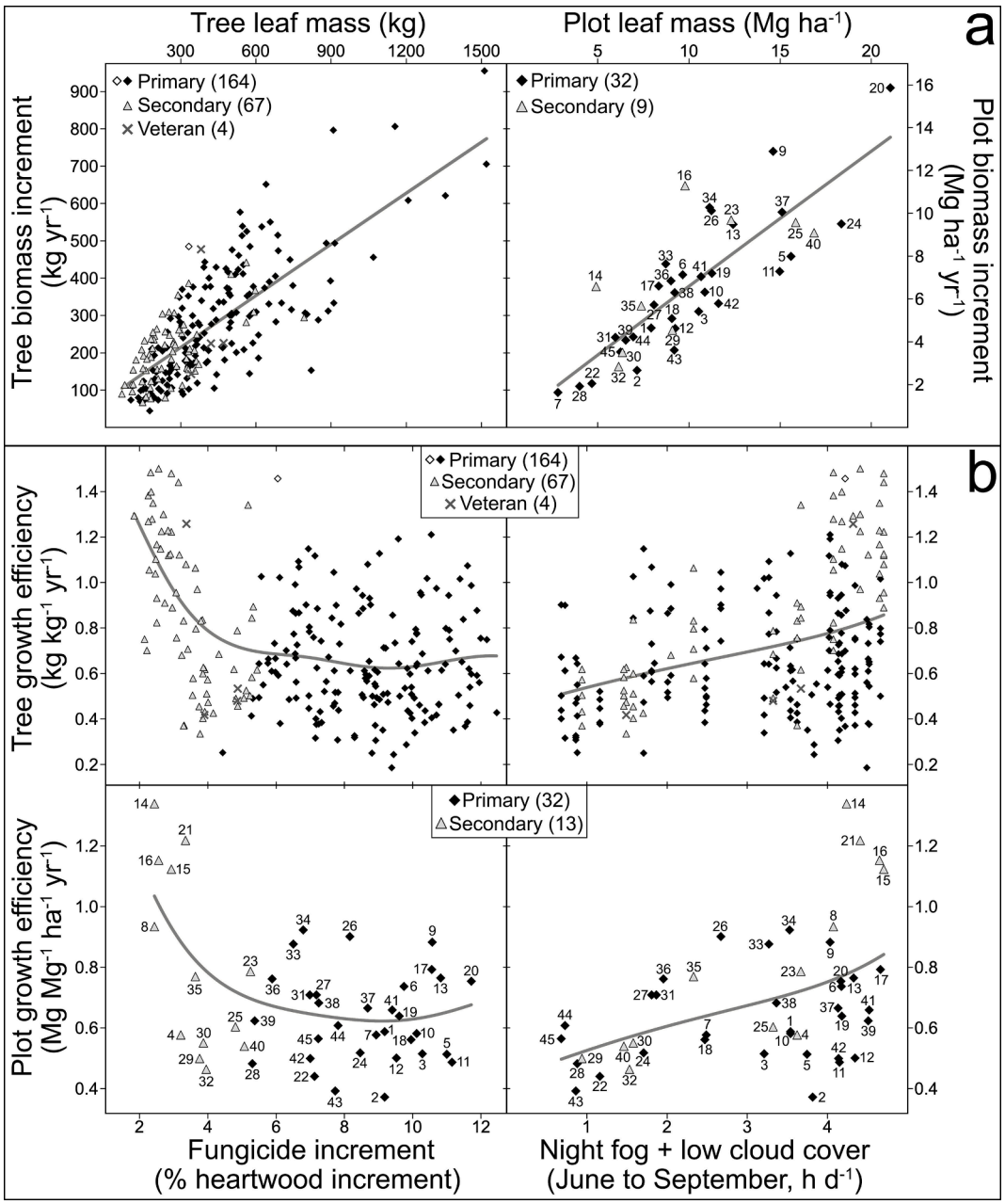

Fig. 10. *Sequoia* productivity during 11-yr period (1999–2009 mean). Gray lines are response curves from best nonparametric regression models (Table 9). (**a**) Biomass increment of 235 trees (left) and 41 locations with plots (right) versus leaf mass. (**b**) Growth efficiency of 235 trees (upper panel) and 45 locations (lower panel) versus fungicide investment (% heartwood increment, left) and nocturnal summer fog + low cloud cover (night FLCC, right). Growth efficiency is computed as biomass increment divided by leaf mass. At four locations lacking plots (4, 8, 15, 21), growth efficiency is estimated as study tree average (kg kg^{-1} yr^{-1}, $N = 4$–8 trees). Symbols indicate forest type for trees and locations. Veteran trees in secondary forests are survivors of logging in late 19th or early 20th centuries. Numbers adjacent to symbols indicate locations ranked by latitude (Table 2, Fig. 1). Numbers in parentheses indicate trees or locations per category. (For interpretation of the references to color in this figure legend, the reader is referred to the web version of this article.)

aboveground attributes—tree age, leaves, heartwood, biomass, crown structure, epiphytes—but also to reconstruct growth histories for long- and short-term analyses of tree performance as it relates to climatic variation, hotter drought, and carbon sequestration.

4.1. Range-wide variation in growth trends

The 20th century growth surge previously observed in primary *Sequoia* forests (Dangerfield et al. 2021; Sillett et al. 2015b, 2021) is widely distributed but does not extend throughout the species' range. After ~ 1970, *Sequoia* in many primary forests from the Santa Cruz Mountains to Oregon began producing more biomass than expected for their size (Fig. 3**a**). This unprecedented and increasing trend in radial and wood volume increments continues for > 30 yr in some forests until the end of the 20th century (Fig. 2) and is not followed by a comparable downward trend such that these forests are still producing more biomass annually than expected for their size during the 21st century (Fig. 11**e**). A smaller growth surge occurs in most primary forests during the 1940 s followed by growth suppression in the 1950s and 1960s (Figs. 2, 3**a**) that is not associated with drought. As suggested previously (Carroll et al. 2014, Sillett et al. 2015b), these distinctive patterns may be related to air quality. Early to mid-20th century logging generated enormous quantities of smoke and particulates from slash burning (Waggoner 1961), but most of this activity ceased during World War II, perhaps allowing

Table 9
Summary of nonparametric regression models predicting *Sequoia* biomass increments and growth efficiencies from 1999 to 2009 (mean) and for 19 individual years (2001–2019). Sample size is number of locations (41, 45) or trees (71–235). Average neighborhood size (N^*) is amount of data bearing on response estimate per point. Predictors are leaf mass (Mg ha^{-1} for locations, kg for trees), current June to September nocturnal and diurnal fog + low cloud cover (night FLCC and day FLCC, h/d) from 1999 to 2009 (Torregrosa et al. 2016), latitude (°N), current June to July mean precipitation (JJ rain, mm yr^{-1}), previous October to November mean precipitation (pON rain, mm yr^{-1}), fungicide proportion of heartwood increment, tree age (yr), current March to October mean standardized precipitation evapotranspiration index (gs SPEI), elevation (m), distance to ocean (km), and previous October to November mean maximum temperature (pON T_{max}, °C). Sensitivity is mean absolute difference resulting from nudging predictor (delta = 0.05) expressed as proportion of dependent variable's range. Cross-validated correlation (xR^2) is computed as 1 – (residual sum of squares / total sum of squares) and based on leave-one-out cross validation. In models with multiple predictors, strongest predictor (highest sensitivity) is highlighted **bold**, and xR^2 change indicates dependence of final model on number of predictors. Asterisks indicate models illustrated in Fig. 10. Note that 41 locations had fixed-area plots (see Table 5, Fig. 11). Growth efficiency at four locations lacking plots (4, 8, 15, 21) is computed as study tree average (kg kg^{-1} yr^{-1}, 4–8 trees per location).

Dependent variable	Units	Sample size	N^*	Predictor(s)	Sensitivity	xR^2	xR^2 change
Biomass increment							
* 1999 to 2009	Mg ha^{-1} yr^{-1}	41	37	Leaf mass	0.82	0.64	—
* 1999 to 2009	kg yr^{-1}	235	226	Leaf mass	0.74	0.57	—
2001	kg yr^{-1}	235	196	**Leaf mass**, Night FLCC	**0.63**, 0.11	0.64	0.58, 0.06
2002	kg yr^{-1}	235	226	Leaf mass	0.76	0.59	—
2003	kg yr^{-1}	235	58	**Leaf mass**, Latitude	**0.77**, 0.46	0.60	0.49, 0.10
2004	kg yr^{-1}	235	59	**Leaf mass**, Latitude	**0.78**, 0.37	0.60	0.54, 0.06
2005	kg yr^{-1}	235	198	Leaf mass	0.75	0.52	—
2006	kg yr^{-1}	235	198	Leaf mass	0.85	0.52	—
2007	kg yr^{-1}	231	58	**Leaf mass**, Latitude	**0.77**, 0.28	0.61	0.55, 0.06
2008	kg yr^{-1}	231	193	**Leaf mass**, Night FLCC	**0.71**, 0.14	0.60	0.54, 0.07
2009	kg yr^{-1}	231	61	**Leaf mass**, JJ rain	**0.67**, 0.38	0.63	0.53, 0.10
2010	kg yr^{-1}	231	128	**Leaf mass**, Night FLCC	**0.66**, 0.13	0.58	0.51, 0.07
2011	kg yr^{-1}	230	170	**Leaf mass**, Night FLCC	**0.80**, 0.13	0.56	0.51, 0.05
2012	kg yr^{-1}	228	191	**Leaf mass**, Night FLCC	**0.63**, 0.13	0.58	0.50, 0.08
2013	kg yr^{-1}	225	158	**Leaf mass**, Night FLCC	**0.69**, 0.14	0.59	0.50, 0.08
2014	kg yr^{-1}	215	48	**Leaf mass**, Day FLCC	**0.57**, 0.22	0.57	0.48, 0.09
2015	kg yr^{-1}	202	53	**Leaf mass**, Night FLCC, Latitude	**0.60**, 0.14, 0.15	0.59	0.48, 0.06, 0.05
2016	kg yr^{-1}	188	56	**Leaf mass**, Night FLCC, Latitude	**0.64**, 0.19, 0.13	0.63	0.45, 0.11, 0.06
2017	kg yr^{-1}	158	40	**Leaf mass**, Night FLCC, Latitude	**0.60**, 0.16, 0.22	0.64	0.47, 0.11, 0.07
2018	kg yr^{-1}	120	28	**pON rain**, Leaf mass	**0.73**, 0.45	0.53	0.35, 0.18
2019	kg yr^{-1}	71	23	Leaf mass	0.74	0.40	—
Growth efficiency							
* 1999 to 2009	Mg Mg^{-1} yr^{-1}	45	10	Fungicide increment, **Night FLCC**	0.33, **0.39**	0.47	0.25, 0.21
* 1999 to 2009	kg kg^{-1} yr^{-1}	235	46	**Fungicide increment**, Night FLCC	**0.33**, 0.27	0.39	0.24, 0.15
2001	kg kg^{-1} yr^{-1}	235	46	**Fungicide increment**, Night FLCC	**0.32**, 0.20	0.39	0.24, 0.15
2002	kg kg^{-1} yr^{-1}	235	47	**Fungicide increment**, Night FLCC	**0.28**, 0.28	0.36	0.20, 0.17
2003	kg kg^{-1} yr^{-1}	235	42	**Fungicide increment**, Night FLCC, JJ rain, Elevation	**0.32**, 0.14, 0.20, 0.23	0.50	0.23, 0.13, 0.07, 0.06
2004	kg kg^{-1} yr^{-1}	235	40	**Fungicide increment**, Night FLCC, JJ rain	**0.36**, 0.25, 0.17	0.41	0.21, 0.14, 0.06
2005	kg kg^{-1} yr^{-1}	235	46	**Fungicide increment**, Night FLCC	**0.27**, 0.22	0.38	0.24, 0.14
2006	kg kg^{-1} yr^{-1}	235	46	**Fungicide increment**, Night FLCC	**0.25**, 0.20	0.34	0.21, 0.13
2007	kg kg^{-1} yr^{-1}	231	46	**Fungicide increment**, Night FLCC	**0.27**, 0.25	0.39	0.24, 0.14
2008	kg kg^{-1} yr^{-1}	231	46	**Fungicide increment**, Night FLCC	**0.28**, 0.26	0.40	0.25, 0.16
2009	kg kg^{-1} yr^{-1}	231	47	**Fungicide increment**, Night FLCC	**0.30**, 0.29	0.45	0.27, 0.18
2010	kg kg^{-1} yr^{-1}	231	45	Fungicide increment, Night FLCC, **Age**	0.26, 0.31, **0.38**	0.44	0.24, 0.15, 0.05
2011	kg kg^{-1} yr^{-1}	230	62	**Age**, Night FLCC	**0.53**, 0.45	0.36	0.16, 0.20
2012	kg kg^{-1} yr^{-1}	228	43	Fungicide increment, Night FLCC, **Age**	0.30, 0.31, **0.34**	0.48	0.27, 0.14, 0.06
2013	kg kg^{-1} yr^{-1}	225	40	**Fungicide increment**, Night FLCC, Elevation	**0.40**, 0.35, 0.25	0.46	0.24, 0.16, 0.07
2014	kg kg^{-1} yr^{-1}	215	43	Fungicide increment, Night FLCC, Elevation	**0.37**, 0.32, 0.23	0.51	0.29, 0.16, 0.06
2015	kg kg^{-1} yr^{-1}	202	49	**pON rain**, Night FLCC, Age	**0.46**, 0.26, 0.24	0.37	0.20, 0.10, 0.06
2016	kg kg^{-1} yr^{-1}	188	37	**Night FLCC**, Fungicide increment	**0.38**, 0.23	0.44	0.27, 0.17
2017	kg kg^{-1} yr^{-1}	158	29	Latitude, **pON T_{max}**, Ocean	0.61, **0.62**, 0.28	0.49	0.28, 0.15, 0.06
2018	kg kg^{-1} yr^{-1}	120	22	**pON rain**, Night FLCC	**0.96**, 0.22	0.54	0.38, 0.16
2019	kg kg^{-1} yr^{-1}	71	15	Latitude	1.12	0.36	—

skies to clear and explaining some of the 1940 s growth surge. After the war, the pace and intensity of logging increased rapidly, especially in Humboldt County (Farnsworth 1996, see Figure 18), where local oral history suggests that air quality was very poor with smoggy skies obscuring sunlight and deposition of pollutants decreasing cambial activity (Myśkow et al. 2019), which helps to explain the 1950s and 1960s growth suppression. In the location with the lowest residual increments during this period (13), where trees produced > 200 kg yr^{-1} less than expected for their size for ~20 yr (Fig. 3**a**), the growth suppression coincided with logging activity in the Redwood Creek basin (Best 1991). Most of this lumber was processed in several local mills capable of delivering smog to these trees via prevailing winds (R. Van Pelt, unpublished). After 1970, the Clean Air Act promoted clear skies as 'beehive burners' were banned, perhaps allowing *Sequoia* in these forests to take advantage of abundant sunlight and less air pollution. Primary forests near the northern (1, 2), eastern (7, 22, 24, 28), and southern (41–45) range limits do not exhibit similar patterns. Two potential contributors to this discrepancy are 1) differences in logging history and 2) climatic factors (e.g., higher temperatures, less rainfall) limiting growth. Further research on the air pollution hypothesis is warranted, especially as it relates to deposition of toxins on leaf surfaces and their effects on wood production.

In secondary forests, decreasing trends in radial increment and increasing trends in volume increment (Fig. 2) are expected consequences of post-logging stand development. Most of the study trees arise as trunk reiterations from stumps (Sillett et al. 2019a, see Figure 9). After logging, these reiterations gained height rapidly and are now the tallest trees in the regenerating forest. Prior to 1950, when these trees (excluding veterans) average 71 yr old and 43 m tall, radial increments decrease as volume increments increase, because height increments are

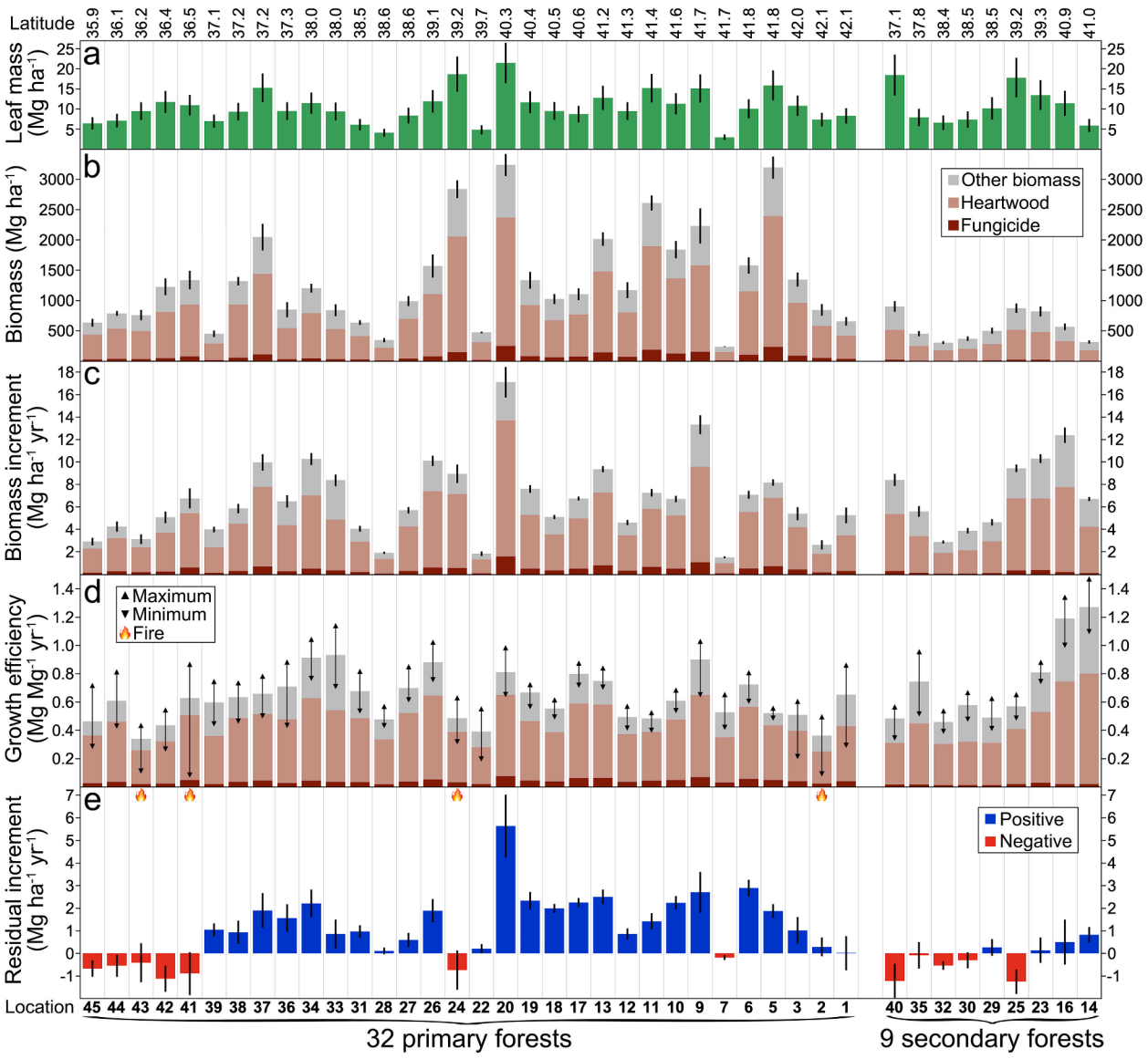

Fig. 11. Twenty-first century (2001–2020) biomass and growth increments for 32 primary and 9 secondary forest locations with sample plots (Table 5). (**a**) Plot leaf mass is computed by summing allometric estimates for all dominant and codominant *Sequoia* trees and dividing by plot area. Values are most recent estimates ± 1 S_E. (**b**) Plot biomass is computed by summing allometric estimates for all dominant and codominant *Sequoia* trees, dividing by plot area, and partitioning into heartwood, fungicide, and other (leaf, bark, sapwood, dead) components. Values are most recent estimates ± 1 S_E. (**c**) Plot biomass increment is computed by summing allometric estimates for all dominant and codominant *Sequoia* trees, dividing by plot area, and partitioning into heartwood, fungicide, and other components. Values are 21st century means ± 95 % confidence intervals. (**d**) Plot growth efficiency is computed as biomass increment divided by leaf mass. Values are 21st century means with error bars showing maximum (▲) and minimum (▼) annual values per location. Fire symbols beneath bars highlight locations burning during measurement period (2 = 2017 Chetco Bar Fire, 24 = 2008 Orr Fire, 41 and 43 = 2016 Soberanes Fire). (**e**) Plot residual increment is calculated as difference between observed and expected biomass increments based on null hypothesis of uniform growing conditions since 1901 (see Fig. 3). Faster-than-expected growth is highlighted blue, and slower-than-expected growth is highlighted red. Values are 21st century means ± 95 % confidence intervals. Locations are ranked from south (left) to north (right) within forest type. (For interpretation of the references to color in this figure legend, the reader is referred to the web version of this article.)

large (maximum = 200 cm yr^{-1}, mean = 58 cm yr^{-1}) and wood is being deposited over a rapidly expanding cambium surface (maximum = 2.6 m^2 yr^{-1}, mean = 1.1 m^2 yr^{-1}). Unencumbered by taller neighbors and perhaps bolstered by the pre-existing root system of the logged forest (Sillett et al. 2020), dominant trees gain biomass faster than expected for their size when young. Eventually subordinate neighboring trees close the canopy, constraining performance of dominants via competition for light and soil resources until tree mortality and other disturbances eventually re-open the canopy (Franklin et al. 2002, Iberle et al. 2020). Well over a century after logging, mature secondary forests are significantly more crowded than primary forests with 62 ± 3 vs 35 ± 2 dominant and codominant trees per hectare (Table 5, mean ± 95 % confidence interval, t = -7.4, $P < 0.0001$). Thus, positive residual increments during early stand development followed by decades of negative residual increments are typical of mature secondary *Sequoia* forests, as evident in most of the locations we studied (Fig. 3**b**). Growth suppression in the 1950s and 1960s in at least three northern locations (4, 15, 16) may be related to poor air quality associated with logging of nearby primary forests as previously discussed. A 20th century growth surge is shorter in duration and less pronounced in secondary forests, most of which exhibit growth suppression coincident with recent drought (Fig. 3**b**) and all but one of which have 21st century plot residual increments that are negative or indistinguishable from zero (Fig. 11**e**). This performance discrepancy between primary and

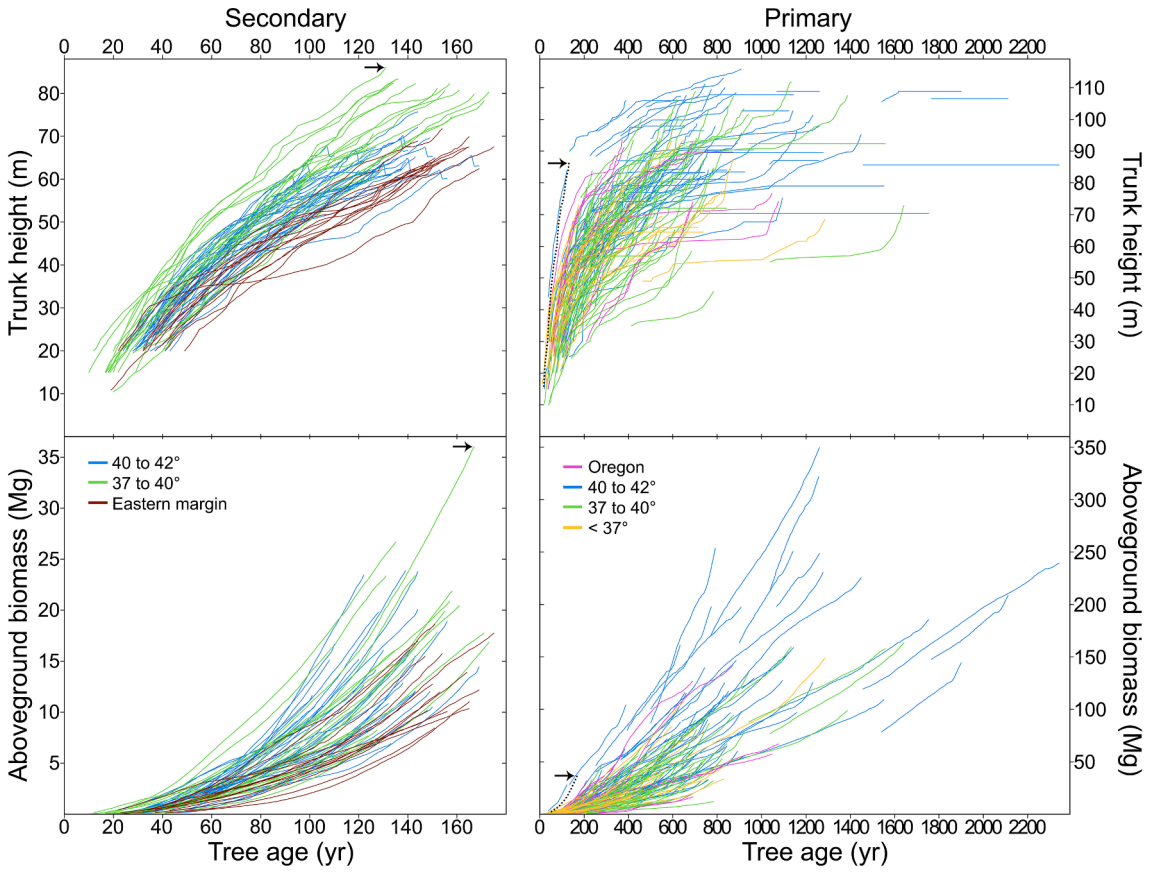

Fig. 12. Reconstructed height and biomass development of 235 study trees in secondary and primary forests. Individual tree size histories (time series) are represented with lines color-coded by latitude and geography (eastern margin includes 3 locations [29, 32, 35] in Napa and Contra Costa Counties). In upper panels, trunk piths accessed by core-sampling reveal heights back through time with interpolation occurring in proportion to radial increments of nearest tree-ring samples. Twelve secondary forest trees (40 to 42° latitude) experimentally topped in 2014 show late dips in trunk height. Flat lines indicate long dead or broken tops in trees lacking core samples from reiterated trunks above break. In lower panels, aboveground biomass is reconstructed in proportion to main trunk wood volume at annual increments. Note that height and biomass dimensions are scaled differently on left and right. Arrows indicate tallest and highest-biomass trees in secondary forests, whose reconstructed development are shown as dotted lines on right.

secondary forests may be related to differences in climatic sensitivity.

4.2. Changing dendroclimatic responses since 1901

Using monthly climatic data available since the start of the 20th century, our approach to dendroclimatic analysis first utilizes traditional methods to identify key variables affecting radial growth, quantifies the temporal stability of these relationships, and then examines how climatic variation influences biomass production across the *Sequoia* range. Climatic variables are generally poor predictors of radial growth variation in tall *Sequoia* forests. Strong correlations between tree-ring indices and climatic drivers are expected if carbon assimilation is the predominant factor limiting wood production (i.e., source limitation), but cambial activity in tall *Sequoia* forests may be largely controlled by the drying power of air. Ample photosynthesis under favorable conditions can yield little woody biomass if cambial cell division and enlargement are inhibited by high nocturnal VPD (Zweifel et al. 2021), thereby leaving few cells available for deposition of cellulose and lignin in secondary cell walls to become sapwood tracheids (Rathgeber et al. 2016). Such sink limitation in which tissue formation controls assimilation is evident in the decoupling of radial growth (measured by tree rings) and gross primary productivity (GPP, measured by eddy-covariance flux towers) recently observed in 78 temperate forests, where radial growth is more sensitive to water availability and GPP is more sensitive to temperature constraints (Cabon et al. 2022). We see evidence that sink limitations largely control wood production in *Sequoia* and are becoming increasingly prominent as temperatures rise.

The most influential monthly climatic variable we examined (SPEI) is a drought index that accounts for the effects of temperature variability (Vicente-Serrano et al. 2010). Our calculation of SPEI expresses the water balance over a 12-month window, where high values indicate wet years and low values indicate dry years. Significantly less radial growth occurs during dry years, and vice versa, in 15 of 19 (79 %) locations south of 39° but only 2 of 26 (8 %) locations north of 39° (Fig. 4). The most extreme latitudinal anomalies with respect to SPEI are attributable to local water availability. Trees from a primary forest at 36.2° (43) exhibit no ring index correlations with SPEI, similar to the situation in all primary forests north of 40° and unlike other locations near the southern range margin. With easy access to a spring-fed stream (2 ± 1 m vertical distance, 6 ± 2 m horizontal distance, mean ± 1 S_E), these trees occupy a hydrologic refugium (McLaughlin et al. 2017) amidst a landscape that becomes climatically unsuitable for *Sequoia* over relatively short distances (Fig. 1). In contrast, trees from a secondary forest at 40.9° (15), which receives the least annual rainfall north of 40° and less rainfall than all but four locations south of 40° (Table 2), stand farther from streams (5 ± 2 m vertical distance, 17 ± 7 m horizontal distance, mean ± 1 S_E) and exhibit a strong radial growth response to SPEI. Several locations (2, 6, 7, 8, 14, 18, 19, 22) have trees standing much farther from streams, but the hydrological environment of *Sequoia* is difficult to define accurately without knowledge of soil water storage and subsurface flows (Francis et al. 2020).

From a water balance perspective, California's climate is undergoing

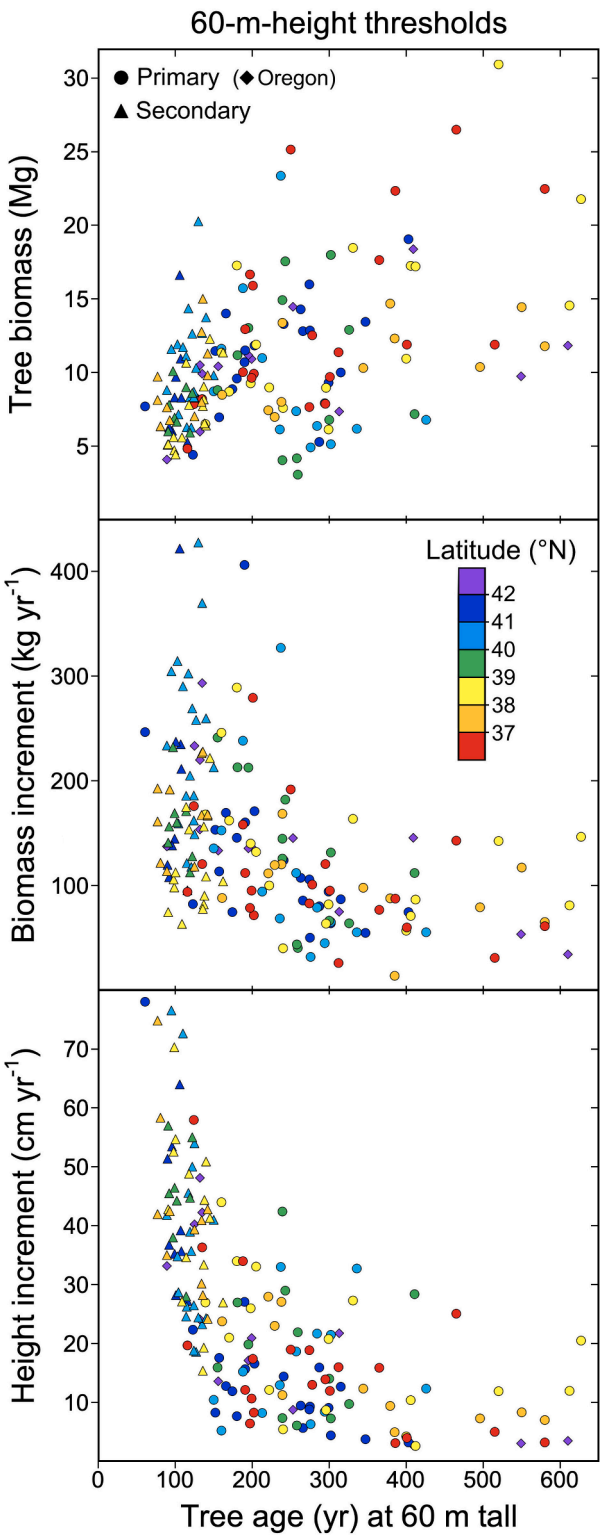

Fig. 13. Reconstructed age, biomass, and growth increments for 169 study trees whose trunk pith was reached by core sampling 60 m above ground level. Biomass increment and height increment are 5-yr means centered on year tree first exceeds 60 m tall. Symbols for primary and secondary forest trees are color-coded by latitude. All trees are in California except those north of 42° (Oregon).

aridification even without substantial changes in precipitation due to rising temperatures (Williams et al. 2019). The sensitivity of radial growth and biomass increment to drought is increasing in most locations (Fig. 6**a**), including forests where significant positive ring index vs SPEI and rain correlations are strengthening and those where correlations are becoming positive (Fig. 5). Such shifts are occurring in forests worldwide as rising temperature and associated VPD increases limit wood production even under conditions of high soil water availability (Novick et al. 2016, Babst et al. 2019, Anderson-Teixeira et al. 2021). In *Sequoia* forests, positive correlations between ring index and summer minimum temperatures (JA T_{min}) are weakening and disappearing in all but one location (Fig. 5). This secondary forest (14) in northern Humboldt County, which has the lowest growing season temperatures among the 45 locations (Table 2), may be the last *Sequoia* forest operating below its thermal optimum for wood production (Pedlar & McKenney 2017). The situation in *Sequoia* may be similar to that observed in many other tree species, where positive ring width vs. summer temperature correlations are prevalent in cooler forests, and the opposite is true in warmer forests (Wettstein et al. 2011, George & Ault 2014). The sensitivity of radial growth to maximum temperatures, which are rising less rapidly than minimum temperatures (Davy et al. 2017, Zhao et al. 2020) and may even be decreasing in some parts of coastal California due to warming of inland areas stimulating sea-breeze activity (Lebassi et al. 2009), is weakening in some northern locations but increasing or stable in most locations south of 39° (Fig. 5). Since *Sequoia* in central and southern forests are generally more responsive to drought than in northern forests, it makes sense that rising temperatures would exacerbate the situation.

The changing magnitude of extreme climatic effects on *Sequoia* productivity is illustrated by latitudinal response curves for relative increments (Fig. 6**a**). Latitude is especially useful for modeling *Sequoia* growth responses to climate, because the 45 locations are widely distributed with little overlap, and latitude integrates substantial climatic variation (Fig. 1, Table 6). Shifts in tree performance between the 60-yr series show which portions of the *Sequoia* range are responding the most to changing conditions. In *Sequoia* forests north of 39°, the wettest relative increments are lower (< 1) during the earlier period and higher (> 1) during the later period. Lower biomass production during extremely wet years in rainforests might be attributable to the shading effects of heavy cloud cover. If CO_2 is more limiting than light availability, much higher atmospheric CO_2 concentrations during the later period (Fig. 6**b**) may stimulate photosynthetic activity and biomass production (Yang et al. 2016, Haverd et al. 2019, Chen et al. 2022). During extremely dry years of the earlier period, relative increments are consistently low (0.7–0.9), but during the later period these relative increments are substantially higher (1.0–1.1) north of 40° (Fig. 6**a**). This upward shift in the driest relative increments may be attributable to increasing water use efficiency accompanying higher atmospheric CO_2 concentrations where VPD is low enough to prevent stomatal closure (Grossiord et al. 2020, Mathias & Thomas 2021). Furthermore, relatively slow leaf turnover may induce a lag in structural responses of *Sequoia* crowns to elevated CO_2, including lower stomatal density (Kouwenberg et al. 2003, Konrad et al. 2008, Engineer et al. 2014), while reduced stomatal aperture enhances water use efficiency in existing leaves before new leaves acclimate (Konrad et al. 2008, Engineer et al. 2016). During both periods, the driest years—as indexed by SPEI—exhibit lower biomass production than the wettest years across most of the range, but north of ~41° the response curves converge. *Sequoia* in these rainforests may be the least sensitive to drought in part because they receive substantially more summer fog and low cloud cover (Fig. 1), which can be readily absorbed by leaves and reduce evapotranspiration (Burgess & Dawson 2004, Fischer et al. 2009, Limm et al. 2009).

Table 10
Summary of crown structures and arboreal biodiversity encountered in 235 study trees across 45 locations. Epiphyte species include only vascular plants (**Supplementary Fig. 3**). Number of trees per location harboring two most frequent epiphyte species (*Polypodium scouleri*, *Vaccinium ovatum*) is indicated. Other types of biodiversity are defined as follows: A = *Aneides vagrans* salamander, D = dead spire top, G = granary of woodpecker (*Melanerpes formicivorous*), H = hollow trunk, M = murrelet nest (*Brachyramphus marmoratus*), P = poison vine (*Toxicodendron diversilobum*), R = raven nest (*Corvus corax*), S = squirrel nest (*Glaucomys* or *Tamiasciurus* spp.), T = termites, V = vole nest (*Arborimus* sp.), W = wasp or bee nest (*Vespula* or *Apis* spp.).

		Measurements		Diameter (cm)		Epiphyte	Trees with	Trees with	Other
Location	Trees	Limbs	Trunks	Mean	Maximum	Species	*P. scouleri*	*V. ovatum*	Biodiversity
Primary forests									
1	5	0	0	—	—	0	0	0	—
2	5	6	44	13	50	3	0	2	—
3	5	32	90	17	56	4	1	1	—
5	6	194	498	28	197	6	4	2	A, H, S, W
6	5	82	249	16	141	6	2	2	D, H
7	5	0	7	5	13	0	0	0	P
9	6	22	81	29	55	3	2	1	H
10	5	228	892	27	180	8	3	2	A, H
11	5	290	1787	27	190	8	5	3	A, M
12	5	70	114	13	67	1	0	0	—
13	8	367	567	22	125	5	3	2	D, M, S, V, W
17	5	0	15	9	28	1	0	2	D
18	5	34	79	25	124	3	1	0	—
19	5	14	128	15	69	0	0	0	S
20	7	86	232	15	143	2	0	1	A, M, S
22	5	2	46	15	48	0	0	0	—
24	4	134	380	16	75	1	0	0	H, T
26	5	16	68	10	54	0	0	0	—
27	5	2	24	25	71	5	0	0	H, P, R
28	5	0	0	—	—	0	0	0	—
31	6	0	4	5	9	0	0	0	H, P
33	5	0	17	9	16	0	0	0	H
34	4	0	45	26	72	0	0	0	—
36	5	0	0	—	—	0	0	0	T
37	5	22	131	17	133	0	0	0	H, S, T
38	5	16	172	21	83	0	0	0	—
39	5	0	5	8	11	0	0	0	
41	6	46	112	37	155	1	0	0	G, T, W
42	5	2	6	12	24	0	0	0	D, G, T, W
43	5	0	3	5	6	0	0	0	T
44	4	0	0	—	—	0	0	0	—
45	5	0	2	3	3	0	0	0	H, T
Secondary forests									
4	4	0	0	—	—	0	0	0	—
8	8	0	0	—	—	0	0	0	—
14	5	10	61	14	45	0	0	0	—
15	8	0	0	—	—	0	0	0	—
16	5	0	14	10	14	0	0	0	—
21	4	0	12	5	8	0	0	0	H
23	5	0	0	—	—	0	0	0	—
25	5	0	0	—	—	0	0	0	P, T
29	5	0	8	6	7	0	0	0	—
30	5	0	3	5	6	0	0	0	—
32	5	0	0	—	—	0	0	0	—
35	5	0	17	7	13	0	0	0	—
40	5	0	0	—	—	0	0	0	—

4.3. *Sequoia responses to hotter drought*

Drought accompanied by warmer temperatures—hotter drought—is now a global environmental concern as forests become increasingly vulnerable to tree mortality (Allen et al. 2015). From 2012 to 2015, forests across California experienced progressively more severe canopy water loss from a drought unprecedented in severity (Asner et al. 2016, Kwon & Lall 2016, Goulden & Bales 2019), and most of these forests are in the midst of another multi-year drought beginning in 2020 (NDMC 2022). After an unusually wet 2011, four consecutive drought years in *Sequoia* forests are accompanied by steadily rising temperatures (Fig. 7), which compound the effects of water stress by increasing both VPD and the need for evaporative cooling of leaves. Unlike central and southern forests, growth efficiency exhibits only modest declines during the first three years of drought in forests north of 40°, plummeting during the fourth year. This sudden decline is similar to the situation in central Europe, where the first of two consecutive hotter drought years (2018–19) result in diminished growth typical of an average drought but the second is much more severe (Schnabel et al. 2022). North of 40°, the cumulative stress of consecutive drought years is worse in secondary than primary forests, contradicting results from a global meta-analysis showing greater reductions in growth of larger trees during drought than smaller trees (Bennett et al. 2015). However, these studies quantify growth as changes in trunk DBH, whereas our metric—growth efficiency—relativizes biomass increment by leaf mass, allowing growth variation unrelated to tree size to be expressed. During the peak of the drought (2014–15), residual increments are negative in 11 of 12 (92 %) secondary forests but only 12 of 32 (38 %) primary forests with location means ($\pm$ 1 S_E) of -37 ± 9 and 28 ± 11 kg yr^{-1}, respectively (Fig. 3). The only primary forest north of 40° with a negative residual increment is near the eastern range margin (location 7). In other words, trees in secondary forests generally produce less biomass than expected for their size during extreme drought, unlike the situation in primary forests, especially those north of 40°. Recovery from extreme drought is another

story.

After four consecutively hotter drought years, growing season temperatures across the *Sequoia* range cool a bit with SPEI returning to normal in 2016 followed by an exceptionally wet 2017 that is considerably cooler in northern but not central or southern locations (Fig. 7). North of 40°, growth efficiency of *Sequoia* recovers to pre-drought (2011) levels with secondary forests recovering faster than primary forests. Compared to northern secondary forests, post-drought recovery of growth efficiency in central secondary forests is slower (Table 8), falling short of pre-drought levels despite unusually high precipitation in 2017. Among primary forests, post-drought recovery in northern and central locations is statistically indistinguishable (Table 8), whereas growth efficiency in southern locations is even lower in 2017 than at the peak of the drought (Fig. 7). Unusually high post-drought temperatures south of 40°, especially T_{min} in 2017, appear to preclude recovery of growth efficiency by maintaining high nocturnal VPD that inhibits cambial activity despite wet soils (Yuan et al. 2019, Zweifel et al. 2021). The extremely low post-drought growth efficiency we observe in southern primary forests (< 0.4 kg kg^{-1} yr^{-1}) occurs despite exclusion of 2017 data from two locations (41, 43) that burned in the Soberanes Fire of July 2016 (Langford et al. 2019). Trees from these locations exhibit a classic post-fire response in which the 2017 annual ring is extremely small or missing (Carroll et al. 2018a). Compared to other *Sequoia* forests, the much higher growth efficiency in northern secondary forests ($>$ 1 kg kg^{-1} yr^{-1} except 2015) and faster post-drought recovery are largely attributable to convergence of a biotic factor that distinguishes these forests—low investment in heartwood defense—and an abiotic factor that promotes cambial activity—summer fog and low cloud cover.

4.4. Biotic and abiotic determinants of 21st century productivity

Widely recognized as a key determinant of *Sequoia*'s restricted coastal distribution, occult precipitation—fog and condensing moisture—ameliorates the negative effects of the summer dry season by extending the period of active photosynthesis and repairing water-stress induced damage (Burgess & Dawson 2004, Limm et al. 2009, Simonin et al. 2009, Chin et al. 2022b). We utilize a static metric of summer fog and low cloud cover (FLCC) based on a 11-yr analysis of satellite data (Fig. 1, Torregrosa et al. 2016). Despite the lack of temporal resolution, we find strong evidence for a positive effect of FLCC on *Sequoia* productivity—it is among the best predictors of biomass increment and growth efficiency in 10 of 19 (53 %) and 17 of 19 (89 %) individual years since 2001, respectively, far more than any other abiotic factor (Table 9). The predominance of night vs. day FLCC as a predictor in these models is striking confirmation of the importance of sink limitations. Nocturnal humidity and leaf wetness are necessary to generate sufficient turgor pressure for cambial activity, allowing photosynthate to be invested in tissue formation (Körner 2015, Zweifel et al. 2021). During the 11-yr period coincident with the satellite data (1999–2009), night FLCC is the second-best predictor of biomass increments, explaining just under 5 % of growth variation (results not shown). Leaf mass is by far the strongest predictor of *Sequoia* biomass increments at both tree and plot levels (Table 9, Fig. 10**a**), confirming results from previous studies of the tallest conifers (Sillett et al. 2015b, 2021). Relativizing biomass increments by leaf mass allows growth variation unrelated to photosynthetic capacity to be expressed, highlighting the critical role of investment in heartwood defense (Loehle 1988).

Sequoia growth efficiency is highest in secondary forests with the least investment in defense as indexed by the fungicide proportion of heartwood increments (Fig. 10**b**). While heartwood proportions of biomass increments increase steadily as trees enlarge with age (Fig. 8**b**) and partly explain the age-related decline in *Sequoia* growth efficiency (Sillett et al. 2020), decay resistance of heartwood correlates with the amount of extractives (Wilcox & Piirto 1974, Taylor et al. 2006) and influences growth efficiency more than the amount of heartwood produced. Deposition of fungicide and other extractives occurs at the transition zone, whose width varies seasonally from one to a few annual rings of the innermost (oldest) sapwood (Hillis 1987). Among the 235 study trees, heartwood deposition occurs across 66 to 1226 m^2 (262 ± 12 m^2, mean ± S_E) of transition zone per trunk into annual rings that are decades old (primary forest mean = 38 yr, range = 8–155 yr; secondary forest mean = 15 yr, range = 5–34 yr; N = 463 and 269 cores, respectively). Numerous molecular constituents of *Sequoia* heartwood have been characterized, including polyphenolic compounds known as sequirins that may account for much of its durability (Balogh & Anderson 1965, 1966; Hatam & Whiting 1969) as well as volatile compounds that are lost upon exposure to dry air (Jones & O'Hara 2012) and convey a distinctive bouquet to fresh samples. After deposition from sapwood ray parenchyma into cells walls and lumens of adjacent tracheids, polymerization of some compounds makes them indistinguishable from (or bound to) lignin such that extraction by solvents may be incomplete (Hillis 1987). Our estimates of fungicide mass at any given height are derived from density differences of sapwood-heartwood pairs collected at 10-m height intervals (Fig. 10**a**) and may be underestimates, because high concentrations of non-structural carbohydrates and other metabolites in sapwood parenchyma are exhausted during its conversion to heartwood at the transition zone (Hillis 1987). Alternatively, if wood density decreases over time as trees respond to environmental changes (e.g., atmospheric fertilization, Pretzsch et al. 2018), heartwood density may be higher merely because the sapwood from which it is derived was denser. We suspect these potentially confounding issues are minor, because our wood density estimates are within the range of those documented 90 yr earlier (Luxford & Markwardt 1932), and the amount of extractives they report for northern primary forests (5–28 % of heartwood mass) is remarkably similar to ours (Fig. 9**a**). For the purpose of estimating each tree's fungicide mass, we assume uniform distribution of extractives along the heartwood radius from transition zone to pith, but decay resistance of *Sequoia* heartwood may diminish toward the pith (Resch & Arganbright 1968, Clark & Scheffer 1983) if less fungicide was deposited when trees were younger, or some decay of inner heartwood has already occurred. Thus, unlike our estimates for fungicide increments (Fig. 11**cd**), which are scaled by measured deposition area to reflect the current situation in outermost (youngest) heartwood, our estimates of plot-level fungicide mass (Fig. 11**b**) may be too high. Further work is needed to understand developmental changes contributing to observed radial gradients of heartwood decay resistance as well as genetic and environmental variation associated with the distribution of specific compounds.

Higher fungicide content of heartwood in primary vs. secondary forests explains why *Sequoia* heartwood decay resistance is more than twice as high in the former (Resch & Arganbright 1968, Clark & Scheffer 1983). Spatial variation in the importance of sink limitations provides an explanation for this difference. Consistently low VPD during summer due to high night FLCC allows *Sequoia* in northern secondary forests to invest a greater proportion of photosynthate in sapwood production, whereas sink limitations farther south constrain sapwood production and may promote heavier fungicide deposition in heartwood fueled by accumulation of non-structural carbohydrates. But why is growth efficiency in northern secondary forests so much higher than in northern primary forests, which also experience high night FLCC? Another form of sink limitation may be operating. As a consequence of gravity, water potential declines with increasing height in tall trees, constraining leaf anatomy and physiology (Woodruff et al. 2004, Koch et al. 2004, Ishii et al. 2008, Oldham et al. 2010) and potentially allowing photosynthate to accumulate far beyond what can be incorporated into wood production. Investment of surplus carbohydrates in heartwood deposition may explain why the fungicide content of heartwood increases with height such that uppermost trunks have similarly high values regardless of forest type or region (Fig. 9**a**) and why taller trees in primary forests have significantly higher fungicide increments than shorter trees in secondary forests. Since upper crowns of dominant trees are well-illuminated, more sugars are locally available for heartwood

deposition. As sugar transport occurs downward through the inner bark (secondary phloem), the interior surface of transition zone expands radially outward, perhaps diluting along the way and leaving less energy available for fungicide biosynthesis in the lower trunk. Wind and animal damage in the upper crown provide frequent opportunities for decay fungi to enter the tree. Investing more in heartwood defense makes biological sense, because most of the photosynthesis and sexual reproduction occur in the upper crown, where fungal decay can promote structural failure and severe loss of reproductive capacity. Incidentally, the portion of trunk within the crown was ignored in previous studies of *Sequoia* heartwood characteristics, as this so-called crown wood has little commercial value. Thus, our finding higher heartwood density and fungicide content of *Sequoia* crown wood compared to the rest of the trunk is new and has implications for both carbon sequestration and conservation of biodiversity.

Before discussing restoration management for non-timber values, brief consideration of two other abiotic determinants of *Sequoia* productivity is warranted. First, after accounting for night FLCC and fungicide increments, elevation explains 6–7 % of additional growth efficiency variation during drought (Table 9). In both 2013 and 2014, growth efficiency steadily declines with increasing elevation in parallel with observed increases in nocturnal VPD (V_{min}, Table 6). This result is further evidence for sink limitations, whereby low atmospheric moisture availability at high elevation reduces recovery of turgor pressure at night and constrains cambial activity (Zweifel et al. 2021). Second, maximum temperature during the previous autumn impacts *Sequoia* productivity during the wettest year of the 21st century so far—2017 (Table 9). Though previous autumn (or winter) temperatures are positively correlated with radial increments in other western North American conifers (Chen et al. 2010, Miyamoto et al. 2010), *Sequoia* exhibits consistently negative correlations between pON T_{max} and ring indices in several locations (Fig. 4). Unusually high previous autumn temperatures might simultaneously reduce photosynthesis and increase stem respiration, depleting non-structural carbohydrates (NSC) that would normally accumulate after radial growth has ceased and leaving fewer resources available for radial growth the following spring—similar to the way climatic extremes deplete carbon reserves in *Fagus sylvatica* (D'Andrea et al. 2021). The opposite scenario—low previous autumn temperatures promoting NSC accumulation and stimulating spring growth—might also occur. Both scenarios are speculative and dependent on a strong relationship between temperature and stem respiration in conifers (Ryan et al. 1995, Zha et al. 2004). However, recently observed trends of rising temperatures and diminished precipitation during autumn across California (Goss et al. 2020) make the former scenario increasingly likely to constrain *Sequoia* productivity.

4.5. Forest management for long-term carbon sequestration

Our focus on tall *Sequoia* forests ignores those lacking trees over 60 m tall, including the vast majority of regenerating forests, which are logged repeatedly, and some primary forests growing in extreme environments such as windswept ridges and the driest margins of the species range. We also ignore subordinate trees that grow far more slowly than any we measured. Thus, our findings are most relevant to restoration management designed to accelerate tree size development toward tall primary (old-growth) forest reference conditions, including any silvicultural practices (e.g., thinning from below) that allow big trees to develop. Our emphasis on dominant and co-dominant trees is justified because these individuals not only create the upper canopy, but they also represent the bulk of forest biomass and control stand-level biomass production (Bastin et al. 2015, 2018; Sillett et al. 2020; Piponiot et al. 2022). For example, among plots where previous inventories quantified the contributions of all vegetation, dominant and co-dominant *Sequoia* trees contribute 49–86 % of the aboveground biomass and 28–79 % of the biomass increment (Table 5). Maximum leaf mass, biomass, and biomass increment occur in an alluvial forest (20) with trees up to 113 m tall, 250 Mg biomass, and 1260 yr old (Fig. 11**abc**, Table 2). Since the original 5-yr re-measurement period included multiple years of hotter drought, the 19.2 Mg ha^{-1} yr^{-1} rate we reported as the maximum primary forest biomass increment (Sillett et al. 2020) may be an underestimate. By scaling the dominant and codominant *Sequoia* contributions to this plot's total, we estimate an average 21st century biomass increment of 24.1 Mg ha^{-1} yr^{-1}, which exceeds the highest productivity observed in a secondary *Sequoia* forest (22.9 Mg ha^{-1} yr^{-1}, Iberle et al. 2020). Scaled in this way, the other primary forest plots exhibit average 21st century plot biomass increments of 11.4–19.1 Mg ha^{-1} yr^{-1}. The mature secondary forests we studied, which have considerably lower aboveground biomass than most primary forests, have biomass increments that are at least as high as all but the most productive primary forests, because they have similar photosynthetic capacities (Fig. 10**a,** **11ac**). Even though very large-crowned *Sequoia* in primary forests have the greatest individual biomass increments known, too few of them can fit into a hectare to increase quantities of well-illuminated leaves beyond what is achievable in much shorter secondary forests containing many more trees per hectare (Sillett et al. 2020).

Despite similar biomass increments, smaller heartwood proportions of biomass and lower fungicide increments imply that secondary forests are generally less effective than primary forests at long-term carbon sequestration. Across the species range, northern secondary forests produce heartwood with the least fungicide and may thus be least effective for maximizing this non-timber value. However, decay resistance will improve as these trees gain height, heartwood deposition area expands in their upper trunks, and the heartwood proportion of biomass increases with tree age (Fig. 9**b**). Lower growth efficiency of *Sequoia* trees in central vs. northern secondary forests (Fig. 11**d**) may be attributed to higher sink limitations south of 40° with higher fungicide increments enhancing their potential for long-term carbon sequestration. Diminishing growth efficiency is expected as temperatures rise and elevated VPD constrains cambial activity, so *Sequoia* forests may produce progressively less biomass, albeit with higher durability. This shift from a period dominated by the positive effects of atmospheric fertilization to a warming-dominated period of increasing sink limitations (Peñuelas et al. 2017, Denissen et al. 2022) coincides with a sharp drop in VPD observed after 1990 (Yuan et al. 2019), leveling off of the photosynthetic response to rising CO_2 (Walker et al. 2021), and cessation of the 20th century growth surge that occurred north of 37° (Fig. 2). The greatest accumulation of durable biomass occurs in primary *Sequoia* forests with relatively few big trees per hectare (Van Pelt et al. 2016, Sillett et al. 2020), and carbon sequestration is maximized when these trees maintain a modest growth efficiency. For example, the plot with the second highest biomass (5) has a relatively low growth efficiency that is least variable among 41 locations (21st century mean = 0.52 ± 0.01 Mg Mg^{-1} yr^{-1}), but this rainforest with trees up to 108 m tall, 350 Mg biomass, and 1280 yr old exhibits the highest heartwood proportion of biomass (83 %), the third highest fungicide proportion of heartwood increment (11 %), and the fourth highest fungicide increment (750 kg ha^{-1} yr^{-1}), which is more than twice as high as any secondary forest we measured (Fig. 10**b, 11d**). Long-term carbon sequestration can be promoted in secondary forests through silviculture that allows a decreasing number of enlarging trees to produce greater amounts of increasingly decay-resistant heartwood.

How long *Sequoia* requires to achieve the sizes necessary for major contributions to non-timber values varies considerably across the species range and can be estimated by considering reconstructed growth histories of the 235 study trees (Fig. 12). Spanning centuries to more than a millennium, these time series of tree size demonstrate what is possible under a cooler climate with far lower concentrations of atmospheric CO_2 than current conditions (Fig. 6**b**). As such the fastest growing individuals establish the limits of tree performance in tall *Sequoia* forests prior to this era of rising sink limitations. Our sampling reveals substantially slower rates of size development in secondary forests near the eastern range margin compared to the main distribution,

and we suspect the same is true in forests south of 37° where water availability is most limiting (Fig. 1, Table 2). The fastest-growing *Sequoia* in secondary forests we document—87 m in 132 ± 1 yr and 36 Mg in 168 ± 3 yr—are probably maxima for the species, far exceeding what is achievable outside the native range (Sillett et al. 2021, see Table 8). Such extraordinary growth rates, which occur in forests of Mendocino and Santa Cruz Counties (25, 40), can be approached in primary forests only under exceptional circumstances (e.g., large canopy gap in alluvial rainforest), such as we document in one tree from Redwood National Park—84 m and 28 Mg in 122 ± 1 yr. Tree biomass increments > 400 kg yr^{-1} are rarely achievable in secondary forests, except among veterans, and tree biomass increments > 700 kg yr^{-1} occur only in primary forests north of 40° latitude, where *Sequoia* with enormous crowns occasionally produce more than a metric ton (Mg) annually (**Supplementary Fig. 2**). This explains why the largest *Sequoia* we measured occur in forests of Humboldt and Del Norte Counties that contain trees capable of surpassing 110 m tall and 250 Mg biomass in < 1000 yr (Fig. 12).

Regenerating beneath the shade of a tall canopy—or within small gaps where light availability is higher—is the normal developmental context in primary forests, explaining why most *Sequoia* in these forests are so old by the time they exceed 60 m tall (Fig. 13). Among dominant and codominant trees in secondary forests, there is great variation in the time required to reach 60 m tall with some *Sequoia* achieving this feat in less than half the time as others. The 60 m threshold is an important benchmark to consider, because beyond this height tree crowns develop long-lasting structural complexity in the form of reiterated trunks and limbs (Sillett & Van Pelt 2007, Sillett et al. 2018a). It comes as no surprise trees reaching this height faster tend to be smaller (less biomass), because height increments are initially prioritized over biomass increments, especially in dense stands (Oliver & Larson 1996). After trees achieve stand dominance, crown expansion and the concomitant increase of photosynthetic capacity—more leaves—lead to increasing biomass increments. In primary forests with maximum tree heights ≤ 80 m, including eight study locations (Table 2), reaching 60 m tall is a long-term proposition not likely to be achieved for centuries. Silviculture prioritizing height increment over volume increment during stand development will minimize the time required for dominant trees to reach the 60 m threshold, after which selective logging that reduces stand density and allows crown expansion of retained trees has great potential to supply merchantable timber while simultaneously promoting non-timber values. Since *Sequoia* prolifically sprouts (O'Hara et al. 2017), competing reiterated trunks often arise in clusters per stump, so reducing their number over time may promote rapid development of tall co-dominants.

4.6. Forest management for biodiversity

Beyond biomass production and carbon sequestration, the size and structural complexity of tree crowns are important considerations in management. Even in the most impressive primary *Sequoia* forests, a few exceptional individuals per hectare (hereafter Elder Trees, Antoine & Sillett 2022) carry the vast majority of arboreal biodiversity, because their crowns have large appendages—branches, reiterated trunks, limbs—that are in short supply elsewhere (Sillett & Van Pelt 2007). Horizontal surfaces of big limbs and crotches between reiterated trunks promote debris accumulation and local water storage, where opportunistic epiphytes may find more favorable conditions aloft than terrestrially (Hoeber & Zotz 2021). Decay-resistant heartwood inside damaged trunks and limbs creates persistent deadwood substrates with stable water and temperature regimes that are readily colonized by *Vaccinium ovatum* and other ericads (Sillett & Van Pelt 2007, see Ishii et al. 2018 for a similar situation in a related tree species, *Cryptomeria japonica*). The evergreen fern *Polypodium scouleri* forms large mats with live fronds atop accumulations of rhizomes, roots, and humus that may individually exceed 100 kg dry mass (Sillett & Bailey 2003). Such arboreal soils, which may be up to a meter thick, are critically important in canopy hydrology and habitat creation (Enloe et al. 2006, Sillett & Van Pelt 2007, Díaz et al. 2010, Gotsch et al. 2016).

Since epiphytes are, by definition, disconnected from terrestrial soil water and non-parasitic on their hosts, they are entirely dependent on atmospheric resources and responsive to small changes in microclimate, particularly VPD (Darby et al. 2016, Gotsch et al. 2017). The same abiotic factor contributing to sink limitations in *Sequoia* trees may also control the geographic distribution of vascular epiphytes. Well-developed communities of vascular epiphytes occur only in the wettest and foggiest portion of the *Sequoia* range—north of 40° (Table 10, **Supplementary Fig. 3**). Cloud immersion provides water to drought-stressed epiphytes (Ferguson et al. 2022), and ocean fog is also enriched in nutrients (Nyaga et al. 2015). Foliar uptake of water and nutrients is important for many epiphytes just as it is for *Sequoia* (Gotsch et al. 2015, Templer et al. 2015, Chin et al. 2022ab), but the dominant vascular epiphyte in *Sequoia* crowns may rely instead on drought avoidance and harvesting fog drip via roots embedded in arboreal soil; mature *P. scouleri* is xeromorphic with coriaceous fronds and slow water exchange through a waxy cuticle (Kessler & Siorak 2007, Fig. 14**a**).

Among the secondary forests we studied, no limbs and very few reiterated trunks are available as substrates for epiphytes, whereas primary forests often contain trees requiring hundreds of diameter measurements to quantify appendages whose average diameters far exceed the maximum observed in secondary forests (Table 10). There is a clear linkage between crown structural complexity and vascular epiphyte abundance where relatively few large trees serve as biodiversity hubs (Sillett & Van Pelt 2007, Ishii et al. 2018, Tejo & Fontúrbel 2019). Accelerating development of sufficiently large-diameter appendages to serve as substrates for soil-forming epiphytes and habitat for arboreal animals requires intervention in secondary forests, unless we are prepared to wait centuries for their natural development in response to storm damage (Sillett et al. 2018a). Among 235 study trees, only 34—averaging 1157 yr old ($S_E = 75$)—support epiphytic vascular plants in their crowns, and none occur in secondary forests (**Supplementary Fig. 3**). Elder Trees are therefore critical for biodiversity conservation in the portion of the *Sequoia* range with sufficient moisture availability.

Vascular epiphytes are rare in primary *Sequoia* forests south of 40°, so efforts to promote structural complexity in secondary forests for benefits of arboreal soil development, canopy water storage, and ericad flowering/fruiting (especially *Vaccinium ovatum*) are best focused north of 40°. Identification of Potential Elder Trees (PETs) has begun in one such location (14), where five *Sequoia* PETs are now protected in perpetuity for their habitat value and contributions to long-term carbon sequestration. Freshly fallen *P. scouleri* ferns—collected from primary forests after winter storms—were transplanted into their crowns and are being monitored (Fig. 14**b**). These ferns likely require substrates with high water-holding capacity for establishment (Callaway et al. 2002), which Elder Trees provide as soil accumulations and drip zones beneath crotches (Fig. 14**c**). Fern establishment is limited by the precarious gametophyte stage (Fig. 14**d**), which lacks a waxy cuticle and stomata, making it extremely vulnerable to desiccation (Anderson 2021, Krieg & Chambers 2021). Transplanting fern mats bypasses the gametophyte stage and—provided adequate moisture—can promote accumulation of *P. scouleri* and arboreal soil in *Sequoia* PETs. The highly decay-resistant heartwood occurring within upper trunks of tall *Sequoia*, regardless of age (Fig. 9**a**), mitigates concerns that judicious injury will compromise crown structural integrity and suggests that transplanting ericads like *V. ovatum* into freshly exposed heartwood may also be feasible. The PET idea is worth implementing beyond *Sequoia* forests, because large trees are ecologically important and declining globally (Lindenmayer et al. 2012). Thus, promoting and retaining at least a few large trees per hectare can make substantial contributions to forest biodiversity. Regardless of whether climatic conditions permit vascular epiphytes to colonize a particular forest, large trees are important for hosting non-vascular epiphytes (i.e., lichens and bryophytes), including rare and

Fig. 14. Dominant epiphyte of *Sequoia* rainforest canopies is evergreen fern, *Polypodium scouleri*. (**a**) Large *Sequoia* limb 80 m above ground supports sprawling *P. scouleri* mat with *Vaccinium ovatum* (on right) and 50-cm-deep arboreal soil. (**b**) Transplanted *P. scouleri* mat lashed to branch with hemp twine 56 m above ground in secondary forest nearly 1 yr after transplanting. (**c**) Beneath crotch formed by main trunk and reiterated trunk 60 m above ground, *P. scouleri* establishes on wet bark of drip zone. (**d**) Close-up of *P. scouleri* gametophytes with young sporophyte fronds along with pale powdery lichens. White arrow points to 1-cm-wide gametophyte.

previously undescribed taxa (Williams & Sillett 2007; Williams & Tibell 2008, Reese Næsborg et al. 2019). PETs can be incorporated wherever management is amenable to some form of retention forestry in which wood production and conservation are not mutually exclusive (Gustafsson et al. 2012).

4.7. Conclusion

Climatic instability associated with rising temperatures and hotter drought is diminishing resilience—the capacity of forests to withstand and recover from perturbations—and shifting forest dynamics on a global scale (McDowell et al. 2020, Forzieri et al. 2022). Compounding other environmental changes, 11 of our 45 study locations (2, 5, 28, 29, 32, 37, 38, 39, 41, 43, 44) burned in wildfires since 2016, which can cause dramatic post-fire reductions in growth efficiency (Fig. 11**d**, Carroll et al. 2018ab). Extreme fire-resistance and prolific reiteration (sprouting) allow *Sequoia* not only to benefit from prescribed burning but also to recover faster than co-occurring tree species (e.g., *Pseudotsuga menziesii*) after high-severity events (Woodward et al. 2020, Cowman & Russell 2021, Mahdizadeh & Russell 2021). Deployment of pyrosilviculture that involves stand density reductions, use of prescribed burning, and leveraging wildfire treatment effects (North et al. 2021, York et al. 2021) may be effective at promoting non-timber values across the *Sequoia* range, much of which has a fire deficit (Parks et al. 2015). When combined with a PET strategy, reducing stand density by selective logging and prescribed burning can simultaneously promote development of increasingly decay-resistant heartwood, conserve arboreal biodiversity, and improve the resilience of *Sequoia* forests. Despite a limited geographic extent, these forests should be given high priority for conservation, because they protect regionally significant biodiversity (**Supplementary Figs. 3, 4**), possess unrivalled carbon storage capacity, and exhibit tremendous potential for long-term carbon sequestration (Law et al. 2021). Restoring *Sequoia* over 100 m tall to previously logged forests may be possible, but centuries will be required for dominant trees currently < 60 m tall to reach these heights (Fig. 12), and rising temperatures are making this increasingly unlikely (McDowell & Allen 2015). If tree size development is promoted in stages such that the 60 m threshold is reached quickly and at least a few dominant individuals per hectare are thereafter allowed to become Elder Trees, reasonably tall *Sequoia* will be able to repopulate much of the landscape and contribute great values.

Declaration of Competing Interest

The authors declare that they have no known competing financial interests or personal relationships that could have appeared to influence the work reported in this paper.

Data availability

Data will be made available on request.

Acknowledgments

Funding for this research was generously provided by the Save the Redwoods League (Redwoods and Climate Change Initiative, Phase 3) and Kenneth L. Fisher (Chair in Redwood Forest Ecology at Cal Poly Humboldt). We thank California State Parks, Redwood National Park, Siskiyou National Forest, Six Rivers National Forest, Los Padres National Forest, City of Arcata, Bureau of Land Management (Headwaters Forest Reserve), University of California (Angelo Preserve), Land Trust of Napa County, Marin County Parks, East Bay Regional Park District, Santa Lucia Preserve, Santa Lucia Conservancy, the Save the Redwoods League, and other landowners for permission to climb and measure trees as well as logistical support. Jim Campbell-Spickler and Russell Kramer assisted with footprint analyses and fieldwork (tree rigging, core

sampling). We are grateful to Michael Taylor, Zane Moore, John Montague, Mike Palladini, Jay Harris, David Anthon, Terra Fuller, Joanne Kerbavaz, Peter Steel, Serena Hubert, Brian Woodward, Ken Fisher, Shawn Byers, Laurie Wayburn, and Alayna Gray for help selecting study locations; Giacomo Renzullo for help collecting, nurturing, and transplanting *Polypodium scouleri*; Bruce McCune for helpful advice on use of NPMR and interpretation of results; Laurence Schimleck for stimulating discussions and references pertaining to heartwood characteristics; and Emily Burns Hartley for encouraging this study in 2017.

Appendix A. Supplementary data

Supplementary data to this article can be found online at https://doi.org/10.1016/j.foreco.2022.120573.

References

Allen, C.D., Breshears, D.B., McDowell, N.G., 2015. On underestimation of global vulnerability to tree mortality and forest die-off from hotter drought in the Anthropocene. Ecosphere 6, 1–55.

Anderson, O.R., 2021. Physiological ecology of ferns: biodiversity and conservation perspectives. International *Journal of Biodiversity and Conservation* 13, 49–63.

Anderson-Teixeira, K.J., Herrmann, V., Rollinson, C.R., Gonzalez, B., Gonzalez-Akre, E. B., Pederson, N., Alexander, M.R., Allen, C.D., Alfaro-Sánchez, R., Awada, T., Baltzer, J.L., Baker, P.J., Birch, J.D., Bunyavejchewin, S., Cherubini, P., Davies, S.J., Dow, C., Helcoski, R., Kašpar, J., Lutz, J.A., Margolis, E.Q., Maxwell, J.T., McMahon, S.M., Piponiot, C., Russo, S.E., Šamonil, P., Sniderhan, A.E., Tepley, A.J., Vašíčková, I., Vlam, M., Zuidema, P.A., 2022. Joint effects of climate, tree size, and year on annual tree growth derived from tree-ring records of ten globally distributed forests. Global Change Biology 28 (1), 245–266.

Antoine, M.E., Sillett, S.C., 2022. Intentional forests: growing hope for the future. International Dendrology Society Yearbook 2021, 55–67.

Asner, G.P., Brodrick, P.G., Anderson, C.B., Vaughn, N., Knapp, D.E., Martin, R.E., 2016. Progressive forest canopy water loss during the 2012–2015 California drought. Proceedings of the National Academy of Sciences 113, E249–E255.

Babst, F., Bouriaud, O., Poulter, B., Trouet, V., Girardin, M.P., Frank, D.C., 2019. Twentieth century redistribution in climatic drivers of global tree growth. *Science. Advances* 5, eaat4313.

Balogh, B., Anderson, A.B., 1965. Chemistry of the genus *Sequoia*—II: isolation of sequirins, new phenolic compounds from the coast redwood (*Sequoia sempervirens*). Phytochemistry 4 (4), 569–575.

Balogh, B., Anderson, A.B., 1966. Chemistry of the genus *Sequoia*—III: structural studies of isosequirin. Phytochemistry 5 (3), 325–330.

Bastin, J.-F., Barbier, N., Réjou-Méchain, M., Fayolle, A., Gourlet-Fleury, S., Maniatis, D., de Haulleville, T., Baya, F., Beeckman, H., Beina, D., Couteron, P., Chuyong, G., Dauby, G., Doucet, J.-L., Droissart, V., Dufrêne, M., Ewango, C., Gillet, J.F., Gonmadje, C.H., Hart, T., Kavali, T., Kenfack, D., Libalah, M., Malhi, Y., Makana, J.-R., Pélissier, R., Ploton, P., Serckx, A., Sonké, B., Stevart, T., Thomas, D.W., De Cannière, C., Bogaert, J., 2015. Seeing Central African forests through their largest trees. Scientific Reports 5 (1).

Bastin, J.-F., Rutishauser, E., Kellner, J.R., Saatchi, S., Pélissier, R., Hérault, B., Slik, F., et al., 2018. Pan-tropical prediction of forest structure from the largest trees. Global Ecology and Biogeography 27, 1366–1383.

Bates, D., R. Kliegl, S. Vasishth, R.H. Baayen, 2018. Parsimonious mixed models. ArXiv: 1506.04967v2.

Bates, D., Mächler, M., Bolker, B.M., Walker, S.C., 2015. Fitting linear mixed-effects models using lme4. Journal of Statistical Software 67, 1–48.

Beguería, S., Vicente-Serrano, S.M., Reig, F., Latorre, B., 2014. Standardized precipitation evapotranspiration index (SPEI) revisited: parameter fitting, evapotranspiration models, tools, datasets and drought monitoring. International Journal of Climatology 34 (10), 3001–3023.

Bennett, A.C., McDowell, N.G., Allen, C.D., Anderson-Teixeira, K.J., 2015. Larger trees suffer most during drought in forests worldwide. Nature Plants 1, 15139.

Berrill, J.-P., Beal, C.B., LaFever, D.H., Dagley, C.M., 2013. Modeling young stand development towards the old-growth reference condition in evergreen mixed-conifer stands at Headwaters Forest Reserve, California. Forests 4, 455–470.

Best, D.W., 1991. History of timber harvest in the Redwood Creek Basin, northwestern California. U.S. Geological Survey Professional Paper 1454-C, 7 pp.

Briffa K.R., 1995. Interpreting high-resolution proxy climate data—the example of dendroclimatology. Pages 77-94 *in* H. von Storch, A. Navarra (eds.), Analysis of Climate Variability. Springer, Berlin, Heidelberg.

Brodrick, P.G., Asner, G.P., 2017. Remotely sensed predictors of conifer tree mortality during severe drought. Environmental Research Letters 12 (11), 115013.

Bunn, A.G., 2008. A dendrochronology program library in R (dplR). Dendrochronologia 26 (2), 115–124.

Burgess, S.S.O., Dawson, T.E., 2004. The contribution of fog to the water relations of *Sequoia sempervirens*: foliar uptake and prevention of dehydration. Plant Cell and Environment 27, 1023–1034.

Burns, E., R. Campbell, P.D. Cowan, 2018. State of redwoods conservation report. Save the Redwoods League, San Francisco, pp. 50. https://www.savetheredwoods.org/about-us/publications/state-of-redwoods-conservation-report-2018/.

Cabon, A., S.A., Kannenberg, A. Arain, F. Babst, D. Baldocchi, S. Belmecheri, N. Delpierre, et al., 2022. Cross-biome synthesis of source versus sink limits to tree growth. *Science* **376**: 758-761.

Canham, C.D., Murphy, L., Riemann, R., McCullough, R., Burrill, E., 2018. Local differentiation in tree growth responses to climate. Ecosphere 9, e02368.

Carroll, A.L., Sillett, S.C., Kramer, R.D., 2014. Millennium-scale crossdating and interannual climate sensitivities of standing California redwoods. PLoS ONE 9 (1–18), 0102545.

Carroll, A.L., Sillett, S.C., Van Pelt, R., 2018a. Tree-ring indicators of fire in two old-growth coast redwood forests. Fire Ecology 14, 85–105.

Carroll, A.L., Sillett, S.C., Palladini, M., Campbell-Spickler, J., 2018b. Dendrochronological analysis of *Sequoia sempervirens* in an interior old-growth forest. Dendrochronologia 52, 29–39.

Chen, C., Riley, W.J., Prentice, I.C., T.F. Keenan, 2022. CO_2 fertilization of terrestrial photosynthesis inferred from site to global scales. *Proceedings of the National Academy of Sciences* **119**: e2115627119.

Chen, P.-Y., Welsh, C., Hamann, A., 2010. Geographic variation in growth response of Douglas-fir to interannual climate variability and projected climate change. Global Change Biology 16, 3374–3385.

Chin, A.R.O., Guzmán-Delgado, P., Sillett, S.C., Orozco, J., Kramer, R.D., Kerhoulas, L.P., Moore, Z.J., Reed, M., Zwieniecki, M., 2022a. Shoot dimorphism enables *Sequoia sempervirens* to separate requirements for foliar water uptake and photosynthesis. American Journal of Botany 109, 564–579.

Chin, A.R.O., Guzmán-Delgado, P., Sillett, S.C., Kerhoulas, L.P., Ambrose, A.R., McElrone, A.R., Zwieniecki, M.A., 2022b. Tracheid buckling buys time, foliar water uptake pays it back: coordination of leaf structure and function in tall redwood trees. Plant, Cell & Environment 45, 2607–2616.

Chin, A.R.O., Sillett, S.C., 2019. Within-crown plasticity in leaf traits among the tallest conifers. American Journal of Botany 106, 1–13.

Clark, J.W., Scheffer, T.C., 1983. Natural decay resistance of the heartwood of coast redwood *Sequoia sempervirens*. Forest Products Journal 33, 15–20.

Coffield, S.R., K.S., Hemes, C.D. Koven, M.L. Goulden, J.T. Randerson, 2021. Climate-driven limits to future carbon storage in California's wildland ecosystems. *AGU Advances* **2**: e2021AV000384.

Cook, E.R., L.A. Kairiukstis, 2013. Methods of Dendrochronology: Applications in the Environmental Sciences. Springer, Dordrecht, 393 pp.

Cook, E.R., 1985. A Time Series Analysis Approach to Tree-ring Standardization. Ph.D. dissertation. University of Arizona, Tucson, AZ.

Cowman, D., Russell, W., 2021. Fuel load, stand structure, and understory species composition following prescribed fire in an old-growth coast redwood (*Sequoia sempervirens*) forest. Fire Ecology 17, 1–13.

D'Andrea, E., Scartazza, A., Battistelli, A., Collalti, A., Proietti, S., Rezaie, N., Matteucci, G., Moscatello, S., 2021. Unravelling resilience mechanisms in forests: role of non-structural carbohydrates in responding to extreme weather events. Tree Physiology 41, 1808–1818.

D'Arrigo, R., Wilson, R., Liepert, B., Cherubini, P., 2008. On the 'divergence problem' in northern forests: a review of the tree-ring evidence and possible causes. Global and Planetary Change 60, 289–305.

Dagley, C.M., Berrill, J.-P., Leonard, L.P., Kim, Y.G., 2018. Restoration thinning enhances growth and diversity in mixed redwood/Douglas-fir stands in northern California. Restoration Ecology 26, 1170–1179.

Dangerfield, C.R., Voelker, S.L., Lee, C.A., 2021. Long-term impacts of road disturbance on old-growth coast redwood forests. Forest Ecology and Management 499, 119595.

Darby, A., Dragulјić, D., Glunk, A., Gotsch, S.G., 2016. Habitat moisture is an important driver of patterns of sap flow and water balance in tropical montane cloud forest epiphytes. Oecologia 182, 357–371.

Davy, R., Esau, I., Chernokulsky, A., Outten, S., Zilitinkevich, S., 2017. Diurnal asymmetry to the observed global warming. International Journal of Climatology 37, 79–93.

Denissen, J.M.C., Teuling, A.J., Pitman, A.J., Koirala, S., Migliavacca, M., Li, W., Reichstein, M., Winkler, A.J., Zhan, C., Orth, R., 2022. Widespread shift from ecosystem energy to water limitation with climate change. Nature Climate Change 12, 677–684.

Díaz, I.A., Sieving, K.E., Peña-Foxon, M.E., Larraín, J., Armesto, J.J., 2010. Epiphyte diversity and biomass loads of canopy emergent trees in Chilean temperate rain forests: a neglected functional component. Forest Ecology and Management 259, 1490–1501.

Diffenbaugh, N.S., Swain, D.L., Touma, D., 2015. Anthropogenic warming has increased drought risk in California. Proceedings of the National Academy of Sciences 112, 3931–3936.

Disney, M., Burt, A., Wilkes, P., Armston, J., Duncanson, L., 2020. New 3D measurements of large redwood trees for biomass and structure. Scientific Reports 10, 16721.

Engbeck Jr., J.H., 2018. Saving the Redwoods: The Movement to Rescue a Wonder of the Natural World. California, Save the Redwoods League, San Francisco, pp. 709.

Engineer, C.B., Ghassemian, M., Anderson, J.C., Peck, S.C., Hu, H., Schroeder, J.I., 2014. Carbonic anhydrases, EPF2 and a novel protease mediate CO_2 control of stomatal development. Nature 513, 246–250.

Engineer, C.B., Hashimoto-Sugimoto, M., Negi, J., Israelsson-Nordström, M., Azoulay-Shemer, T., Rappel, W.J., Iba, K., Schroeder, J.I., 2016. CO_2 sensing and CO_2 regulation of stomatal conductance: advances and open questions. Trends in Plant Science 21, 16–30.

Enloe, H.A., Graham, R.C., Sillett, S.C., 2006. Arboreal histols in old-growth redwood forest canopies, Northern California. Soil Science Society of America Journal 70, 408–418.
Evans, M.E.K., Derose, R.J., Klesse, S., Girardin, M.P., Heilman, K.A., et al., 2022. Adding tree rings to North America's national forest inventories: an essential tool to guide drawdown of atmospheric CO_2. BioScience 72, 233–246.
Farnsworth, K.F., 1996. Gyppo logging in Humboldt County: a boom-bust cycle on the California forest frontier. Master's Thesis, Humboldt State University, Arcata, CA, 117 pp.
Ferguson, B.N., Gotsch, S.G., Williams, C.B., Wilson, H., Barnes, C.N., Dawson, T.E., Nadkarni, N.M., 2021. Variation in cloud immersion, not precipitation, drives leaf trait plasticity and water relations in vascular epiphytes during an extreme drought. American Journal of Botany 109, 550–563.
Fernández, M., Hamilton, H.H., Kueppers, L.M., 2015. Back to the future: using historical climate variation to project near-term shifts in habitat suitable for coast redwood. Global Change Biology 21, 4141–4152.
Fettig, C.J., Mortenson, L.A., Bulaon, B.B., Foulk, P.G., 2019. Tree mortality following drought in the central and southern Sierra Nevada, California, U.S. Forest Ecology and Management 432, 164–178.
Fischer, D.T., Still, C.J., Williams, A.P., 2009. Significance of summer fog and overcast for drought stress and ecological functioning of coastal California endemic plant species. Journal of Biogeography 36, 783–799.
Forzieri, G., V. Dakos, N.G. McDowell, A. Ramdane, A. Cescatti, 2022. Emerging signals of declining forest resilience under climate change. *Nature*, doi.org/10.1038/s41586-022-04959-9.
Francis, E., Asner, G.P., Mach, K.J., Field, C.B., 2020. Landscape scale variation in the hydrological niche of California coast redwood. Ecography 43, 1305–1315.
Franklin, J.F., Spies, T.A., Van Pelt, R., Carey, A.B., Thornburgh, D.A., Berg, D.R., Chen, J., 2002. Disturbances and structural development of natural forest ecosystems with silvicultural implications, using Douglas-fir as an example. Forest Ecology and Management 155, 399–423.
Frankson, R., L.E. Stevens, K.E. Kunkel, S.M. Champion, D.R. Easterling, W. Sweet, M. Anderson, 2022. California State Climate Summary 2022. NOAA Technical Report NESDIS 150-CA. NOAA/NESDIS, Silver Spring, MD, 6 pp.
Fritts, H.C., 2012. Tree Rings and Climate. Academic Press, New York, NY, 582 pp.
George, S.S., Ault, T.R., 2014. The imprint of climate within Northern Hemisphere trees. Quaternary Science Reviews 89, 1–4.
Goss, M., Swain, D.L., Abatzoglou, J.T., Sarhadi, A., Kolden, C.A., Williams, A.P., Diffenbaugh, N.S., 2020. Climate change is increasing the likelihood of extreme autumn wildfire conditions across California. Environmental Research Letters 15, 094016.
Gotsch, S.G., Nadkarni, N., Darby, A., Glunk, A., Dix, M., Davidson, K., Dawson, T.E., 2015. Life in the treetops: ecophysiological strategies of canopy epiphytes in a tropical montane forest. Ecological Monographs 85, 393–412.
Gotsch, S.G., Nadkarni, N., Amici, A., 2016. The functional roles of epiphytes and arboreal soils in tropical montane cloud forests. Journal of Tropical Ecology 32, 455–468.
Gotsch, S.G., Davidson, K., Murray, J.G., Duarte, V.J., Draguljić, D., 2017. Vapor pressure deficit predicts epiphyte abundance across an elevational gradient in a tropical montane region. American Journal of Botany 104, 1790–1801.
Goulden, M.L., Bales, R.C., 2019. California forest die-off linked to multi-year deep soil drying in 2012–2015. Nature Geosciences 12, 632–637.
Grissino-Mayer, H.D., 2001. Evaluating crossdating accuracy: a manual and tutorial for the computer program COFECHA. Tree-Ring Research 57, 205–221.
Grossiord, D., Buckley, T.N., Cernusak, L.A., Novick, K.A., Poulter, B., Siegwolf, R.T.W., Sperry, J.S., McDowell, N.G., 2020. Plant responses to rising vapor pressure deficit. New Phytologist 226, 1550–1566.
Gustafsson, L., Baker, S.C., Bauhus, J., Beese, W.J., Brodie, A., Kouki, J., Lindenmayer, D. B., et al., 2012. Retention forestry to maintain multifunctional forests: a world perspective. BioScience 62, 633–645.
Hatam, R.A.R., Whiting, D.A., 1969. The constituents of Californian redwood: the constitution, absolute stereochemistry, and chemistry of sequirin-B and sequirin-C. Journal of the Chemical Society C: Organic 14, 1921–1932.
Haverd, V., Smith, B., Canadell, J.G., Cuntz, M., Mikaloff-Fletcher, S., Farquhar, G., Woodgate, W., Briggs, P.R., Trudinger, C.M., 2019. Higher than expected CO_2 fertilization inferred from leaf to global observations. Global Change Biology 26, 2390–2402.
Hillis, W.E., 1987. Heartwood and Tree Exudates. Springer, Berlin, Heidelberg, 268 pp.
Hoeber, V., Zotz, G., 2021. Not so stressful after all: epiphytic individuals of accidental epiphytes experience more favorable abiotic conditions than terrestrial conspecifics. Forest Ecology and Management 479, 118529.
Holmes, R.L., 1983. Computer-assisted quality control in tree-ring dating and measurement. Tree Ring Bulletin 43, 69–75.
Iberle, B.G., Van Pelt, R., Sillett, S.C., 2020. Development of mature second-growth *Sequoia sempervirens* forests. Forest Ecology and Management 459, 117816.
Ishii, H. Roaki, Azuma, Wakana, Kuroda, Keiko, Sillett, Stephen C., 2014. Pushing the limits to tree height: could foliar water storage compensate for hydraulic constraints in *Sequoia sempervirens*? Functional Ecology 28, 1087–1093. https://doi.org/10.1111/1365-2435.12284.
Ishii, H.T., Jennings, G.M., Sillett, S.C., Koch, G.W., 2008. Hydrostatic constraints on morphological exploitation of light in tall *Sequoia sempervirens* trees. Oecologia 156, 751–763.
Ishii, H.R., Minamino, T., Azuma, W., Hotta, K., Nakanishi, A., 2018. Large, retained trees of *Cryptomeria japonica* functioned as refugia for canopy woody plants after logging 350 years ago in Yakushima, Japan. Forest Ecology and Management 457, 457–467.
Jones, D.A., O'Hara, K.L., 2012. Carbon density in managed coast redwood stands: implications for forest carbon estimation. Forestry 85, 99–110.
Keeley, J.E., Syphard, A.D., 2021. Large California wildfires: 202 fires in historical context. Fire Ecology 17, 22.
Kessler, M., Siorak, Y., 2007. Desiccation and rehydration experiments on leaves of 43 pteridophyte species. American Fern Journal 97, 175–185.
Klesse, S., DeRose, R.J., Babst, F., Black, B., Anderegg, L.D.L., Axelson, J., Ettinger, A., Griesbauer, J., Guiterman, C.H., Harley, G., Harvey, J.E., Lo, Y.H., Lynch, A.M., O'Connor, C., Restaino, C., Sauchyn, D., Smith, D., Wood, L., Villanueva, J., Evans, M.E.K., 2020. Continental-scale tree-ring-based projection of Douglas-fir growth – testing the limits of space-for-time substitution. Global Change Biology 26, 5146–5163.
Koch, G.W., Sillett, S.C., Jennings, G.M., Davis, S.D., 2004. The limits to tree height. Nature 428, 851–854.
Konrad, W., Roth-Nebelsick, A., Grein, M., 2008. Modelling of stomatal density response to atmospheric CO_2. Journal of theoretical Biology 253, 638–658.
Körner, C., 2015. Paradigm shift in plant growth control. Current Opinion in Plant Biology 25, 107–114.
Kouwenberg, L.L., McElwain, J.C., Kürschner, W.M., Wagner, F., Beerling, D.J., Mayle, F. E., Visscher, H., 2003. Stomatal frequency adjustment of four conifer species to historical changes in atmospheric CO_2. American Journal of Botany 90, 610–619.
Kramer, R.D., Sillett, S.C., Van Pelt, R., 2018. Quantifying aboveground components of *Picea sitchensis* for allometric comparisons among tall conifers in North American rainforests. Forest Ecology and Management 430, 59–77.
Krieg, C.P., Chambers, S.M., 2021. The ecology and physiology of fern gametophytes: a methodological synthesis. Applications in Plant Sciences 10, e11464.
Kwon, H.-H., Lall, U., 2016. A copula-based nonstationary frequency analysis for the 2012–2015 drought in California. Water Resources Research 52, 5662–5675.
Langford, A.O., R.J. Alvarez, J. Brioude, D. Caputi, S.A. Conley, S. Evan, I.C. Faloona, L. T. Iraci, G. Kirgis, J.E. Marrero, J.M. Ryoo, C.J. Senff, E.L. Yates, 2019. Ozone production in the Soberanes smoke haze: implications for air quality in the San Joaquin Valley during the California Baseline Ozone Transport Study. *Journal of Geophysical Research: Atmospheres* **125**: e2019JD031777.
Law, B.E., Berner, L.T., Buotte, P.C., Mildrexler, D.J., Ripple, W.J., 2021. Strategic forest reserves can protect biodiversity in the western United States and mitigate climate change. Communications Earth & Environment 2, 1–13.
Lebassi, B., González, J., Fabris, D., Maurer, E., Miller, N., Milesi, C., Switzer, P., Bornstein, R., 2009. Observed 1970–2005 cooling of summer daytime temperatures in coastal California. Journal of Climate 22, 3558–3573.
Limm, E.B., Simonin, K.A., Bothman, A.G., Dawson, T.E., 2009. Foliar water uptake: a common water acquisition strategy for plants of the redwood forest. Oecologia 161, 449–459.
Lindenmayer, D.B., Laurance, W.F., Franklin, J.F., 2012. Global decline in large old trees. Science 338, 1305–1306.
Loehle, C., 1988. Tree life history strategies: the role of defense. Canadian Journal of Forest Research 18, 209–222.
Luxford, R.F., L.J. Markwardt, 1932. The strength and related properties of redwood. Technical Bulletin No. 305, U.S. Department of Agriculture, Washington, D.C., 48 pp.
Mahdizadeh, M., Russell, W., 2021. Initial floristic response to high severity wildfire in an old-growth coast redwood (*Sequoia sempervirens*) forest. Forests 12, 1135.
Mathias, J.M., R.B. Thomas, 2021. Global tree intrinsic water use efficiency is enhanced by increased atmospheric CO_2 and modulated by climate and plant functional types. *Proceedings of the National Academy of Sciences* **118**: e2014286118.
McCune, B., 2007. Improved estimates of incident radiation and heat load using non-parametric regression against topographic variables. Journal of Vegetation Science 18, 751–754.
McCune, B., M.J. Mefford, 2009. HyperNiche. Nonparametric Multiplicative Habitat Modeling, version 2.30. MjM Software, Gleneden Beach, Oregon.
McCune, B., 2011. Nonparametric multiplicative regression for habitat modeling, http://www.pcord.com/NPMRintro.pdf, Oregon State University, Corvallis OR.
McDowell, N.G., Allen, C.D., Anderson-Teixeira, K., Aukema, B.H., Bond-Lamberty, B., Chini, L., Clark, J.S., et al., 2020. Pervasive shifts in forest dynamics in a changing world. Science 368, eaaz9463.
McLaughlin, B.C., Ackerly, D.D., Klos, P.Z., Natali, J., Dawson, T.E., Thompson, S.E., 2017. Hydrologic refugia, plants, and climate change. Global Change Biology 23, 2941–2961.
Miyamoto, Y., Griesbauer, H.P., Green, D.S., 2010. Growth responses of three coexisting conifer species to climate across wide geographic ranges in Yukon and British Columbia. Forest Ecology and Management 259, 514–523.
Myśkow, E., Błaś, M., Sobik, M., Godek, M., Owczarek, P., 2019. The effect of pollutant fog deposition on the wood anatomy of subalpine Norway spruce. European Journal of Forest Research 138, 187–201.
NDMC, 2022. National Drought Mitigation Center, US Department of Agriculture and National Oceanic and Atmospheric Administration. www.droughtmonitor.unl.edu/maps/maparchive.aspx.
North, M.P., York, R.A., Collins, B.M., Hurteau, M.D., Jones, G.M., Knapp, E.E., Kobziar, L., Meyer, M.D., Stephens, S.L., Tompkins, R.E., Tubbesing, C.L., 2021. Pyrosilviculture needed for landscape resilience of dry western United States forests. Journal of Forestry 119, 520–544.
Novick, K.A., Ficklin, D.L., Stoy, P.C., Williams, C.A., Bohrer, G., Oishi, A.C., Papuga, S. A., Blanken, P.D., et al., 2016. The increasing importance of atmospheric demand for ecosystem water and carbon fluxes. Nature Climate Change 6, 1023–1027.
Nyaga, J.M., Neff, J.C., Cramer, M.D., 2015. The contribution of occult precipitation to nutrient deposition on the west coast of South Africa. PLOS One 10, e0126225.

O'Hara, K.L., Cox, L.E., Nikolaeva, S., Bauer, J.J., Hedges, R., 2017. Regeneration dynamics of coast redwood, a sprouting conifer species: a review with implications for management and restoration. Forests 8, 144.
Oldham, A.R., Sillett, S.C., Tomescu, A.M.F., Koch, G.W., 2010. The hydrostatic gradient, not light availability, drives height-related variation in *Sequoia sempervirens* (Cupressaceae) leaf anatomy. American Journal of Botany 97, 1–12.
Oliver, C.D., B.A. Larson, 1996. Forest Stand Dynamics, Update Edition. Yale School of the Environment Other Publications 1, 541 pp.
Parks, S.A., Miller, C., Parisien, M.-A., Holsinger, L.M., Dobrowski, S.Z., Abatzoglou, J., 2015. Wildland fire deficit and surplus in the western United States. Ecosphere 6, 1–13.
Pedlar, J.H., McKenney, D.W., 2017. Assessing the anticipated growth response of northern conifer populations to a warming climate. Scientific Reports 7, 43881.
Peñuelas, J., Ciais, P., Canadell, J.G., Janssens, I., Fernandez-Martinez, M., Carnicer, J., Obersteiner, M., Piao, S., Vautard, R., Sardans, J., 2017. Shifting from a fertilization-dominated to a warming-dominated period. Nature Ecology and Evolution 1, 1438–1445.
Piponiot, C., K.J. Anderson-Teixeira, S.J. Davies, D. Allen, N.A. Bourg, et al., 2022. Distribution of biomass dynamics in relation to tree size in forests across the world. *New Phytologist*, doi 10.111/nph.17995.
Pretzsch, H., Biber, P., Schütze, G., Kemmerer, J., Uhl, E., 2018. Wood density reduced while wood volume growth accelerated in Central European forests since 1870. Forest Ecology and Management 429, 589–616.
R Core Team, 2021. R: A language and environment for statistical computing. R Foundation for Statistical Computing, Vienna, Austria. URL https://www.R-project.org/.
Rathgeber, C.B.K., Cuny, H.E., Fonti, P., 2016. Biological basis of tree-ring formation: a crash course. Frontiers in Plant Science 7, 734.
Reese Næsborg, R., Peterson, E.B., Tibell, L., 2019. *Chaenotheca longispora* (Coniocybaceae), a new lichen from coast redwood trees in California, U.S.A. Bryologist 122, 31–37.
Resch, H., Arganbright, D.G., 1968. Variation of specific gravity, extractive content, and tracheid length in redwood trees. Forest Science 14, 148–155.
Ripple, W.J., Wolf, C., Newsome, T.M., Gregg, J.W., Lenton, T.M., Palomo, I., Eikelboom, J.A.J., Law, B.E., Huq, S., Duffy, P.B., Rockström, J., 2021. World scientists' warning of a climate emergency 2021. BioScience 71, 894–898.
Ryan, M.G., Gower, S.T., Hubbard, R.M., Waring, R.H., Gholz, H.L., Cropper Jr., W.P., Running, S.W., 1995. Woody tissue maintenance respiration of four conifers in contrasting climates. Oecologia 101, 133–140.
Schnabel, F., Purrucker, S., Schmitt, L., Engelmann, R.A., Kahl, A., Richter, R., Seele-Dilbat, C., Skiadaresis, G., Wirth, C., 2022. Cumulative growth and stress responses to the 2018–2019 drought in a European floodplain forest. Global Change Biology 28, 1870–1883.
Shenkin, A., C.J. Chandler, D.S. Boyd, T. Jackson, M. Disney, N. Majalap, R. Nilus, G. Foody, J. bin Jami, G. Reynolds, P. Wilkes, M.E.J. Cutler, G.M.F. van der Heijden, D. F.R.P. Burslem, D.A. Coomes, L.P. Bentley, Y. Malhi, 2019. The world's tallest tropical tree in three dimensions. *Frontiers in Forests and Global Change* **2**: 32.
Shive, K.L., Wuenschel, A., Harlund, L.J., Morris, A., Meyer, D., Hood, S.M., 2022. Ancient trees and modern wildfires: declining resilience to wildfire in the highly fire-adapted giant sequoia. Forest Ecology and Mangement 511, 120220.
Sillett, S.C., Bailey, M.G., 2003. Effects of tree crown structure on biomass of the epiphytic fern *Polypodium scouleri* (Polypodiaceae) in redwood forests. American Journal of Botany 90, 255–261.
Sillett, S.C., Van Pelt, R., 2007. Trunk reiteration promotes epiphytes and water storage in an old-growth redwood forest canopy. Ecological Monographs 77, 335–359.
Sillett, S.C., Van Pelt, R., Koch, G.W., Ambrose, A.R., Carroll, A.L., Antoine, M.E., Mifsud, B.M., 2010. Increasing wood production through old age in tall trees. Forest Ecology and Management 259, 976–994.
Sillett, S.C., Van Pelt, R., Kramer, R.D., Carroll, A.L., Koch, G.W., 2015a. Biomass and growth potential of *Eucalyptus regnans* up to 100 m tall. Forest Ecology and Management 348, 78–91.
Sillett, S.C., Van Pelt, R., Carroll, A.L., Kramer, R.D., Ambrose, A.R., Trask, D., 2015b. How do tree structure and old age affect growth potential of California redwoods? Ecological Monographs 85, 181–212.
Sillett, S.C., Antoine, M.E., Campbell-Spickler, J., Carroll, A.L., Coonen, E.J., Kramer, R. D., Scarla, K., 2018a. Manipulating tree crown structure to promote old-growth characteristics in second-growth redwood forest canopies. Forest Ecology and Management 417, 77–89.
Sillett, S.C., Van Pelt, R., Freund, J.A., Campbell-Spickler, J., Carroll, A.L., Kramer, R.D., 2018b. Development and dominance of Douglas-fir in North American rainforests. Forest Ecology and Management 429, 93–114.
Sillett, S.C., Van Pelt, R., Carroll, A.L., Campbell-Spickler, J., Coonen, E.J., Iberle, R., 2019a. Allometric equations for *Sequoia sempervirens* in forests of different ages. Forest Ecology and Management 433, 349–363.
Sillett, S.C., Van Pelt, R., Carroll, A.L., Campbell-Spickler, J., Antoine, M.E., 2019b. Structure and dynamics of forests dominated by *Sequoiadendron giganteum*. Forest Ecology and Management 448, 218–239.
Sillett, S.C., Van Pelt, R., Carroll, A.L., Campbell-Spickler, J., Antoine, M.E., 2020. Aboveground biomass dynamics and growth efficiency of *Sequoia sempervirens* forests. Forest Ecology and Management 458, 117740.
Sillett, S.C., Kramer, R.D., Van Pelt, R., Carroll, A.L., Spickler, J.C., Antoine, M.E., 2021. Comparative development of the four tallest conifers. Forest Ecology and Management 480, 118688.
Simonin, K.S., Santiago, L.S., Dawson, T.E., 2009. Fog interception by *Sequoia sempervirens* crowns decouples physiology from soil water deficit. Plant, Cell & Environment 32, 882–892.
Soland, K.R., Kerhoulas, L.P., Kerhoulas, N.J., Teroaka, J.R., 2021. Second-growth redwood forest responses to restoration treatments. Forest Ecology and Management 496, 119370.
Stephenson, N.L., Das, A.J., Ampersee, N.J., Cahill, K.G., Caprio, A.C., Sanders, J.E., Williams, A.P., 2018. Patterns and correlates of giant sequoia foliage dieback during California's 2012–2016 hotter drought. Forest Ecology and Management 419–420, 268–270.
Swain, D.L., Langenbrunner, B., Neelin, J.D., Hall, A., 2018. Increasing precipitation volatility in twenty-first-century California. Nature Climate Change 8, 427–433.
Tatsumi, S., Yamaguchi, K., Furuya, N., 2022. ForestScanner: a mobile application for measuring and mapping trees with LiDAR-equipped iPhone and iPad. Methods in Ecology and Evolution. https://doi.org/10.1111/2041-210X.13900.
Taylor, A.M., Gartner, B.L., Morrell, J.J., 2002. Heartwood formation and natural durability—a review. Wood Fiber Science 34, 587–611.
Taylor, A.M., Gartner, B.L., Morrell, J.J., Tsunoda, K., 2006. Effects of heartwood extractive fractions of *Thuja plicata* and *Chamaecyparis nootkatensis* on wood degradation by termites or fungi. Journal of Wood Science 52, 147–153.
Tejo, C.M., Fontúrbel, F.E., 2019. A vertical forest within the forest: millenary trees from the Valdivian rainforest as biodiversity hubs. Ecology 100, e02584.
Templer, P.H., Weathers, K.C., Ewing, H.A., Dawson, T.E., Mambelli, S., Lindsey, A.M., Webb, J., Boukili, V.K., Firestone, M.K., 2015. Fog as a source of nitrogen for redwood trees: evidence from fluxes and stable isotopes. Journal of Ecology 103, 1397–1407.
Torregrosa, A., Combs, C., Peters, J., 2016. GOES-derived fog and low cloud indices for coastal north and central California ecological analyses. Earth and Space Science 3, 46–67.
Van Pelt, R., Sillett, S.C., Kruse, W.A., Freund, J.A., Kramer, R.D., 2016. Emergent crowns and light-use complementarity lead to global maximum biomass and leaf area in *Sequoia sempervirens* forests. Forest Ecology and Management 375, 279–308.
Vicente-Serrano, S.M., Beguería, S., López-Moreno, J.I., 2010. A multiscalar drought index sensitive to global warming: the standardized precipitation evapotranspiration index. Journal of Climate 23, 1696–1718.
Waggoner, N.E., 1961. The Eureka-Arcata ambient air quality study. Bureau of Air Sanitation, Berkeley, CA, 24 pp.
Walker, A.P., De Kauwe, M.G., Bastos, A., Belmecheri, S., Georgious, K., Keeling, R.F., et al., 2021. Integrating the evidence for a terrestrial carbon sink caused by increasing atmospheric CO_2. New Phytologist 229, 2413–2445.
Wettstein, J.J., Littell, J.S., Wallace, J.M., Gedalof, Z., 2011. Coherent region-, species-, and frequency-dependent local climate signals in northern hemisphere tree-ring widths. Journal of Climate 24, 5998–6012.
Wigley, T.M.L., Briffa, K.R., Jones, P.D., 1984. On the average value of correlated time series, with applications in dendroclimatology and hydrometeorology. Journal of Climate and Applied Meteorology 23, 201–213.
Wilcox, W.W., Piirto, D.D., 1974. Decay resistance in redwood (*Sequoia sempervirens*) heartwood as related to color and extractives. Wood and Fiber Science 7, 240–245.
Williams, A.P., Abatzoglou, J.T., Gershunov, A., Guzman-Morales, J., Bishop, D.A., Balch, J.K., Lettenmaier, D.P., 2019. Observed impacts of anthropogenic climate change on wildfire in California. Earth's Future 7, 892–910.
Williams, C.B., Sillett, S.C., 2007. Epiphyte communities on redwood (*Sequoia sempervirens*) in northwestern California. Bryologist 110, 420–452.
Williams, C.B., Tibell, L., 2008. *Calicium sequoiae*, a new lichen species from northwestern California, USA. The Lichenologist 40, 185–194.
Woodruff, D.R., Bond, B.J., Meinzer, F.C., 2004. Does turgor limit growth in tall trees? Plant, Cell & Environment 27, 229–236.
Woodward, B.D., Romme, W.H., Evangelista, P.H., 2020. Early postfire response of a northern range margin coast redwood forest community. Forest Ecology and Management 462, 117966.
Yamaguchi, D.K., 1991. A simple method for cross-dating increment cores from living trees. Canadian Journal of Forest Research 21, 414–416.
Yang, Y., Donohue, R.J., McVicar, T.R., Roderick, M.L., Beck, H.E., 2016. Long-term CO_2 fertilization increases vegetation productivity and has little effect on hydrological partitioning in tropical rainforests. Journal of Geophysical Research: Biogeosciences 121, 2125–2140.
York, R.A., Noble, H., Quinn-Davidson, L.N., Battles, J.J., 2021. Pyrosilviculture: combining prescribed fire with gap-based silviculture in mixed-conifer forests of the Sierra Nevada. Canadian Journal of Forest Research 51, 781–791.
Yuan, W., Zheng, Y., Piao, S., Cias, P., Lombardozzi, D., Wang, Y., Ryu, Y., Chen, G., et al., 2019. Increased atmospheric vapor pressure deficit reduces global vegetation growth. *Science*. Advances 5, eaax1396.
Zang C., F. Biondi, 2015. Treeclim: an R package for the numerical calibration of proxy-climate relationships. *Ecography* **38**: 431-436.
Zha, T., Kellomäki, K.-Y., Wang, A., Ryyppö, S.N., 2004. Seasonal and annual stem respiration of Scots pine trees under boreal conditions. Annals of Botany 94, 889–896.
Zhao, Z., Pingkuan, D., Chen, S., Avise, K., Kaduwela, A., DaMassa, J., 2020. Assessment of climate change impact over California using dynamical downscaling with a bias correction technique: method validation and analyses of summertime results. Climate Dynamics 54, 3705–3728.
Zweifel, R., F. Sterck, S. Braun, N. Buchmann, W. Eugster, A. Gessler, M. Häni, L. Walthert, M, Wilhelm, K. Zieminska, S. Etzold, 2021. Why trees grow at night. *New Phytologist* **231**: 2174-2185.